Stochastic Heating of Ions in a Tokamak by RF Power

by

Charles Fielding Finch Karney
B.A., Cambridge University, 1972
S.M., Massachusetts Institute of Technology, 1974

Submitted in Partial Fulfillment of the
Requirements for the Degree of
Doctor of Philosophy
at the
Massachusetts Institute of Technology
May, 1977

Note

This thesis, text and figures, was typeset using the facilities of MIT's Project MAC and Artificial Intelligence Laboratory and printed on a Xerox Graphics Printer—a precursor to today's laser printers. The typesetting software consisted of TECO macros written by John Kulp together with graphics routines that I wrote. (Recall that the first version of Knuth's TEX only became available in 1978.)

Unfortunately, the source files are no longer available. So this is a facsimile of the thesis produced by scanning a clean copy, converting the images to png figures, including these figures in a LATEX file, and processing this with pdflatex. The production of the png figures was done with

```
DEV=/dev/scanner
scanimage --device umax:$DEV --mode Gray --resolution 300 \
  -l 0.8in -t 0.6in -x 7in -y 9.5in |
  pnmscale -xysize 1400 1900 |
  pgmnorm -bvalue 32 -wvalue 191 | pnmdepth 7 |
  pnmtopng -compress 9
```

In words: scan a 7 in by 9.5 in area at 300/in, scale resolution down to 200/in (the resolution of the Xerox Graphics Printer), scale the gray levels so that nearly white/black becomes white/black, reduce pixel depth to 3 bits, and convert to png with the highest compression. The resulting png files average about 10^5 bytes/page or about 0.3 bits/pixel.

A list of errata is included at the end.

Charles Karney
February 23, 2004

Stochastic Heating of Ions in a Tokamak by RF Power

by

Charles Fielding Finch Karney

B.A., Cambridge University, 1972

S.M., Massachusetts Institute of Technology, 1974

Submitted in Partial Fulfillment of the

Requirements for the Degree of

Doctor of Philosphy

at the

Massachusetts Institute of Technology

May, 1977

Signature of Author _____

Department of Electrical Engineering and Computer Science, May 25, 1977

Certified by _____

Thesis Supervisor

Accepted by _____

Chairman, Departmental Committee on Graduate Students

Stochastic Heating of Ions in a Tokamak by RF Power

by

Charles Fielding Finch Karney

Submitted to the Department of Electrical Engineering and Computer Science on May 25, 1977, in partial fulfillment of the requirements for the degree of Doctor of Philosphy.

Abstract.

The nonlinear interaction of ions in a plasma with waves excited by RF power near the lower hybrid frequency is considered. The object of this study is to evaluate such an interaction as a method of heating the ions in a tokamak. The problem is simplified by assuming the magnetic field, B_0, to be uniform and the lower hybrid wave (whose frequency, ω, is much greater than the ion cyclotron frequency, Ω_i) to be propagating perpendicular to the magnetic field. It is shown that trapping by the wave significantly increases the energy of the ions on a time scale of a few cyclotron periods. For longer times the motion in a certain region of velocity space becomes stochastic for fields satisfying $E/B_0 > \frac{1}{4}(\Omega_i/\omega)^{1/3}\omega/k$ (k is the wavenumber of the wave). The stochastic region of velocity space extends from a lower limit given by $\omega/k - \sqrt{qE/mk}$ (q and m are the ionic charge and mass, respectively) where the ion dynamics are determined by trapping to an upper limit which scales as $E^{2/3}$. The stochasticity condition is independent of how close ω is to a cyclotron harmonic. These results are extended to the case of propagation at an oblique angle to the magnetic field and to the case of inhomogeneous magnetic field. It is shown that stochastic ion heating can be an efficient method for supplementary heating of the ions in a tokamak.

Thesis Supervisor: Abraham Bers
Professor of Electrical Engineering and Computer Science

Acknowledgements.

The author wishes to thank his supervisor Professor Abraham Bers, with whom he collaborated on the the work presented here. All the members of the Active Plasma Group are thanked for providing a congenial and stimulating atmosphere in which to work. Special thanks go to Nat Fisch, who proof-read this thesis, and to John Kulp, who was primarily responsible for keeping the computational facilities of the group in working order.

Financial sponsorship was provided by a research assistantship from the Research Laboratory of Electronics. The computations were carried out on the Macsyma Consortium machine. This thesis was printed on the Xerox Graphics Printer of the Artificial Intelligence Laboratory.

Table of Contents.

Abstract		Page 2
Acknowlegements		3
Table of Contents		4
Chapter 1.	INTRODUCTION	5
1.1.	Overview of Problem	5
1.2.	Previous Work	7
1.3.	Outline of Following Chapters	10
Chapter 2.	ORBIT EQUATIONS AND THEIR LINEAR SOLUTION	13
2.1.	Derivation of Orbit Equations	13
2.2.	Linear Solution of Orbit Equations	15
2.3.	Interpretation of Linear Solutions	22
2.4.	Iteration of Linear Solutions	28
Chapter 3.	NUMERICAL SOLUTION OF ORBIT EQUATIONS	37
3.1.	Observation of Trapping	37
3.2.	Observation of Stochasticity	41
Chapter 4.	HAMILTONIAN FORMULATION	52
4.1.	Formulation in Terms of Hamiltonian	52
4.2.	Integrals of the Motion	56
4.3.	Origin of Stochasticity	59
4.4.	Derivation of Island and Stochasticity Thresholds	70
4.5.	Inclusion of Small Parallel Propagation	82
4.6.	Inclusion of Weak Magnetic Field Inhomogeneity	87
Chapter 5.	APPLICATION TO RF HEATING	93
5.1.	Simulated Heating Experiment	93
5.2.	Role of Collisions	97
5.3.	Design of Experiment	100
5.4.	Conclusion	112
Appendices		114
A.	Numerical Integration Scheme for Orbit Equations	114
B.	Calculation of Overlap Condition near a Harmonic	118
References		127
Biographical Note		131

STOCHASTIC HEATING OF IONS IN A TOKAMAK BY RF POWER.

Chapter 1. INTRODUCTION.

Section 1.1. Overview of Problem.

The need for supplementary heating of tokamak plasma is well known (Artsimovich, 1972). Its purpose is to raise the ion temperature from the 1 to 2 keV attainable by ohmic heating to about 10 keV required for ignition. Injection of RF power in the lower hybrid frequency range is one of the heating schemes considered (Stix, 1965). This has the advantages that high power (about 1 MW) sources at these frequencies are presently available, and that the power can be easily brought to the wall of the tokamak by means of waveguides. Experiments using RF in tokamaks have been carried out on ALCATOR (Richards and Parker, 1975), ATC (Hooke, 1975; Bernabei *et al.*, 1976; Porkolab *et al.*, 1977), and WEGA (Lallia *et al.*, 1976; Blanc *et al.*, 1976; Hess *et al.*, 1976). With all the experiments hot ion tails are observed; these ion tails decay very rapidly after the RF is turned off. Only preliminary results were obtained with the experiment on ALCATOR; this experiment is currently in the process of being revived. With the experiment on ATC an ion temperature rise was observed, although, due to instrumental deficiencies, it was not possible to establish its decay time accurately. A neutral beam injected into ATC as a diagnostic, was accelerated from 25 keV to 32 keV in the perpendicular direction when the RF was turned on. This indicated that the RF was able to to penetrate into the center of the plasma, and that it was able to couple strongly to the beam. With WEGA the ion temperature rise was more definite, increasing by a factor of 2 in some cases. The ion temperature decayed over a time of several milliseconds.

In this thesis we will deal with a theoretical aspect of the problem of RF heating.

Specifically we ask the question: What is the interaction of ions with the lower hybrid waves? Since lower hybrid waves generally satisfy $k_\perp \gg k_\parallel$ and $\omega \gg \Omega_i$, we begin by looking at the nonlinear motion of a single ion in uniform magnetic field and a perpendicularly propagating electrostatic wave whose frequency is much above the ion cyclotron frequency. The equations of motion exhibit some interesting properties. Over a small portion of the Larmor orbit (times short compared with the cyclotron period) the ion behaves as though it were unmagnetized, so that trapping of the same sort that occurs without a magnetic field can occur, as long as the particle's velocity equals the wave phase velocity. Although the magnetic field eventually detraps the particle, the particle's energy may be significantly increased. An estimate of the energy exchange can be made on the basis of this physical picture. The effect of trapping in this problem has also recently been discussed by Sugihara and Midzuno (1976), but they consider much larger field amplitudes.

In order to be sure that this energy is gained irreversibly, we next numerically compute the motion over many cyclotron periods. What we find is that the motion in a certain region of perpendicular velocity space becomes stochastic above a threshold field. The stochasticity threshold is found to be independent of how close ω is to a cyclotron harmonic. This should be contrasted with the results of Fukuyama *et al.* (1977) which are only applicable very close to a harmonic. In order to derive the threshold analytically we cast the problem in terms of a Hamiltonian. The effect of the wave is to cause a nonlinear shift in the cyclotron frequency, which depends on the particle's speed, so that the cyclotron frequency becomes a rational fraction of the wave frequency. This resonance causes islands to form in phase space. As the amplitude of the field is increased these islands grow and increase in number leading to overlap and stochastic behaviour. By finding the nonlinear frequency shift analytically and by investigating the motion numerically we are able to derive an analytic expression for the stochasticity threshold.

In order to apply these results to lower hybrid heating in tokamaks we include parallel propagation of the wave as a perturbation. We are able to show how our results match to those

of Smith and Kaufman (1975) for an obliquely propagating wave. We also consider an inhomogeneity in the magnetic field as a perturbation and show that for tokamak magnetic field configurations this does not affect our results. We examine the role of collisions in channelling the energy gained by tail particles due to be stochastic heating into the bulk ion distribution. Finally we discuss the ways in which our results may used to design a lower hybrid heating experiment. We find that the field required for the motion to be stochastic is quite moderate, but that the requirement that the heating not occur too far out on the tail of the ion distribution means that the frequency of the wave must be quite close to the maximum lower hybrid frequency in the tokamak.

Section 1.2. Previous Work.

We briefly review some of the work on the basic theory of lower hybrid heating. The previous work on ion heating and stochasticity is covered in more detail.

The suggestion of using RF power near the lower hybrid frequency was first made by Stix (1965), who gave the conditions under which such power could penetrate the plasma. This accessiblity condition was refined by Briggs and Parker (1972), Golant (1971), Troyon and Perkins (1974), and Theilhaber (1976). A detailed analysis of the coupling to RF power in waveguides to plasma waves has been made by Brambilla (1976), although a thorough treatment of the waves in the very low density region of the plasma is still required. The effects of the tokamak geometry on the penetration have been studied by Kulp *et al.* (1976). These studies consider only linear effects; however, in order to heat the plasma effectively large amplitude waves must be used. In fact, it turns out that nonlinear effects can significantly affect the penetration of lower hybrid waves. Morales and Lee (1975) and Bers *et al.* (1976b) have considered the filamentation of the lower hybrid rays. Decay into quasi-modes (Berger and Chen, 1976; Sen *et al.*, 1977) may also play an important role in the penetration problem.

Stix (1965) suggested that the lower hybrid waves would convert near the lower hybrid resonance layer to an ion thermal wave which would damp (and heat the plasma) by linear processes. This idea has been pursued by Glagolev (1972) and Simonutti (1975). This wave conversion is primarily a finite ion temperature effect. One effect of finite electron temperature is to cause the lower hybrid wave to decay by Landau damping. This has been proposed as a heating mechanism by Bers *et al.* (1976a). In addititon there have been a number of studies on the possibility of heating by parametric decay products (Kindel *et al.*, 1972; Porkolab, 1974; Bers and Karney, 1974). A detailed examination of the role of parametric instablilities on the problem of penetration and of heating still remains to be done.

We turn now to the work on ion heating. Linearly a wave propagating at a steep angle to the magnetic field suffers cyclotron harmonic damping only if its frequency is close to a cyclotron harmonic. In a tokamak the magnetic field is inhomogeneous and so the lower hybrid ray crosses a few cyclotron harmonics as it penetrates the plasma. Eldridge *et al.* (1975) considered such a situation, and found the damping of the lower hybrid wave as it crosses the cyclotron harmonic layers by solving for the linear motion of an ion. Antonsen and Ott (1976) considered a similar problem but treated the waves more exactly. They showed that the integrated effect of the wave's crossing many cyclotron harmonic layers is the same as if the wave were suffering linear Landau damping in an unmagnetized plasma; however these conditions are unlikely to be met in a tokamak.

This thesis examines the interaction between a lower hybrid wave and the ions in more detail. Specifically we consider the nonlinear motion of an ion in a magnetic field and a lower hybrid wave. The motion of a particle in various field configurations has been investigated for many years. In the absence of a magnetic field the motion of particles in a single finite amplitude electrostatic wave is well known (O'Neil, 1965). There are a class of particles that are trapped in the potential trough of the wave. For times shorter than the bounce time of the particle in the wave, this leads to Landau damping; for longer times trapping serves to limit the damping

decrement of the wave. The next most simple case to consider is the motion of a particle in the presence of a finite amplitude electrostatic wave travelling at an angle to a constant magnetic field. The equations of motion in this case cannot in general be solved exactly. Various approximations have been used to make the equations tractable. For instance Aamodt (1970) makes the approximation that the Larmor orbit is not grossly perturbed over one cyclotron orbit. A similar restriction is made by Sigmar and Callen (1971), Timofeev (1974), and Schmitt (1976) who in addition concentrates on the long wavelength limit. A somewhat different approach is taken by Sugihara and Midzuno (1976), who consider a large amplitude wave. They show that the process of trapping and detrapping of a particle in the trough of the electrostatic wave can result in a large exchange of energy. However the fields they consider are so large that their results are inapplicable to the case of lower hybrid heating. One of the important results that we shall present here is to show that trapping can indeed play an important role in the short time behaviour of the particle.

In contrast with the studies described above, which seek to find an approximation to the orbit of the particle, is the work of Smith and Kaufman (1974). They look instead at more general properties of the system, and they show that even though the wave is coherent the particle motion can be stochastic if the amplitude of the wave is large enough. Unfortunately the threshold for stochasticity that they give is infinite for waves propagating exactly perpendicularly to the field, and is very large for lower hybrid waves that propagate nearly perpendicularly. Fukuyama *et al.* (1977) consider the case of a perpendicularly propagating wave whose frequency is very close to a cyclotron harmonic and show that the motion is stochastic at a finite amplitude. These results should be constrasted with those of Dum and Dupree (1970) who consider "resonance broadening" effect of the motion of a particle in a randomly phased wave.

There are a number of examples from the field of plasma physics, in addition to the two cited above, where a coherent system can produce stochastic motion. Jaeger *et al.* (1972) and Lieberman and Lichtenberg (1973) found this to be the case for electron cyclotron heating in

mirror machines. In this case the inhomogeneous magnetic field in a mirror machine plays an important role in randomizing the particles phase with repect to the wave. Other examples are the particle motion in two electrostatic waves (Zaslavskii and Filonenko, 1968), magnetic braiding (Rechester and Stix, 1976) and particle motion in a modulated magnetic field (Dunnett *et al.*, 1968). Since this is a relatively unfamiliar subject, we give a brief description of the origin of stochasticity in Sec. 4.3.

The work in progress towards this thesis thesis has been reported in Bers *et al.* (1975), Karney *et al.* (1975), and Karney and Bers (1976a, 1976b, 1976c, 1977a, 1977b).

Section 1.3. Outline of Following Chapters.

In this thesis we will examine the interaction of lower hybrid waves with the ions in a tokamak. We wish to determine whether this interaction can lead to ion heating. We begin by making four simplifying assumptions which we make use of in the next two and a half chapters. They are:

1. That the wave may taken as propagating perpendicular to the magnetic field.
2. That the wave is uniform.
3. That the magnetic field is homogeneous.
4. That the ion doesn't act back on the wave.

These assumptions allow us to study a much simpler problem: the interaction of a single ion with a perpendicularly propagating electrostatic wave in a homogenous magnetic field. We will examine these assumptions later when applying our results to the problem of ion heating in a tokamak. This simpler problem is tackled by three methods: iterating the linear solutions, numerical integration of the orbit equations, and the Hamiltonian formulation.

Chapter 2 deals with the orbit equations and their linear solutions. In Sec. 2.1 we derive the equations describing the motion of an ion in a homogeneous magnetic field and a uniform, perpendicularly propagating, electrostatic wave. We summarize the standard linear solution to the orbit equations in Sec. 2.2 and derive an alternate form for the linear solution, that allows the unperturbed orbit to be corrected every cyclotron period. In Sec. 2.3 we show how this alternate form may be physically interpreted in terms of the zero magnetic field wave particle resonance. In Sec. 2.4 we present the results of numerically iterating the linear equations, with the corrected orbits, and show that when the field is sufficiently large, particles with a perpendicular velocity larger than the phase velocity of the wave may be accelerated.

In order to verify the results of Chapter 2, we look in Chapter 3 at the results of numerically integrating the exact orbit equations. Two interesting phenomena are discovered. In Sec. 3.1 we show that trapping of the particle by the wave can lead to significant energy exchange between the particle and the wave on the time scale of the cyclotron period. Estimates of the energy exchange based on simple physical considerations are given. In Sec. 3.2 we look at the behaviour of the orbit equations over many cyclotron periods, and find that the motion in certain regions of velocity space can become stochastic.

In Chapter 4, we formulate the problem in terms of its Hamiltonian. This enables us to derive an analytic expression for the stochasticity threshold observed in Sec. 3.2. We derive the Hamiltonian in Sec. 4.1. In Sec. 4.2 we derive the integrals of the motion for the case where the electric field is small. In Sec. 4.3 we discuss the origins of stochasticity in Hamiltonian systems, with specific reference to our problem; in particular we trace the relation between stochasticity and island formation and growth. In Sec. 4.4 we derive the conditions for island formation, and from them the stochasticity threshold. Section 4.5 examines to what extent our results hold when we include parallel propagation of the wave. We show how our results tie in with the results of Smith and Kaufman (1975) for oblique propagation. Lastly Sec. 4.6 deals with the inclusion of a weak magnetic field inhomogeneity, where we show that our results are valid for the magnetic

fields typical in Tokamaks.

In Chapter 5 we examine how our results may be applied to the problem of heating a tokamak plasma with RF power near the lower hybrid frequnecy. In Sec. 5.1 we present the results of a numerical simulation of a group of particles. This establishes that the stochastic motion analyzed in the previous chapter does cause particles to get heated. For short times it is shown that the amount of heating in determined by trapping. In Sec. 5.2 we look at collisions. Their effect is to convert the tail heating caused by the wave into bulk heating. The time scale of this is derived. In Sec. 5.3 we discuss some aspects of the design of a lower hybrid heating experiment, which seeks to utilize stochastic ion heating. Section 5.4 is the conclusion.

Chapter 2. ORBIT EQUATIONS AND THEIR LINEAR SOLUTION.

Section 2.1. Derivation of Orbit Equations.

For the major part of this thesis we will assume that the magnetic field is uniform and that the RF field propagates perpendicular to the magnetic field. (We will examine both of these assumptions later in the light of our results.) Thus we consider an ion in the presence of a magnetic field,

$$\mathbf{B} = B_0\hat{\mathbf{z}}, \tag{2.1.1}$$

and an electric field,

$$\mathbf{E} = E_0\hat{\mathbf{y}}\cos(ky - \omega t - \phi). \tag{2.1.2}$$

The equation of motion of such a particle is given by the Lorentz force law,

$$\frac{d\mathbf{v}}{dt} = \frac{q}{m}[\mathbf{E} + \mathbf{v}\times\mathbf{B}] = \frac{q}{m}[E_0\hat{\mathbf{y}}\cos(ky - \omega t - \phi) + \mathbf{v}\times B_0\hat{\mathbf{z}}]. \tag{2.1.3}$$

If we normalize time to Ω^{-1}, length to k^{-1}, and velocity to Ω/k, then (2.1.3) becomes

$$\frac{d\mathbf{v}}{dt} = \alpha\hat{\mathbf{y}}\cos(y - \nu t - \phi) + \mathbf{v}\times\hat{\mathbf{z}}, \tag{2.1.4}$$

where

$$\nu = \omega/\Omega, \tag{2.1.5}$$

and

$$\alpha = \frac{qkE_0}{m\Omega^2} = \frac{E_0/B_0}{\Omega/k}. \tag{2.1.6}$$

Taking the x and y components of (2.1.4) we obtain

$$\ddot{x} = \dot{y}, \tag{2.1.7}$$

$$\ddot{y} = -\dot{x} + \alpha\cos(y - vt - \phi). \tag{2.1.8}$$

Integrating (2.1.7), and suitably choosing the orgin of y we find

$$\dot{x} = y, \tag{2.1.9}$$

and so (2.1.8) becomes

$$\ddot{y} + y = \alpha\cos(y - vt - \phi). \tag{2.1.10}$$

Equations (2.1.9) and (2.1.10) are the orbit equations for the ion.

The orbit equations obey an energy conservation law, which we will now derive. We make use of this law in the numerical integration of the equations described in the next chapter. We begin by making a Galilean transformation to the frame of the wave,

$$y' = y - vt. \tag{2.1.11}$$

Then (2.1.11) becomes

$$\ddot{y}' + y' = \alpha\cos(y' - \phi) - vt. \tag{2.1.12}$$

Multiplying through by $\dot{y}'$ and integrating we find

$$\tfrac{1}{2}\dot{y}'^2 + \tfrac{1}{2}y'^2 - \alpha\sin(y' - \phi) + v\int \dot{y}'\,t\,dt = \text{const.} \tag{2.1.13}$$

Going back to the original frame and integrating the last term in (2.1.13) by parts and using (2.1.9) we obtain

$$\tfrac{1}{2}(\dot{y} - v)^2 + \tfrac{1}{2}\dot{x}^2 - \alpha \sin(y - vt - \phi) - vx = \text{const} = \mathcal{E}. \tag{2.1.14}$$

The first two terms in (2.1.14) are the particle's kinetic energy in the wave frame. The third term is its potential energy in the wave trough and the fourth term its potential energy in the constant electric field obtained by transforming the magnetic field to the wave frame. Thus we identity $\mathcal{E}$ with the total energy of the particle in the wave frame.

Section 2.2. Linear Solution of Orbit Equations.

Many important properties of plasma waves may be found from the linear solution of the orbit equations (2.1.9) and (2.1.10). Most importantly we may find the energy transfer between infinitesimal amplitude waves and a distribution of ions. This result is also embodied in the ion susceptibility as derived by Harris (1961)

$$\chi = -\frac{\omega_p^2}{k^2} \sum_{m=-\infty}^{\infty} \int d^3v \, \frac{J_m^2(k_\perp v_\perp/\Omega)}{k_\parallel v_\parallel - \omega + m\Omega} \left[\frac{m\Omega}{v_\perp} \frac{\partial f_0}{\partial v_\perp} + k_\parallel \frac{\partial f_0}{\partial v_\parallel} \right] \tag{2.2.1}$$

From this we may write down the power gained by the ions, P, (Bers, 1975)

$$P = \tfrac{1}{2}\epsilon_0 \omega |E|^2 \, \mathfrak{Im}(\chi). \tag{2.2.2}$$

where we find $\mathfrak{Im}(\chi)$ by writing

$$\mathfrak{Im}[(k_\parallel v_\parallel - \omega + m\Omega)^{-1}] = \pi \, \delta(\omega - m\Omega - k_\parallel v_\parallel). \tag{2.2.3}$$

This tells us that only particles obeying the resonance condition

$$\omega - k_\parallel v_\parallel = m\Omega \tag{2.2.4}$$

can gain energy from the waves. With $m = 0$ the mechanism for energy gain is the same as in the

Landau problem (with zero magnetic field). For $m \neq 0$ we see that the Doppler-shifted frequency is an integer multiple of Ω. If the wave is propagating perpendicular to the magnetic field, it will experience heavy (in fact, infinite) damping only if $\omega = n\Omega$ (n, an integer). (However the real part of the susceptibility is singular in this case so such a wave cannot exist in a homogeneous plasma, unless it is driven. Also there are physical effects, not accounted for in this model, which can limit the damping. In long wavelength systems, e.g. cyclotron accelerators, relativistic effects cause a change in the cyclotron frequency. In our problem the wave has a short wavelength and this causes nonlinear effects to be important.) These results are given more physical foundation if we look at a single particle obeying the linearized orbit equations. Also we are lead to analyse these equations, for they give valuable insight into the nonlinear equations (2.1.9) and (2.1.10).

In order to linearize (2.1.9) and (2.1.10) we first solve them with $\alpha = 0$ ($E_0 = 0$). The solution to this problem is

$$x = x_0(t) = -r_0 \cos(t - t_0), \quad y = y_0(t) = r_0 \sin(t - t_0), \tag{2.2.5}$$

where r_0 and t_0 are constants. The linearized equations are then obtained by substituting $y = y_0(t)$ in the right hand side of (2.1.10) to give

$$\ddot{y} + y = \alpha \cos(r_0 \sin(t - t_0) - \nu t - \phi) \tag{2.2.6}$$

$$= \alpha \sum_{m=-\infty}^{\infty} J_m(r_0) \cos[(m - \nu)t - \phi - mt_0], \tag{2.2.7}$$

where we have made use of eq. 9.1.41 of Abramowitz and Stegun (1964). We can now straightforwardly solve for y and obtain

$$y = + r_0 \sin(t - t_0)$$

$$+ \alpha \Sigma_{m \neq \nu \pm 1} [1 - (m - \nu)^2]^{-1} J_m(r_0) \cos[(m - \nu)t - \phi - mt_0]$$

$$+ \alpha \Sigma_{m=\nu\pm 1} \tfrac{1}{2} t J_m(r_0) \sin[t \mp (\phi + m t_0)]. \tag{2.2.8}$$

The first term on the right hand side of (2.2.8) is $y_0(t)$, the unperturbed solution, and the remaining terms of the contributions due to α. If ν is not an integer then the last term is zero, and y is bounded for all time, leading to no time-averaged energy exchange between the ion and the wave. However, if $\nu = n$, an integer, the last term in (2.2.8) is unbounded as $t \to \infty$. In this case all the particles in the ion distribution function will be exchanging energy with the wave, leading to the δ function dependence of the power dissipated on frequency. It is clear in this case, that if α is finite that the linearized solution is valid only for a finite time. We will postpone an analysis of the limitations of linear theory until we have solved (2.2.6) by an alternative method.

The alternative approach to solving the linearized equations avoids Fourier transforming the driving term. Instead we use the method of variation of parameters to express the solutions in terms of integrals. These integrals are known if we integrate over one cyclotron period. Thus if we know the particle's position and velocity at the beginning of the kth cyclotron orbit, we can use this solution to compute its state at the beginning of the $(k + 1)^{th}$ orbit. This process can then be repeated. We will define the beginning of the kth cyclotron orbit as being when the particle satisfies

$$\dot{y} = -r_k, \quad y = 0, \quad x = r_k. \tag{2.2.9}$$

At this point the interaction between the particle and the wave is minimum, since the quantity $|\omega - \mathbf{k} \cdot \mathbf{v}|$ (in normalized terms $|\nu - \dot{y}|$) is maximum.

We begin by writing (2.2.6) as a set of coupled first order equations

$$\dot{\mathbf{X}} = \mathbf{A} \cdot \mathbf{X} + \mathbf{F}(t). \tag{2.2.10}$$

where

$$\mathbf{X} = \begin{bmatrix} v \\ y \\ x \end{bmatrix}, \quad \mathbf{A} = \begin{bmatrix} 0 & -1 & 0 \\ 1 & 0 & 0 \\ 0 & 1 & 0 \end{bmatrix}, \quad \mathbf{F}(t) = \begin{bmatrix} f(t) \\ 0 \\ 0 \end{bmatrix}, \tag{2.2.11}$$

and $f(t)$, the driving term, is the right hand side of (2.2.6). Note that $v = \dot{y}$. We take for the unperturbed orbit $[\mathbf{F}(t) = 0]$

$$\mathbf{X} = \mathbf{X}_0(t) = \begin{bmatrix} v_0(t) \\ y_0(t) \\ x_0(t) \end{bmatrix} = \begin{bmatrix} r_k \cos(t - t_k) \\ r_k \sin(t - t_k) \\ -r_k \cos(t - t_k) \end{bmatrix}, \tag{2.2.12}$$

so that the kth unperturbed orbit lasts from $t_k - \pi$ to $t_k + \pi$; t_k is the time at which the ion is at the "top" of its unperturbed orbit (see Fig. 2.2.1). Then $f(t)$ is given by

$$f(t) = \alpha \cos[r_k \sin(t - t_k) - \nu t - \phi]. \tag{2.2.13}$$

Transforming the time origin to t_k using

$$t' = t - t_k \tag{2.2.14}$$

we have

$$\mathbf{X}_0(t') = \begin{bmatrix} r_k \cos t' \\ r_k \sin t' \\ -r_k \cos t' \end{bmatrix}, \tag{2.2.15}$$

and

$$f(t') = \alpha \cos[y_o(t') - \nu t' - \gamma_k] = \alpha \cos(r_k \sin t' - \nu t' - \gamma_k), \tag{2.2.16}$$

where

$$\gamma_k = (\nu t_k + \phi)_{\text{mod } 2\pi}. \tag{2.2.17}$$

We wish to determine the position of the particle at time $t' = \pi$ in terms of its position at time $-\pi$. We can write this result formally as

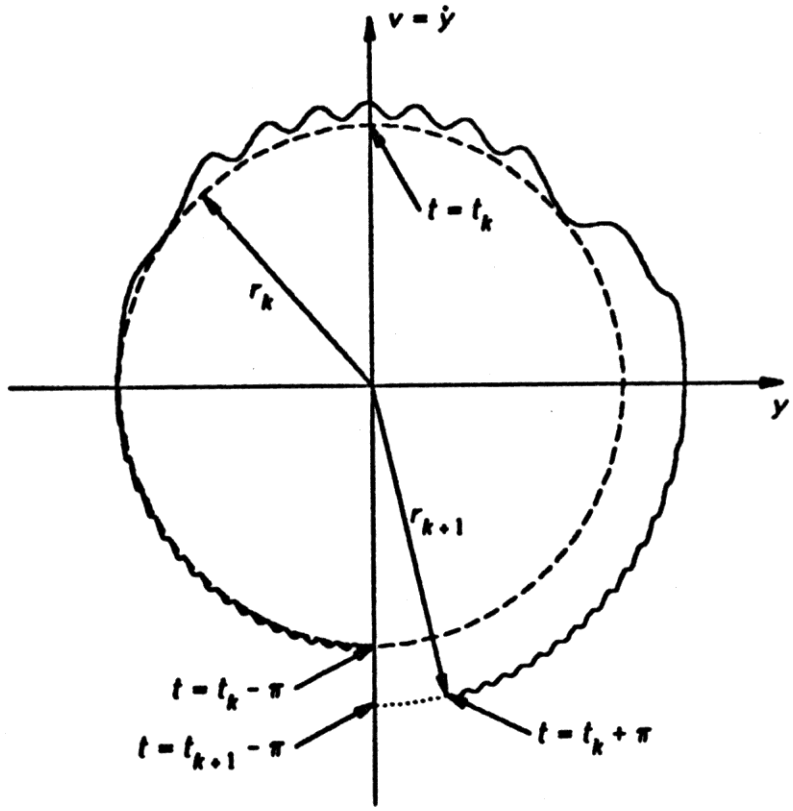

Figure 2.2.1. Integration along the kth unperturbed orbit. The dashed line is the unperturbed orbit and the solid line the result of the integration (schematically). The dotted line extends the kth orbit to the beginning of the $(k + 1)^{th}$ orbit.

$$\mathbf{X}(t'=\pi) = \mathbf{X}_0(\pi) + \mathbf{G}(\pi)\cdot\int_{-\pi}^{\pi}[\mathbf{G}(\tau)]^{-1}\cdot\mathbf{F}(\tau)\,d\tau, \tag{2.2.18}$$

where $\mathbf{X}(-\pi)$ is given by (2.2.15) and $\mathbf{G}$ is the fundamental matrix of independent solutions to the homogeneous equation $\dot{\mathbf{X}} = \mathbf{A}\cdot\mathbf{X}$. Thus we may take

$$\mathbf{G}(t') = \begin{bmatrix} \cos t' & -\sin t' & 0 \\ \sin t' & \cos t' & 0 \\ -\cos t' & \sin t' & 1 \end{bmatrix}. \tag{2.2.19}$$

Making use of eq. 9.1.22 of Abramowitz and Stegun (1964) the integrals in (2.2.18) may be evaluated to give

$$v(t'=\pi) = -r_k - 2\pi\alpha\cos\gamma_k\left[\frac{\nu}{r_k}J_\nu(r_k) - \frac{\sin(\nu\pi)}{\pi}\left[\tfrac{1}{2}Q(\nu-1) + \tfrac{1}{2}Q(\nu+1)\right]\right], \tag{2.2.20}$$

$$y(t'=\pi) = -2\pi\alpha\sin\gamma_k\left[J_\nu'(r_k) - \frac{\sin(\nu\pi)}{\pi}\left[\tfrac{1}{2}Q(\nu-1) - \tfrac{1}{2}Q(\nu+1)\right]\right], \tag{2.2.21}$$

$$x(t'=\pi) = r_k + 2\pi\alpha\cos\gamma_k\left[\frac{r_k+\nu}{r_k}J_\nu(r_k) - \frac{\sin(\nu\pi)}{\pi}\left[\tfrac{1}{2}Q(\nu-1) - Q(\nu) + \tfrac{1}{2}Q(\nu+1)\right]\right], \tag{2.2.22}$$

where

$$Q(\mu) = \int_0^\infty \exp(-r_k\sinh s - \mu s)\,ds. \tag{2.2.23}$$

If $\nu \gg 1$ we can asymptotically expand the terms multiplying $\sin(\nu\pi)/\pi$ (in small []'s) in (2.2.20), (2.2.21), (2.2.22) and so show that these terms are equal to

$$(r_k+\nu)^{-1},\ (r_k+\nu)^{-2},\ (r_k+\nu)^{-3}, \tag{2.2.24}$$

respectively. Since these terms are multiplied by $\sin(\nu\pi)$, They do not contribute when ν is an integer. Also the quantity $(r_k + \nu)$ is the difference in the velocity of the particle and the phase velocity of the wave at the beginning or end of a cyclotron orbit. Thus we interpret these terms in the expressions for $\mathbf{X}(t'=\pi)$ as being the oscillations of particle under the influence of a wave travelling $(r_k + \nu)$ faster than it, which arise because the particle does not experience an integral

number of wave periods in a time 2π. Since we are interested obtaining a estimate for the unperturbed $(k+1)^{\text{th}}$, we do not wish to include these contributions when computing r_{k+1} and t_{k+1}. Thus for our purposes we may write (going back to the original time)

$$v(t_k+\pi)+r_k=-2\pi\alpha\cos\gamma_k\frac{\nu}{r_k}J_\nu(r_k), \tag{2.2.25}$$

$$y(t_k+\pi)=-2\pi\alpha\sin\gamma_k J_\nu'(r_k), \tag{2.2.26}$$

$$x(t_k+\pi)-r_k=+2\pi\alpha\cos\gamma_k\frac{r_k+\nu}{r_k}J_\nu(r_k). \tag{2.2.27}$$

We may define r_{k+1} and t_{k+1} by extending the kth orbit to $y=0$ assuming $\alpha=0$ (Fig. 2.2.1). Then we find

$$t_{k+1}=t_k+2\pi+\tan^{-1}\left[\frac{y(t_k+\pi)}{-v(t_k+\pi)}\right]. \tag{2.2.28}$$

$$r_{k+1}=[v(t_k+\pi)^2+y(t_k+\pi)^2]^{1/2}, \tag{2.2.29}$$

Expanding (2.2.28) and (2.2.27) in the limit of α small (the only limit in which we are justified in integrating along unperturbed orbits) we obtain

$$t_{k+1}=t_k+2\pi-2\pi\alpha\frac{1}{r_k}\sin\gamma_k J_\nu'(r_k). \tag{2.2.30}$$

$$r_{k+1}=r_k+2\pi\alpha\frac{\nu}{r_k}\cos\gamma_k J_\nu(r_k), \tag{2.2.31}$$

Because we are primarily interested in the evolution of the wave-particle system, we find it useful to use only quantities that define the *state* of the system, without regard to the time at which the system is at that state. Thus instead of the time at which the particle is in the middle of its kth orbit, t_k, we will use the wave phase, γ_k, at this point as defined in (2.2.17). From (2.2.30)

$$\gamma_{k+1}=[\gamma_k+2\pi\nu-2\pi\alpha\frac{\nu}{r_k}\sin\gamma_k J_\nu'(r_k)]_{\text{mod } 2\pi}. \tag{2.2.32}$$

Equations (2.2.31) and (2.2.32) constitute a set of difference equations, which may be easily iterated to give us an understanding of some of the basic properties of the orbit equations. Before turning to the solution, we investigate an impulse model that enables us to derive (2.2.31) and (2.2.32) by considering only the interaction of the wave and the particle when they are in resonance.

Section 2.3. Interpretation of Linear Solutions.

It is often supposed that $\omega \gg \Omega$ ($\nu \gg 1$) is a sufficient condition for regarding the ions as being unmagnetized. While this is not so, it is true that phenomena that occur over a time short compared with the cyclotron period can be correctly treated by assuming that the magnetic field is zero. We will use this fact to re-derive (2.2.31) and (2.2.32) from a more physical standpoint. We do this by approximating the force seen by the particle as a delta function whenever the particle passes through (or close to) $\dot{y} = \nu$ ($\omega = \mathbf{k}\cdot\mathbf{v}$), the zero magnetic field wave-particle resonance.

We consider two cases: In Case I, $r_k < \nu$ or $r_k \approx \nu$ (Fig. 2.3.1). The largest kick the particle will receive is at $t = t_k$, when the particle is closest to be in resonance with the wave. As in the previous section we shift the time origin to t_k, so that the unperturbed orbit is given by (2.2.15) and the force due to the electric field by (2.2.16). Expanding the $y_o(t')$ appearing in (2.2.16) in a Taylor series about $t' = 0$ we obtain

$$\ddot{y} = -r_k \sin t' + \alpha \cos(r_k t' - \tfrac{1}{6} r_k t'^3 - \nu t' - \gamma_k). \tag{2.3.1}$$

Integrating once we find

$$\dot{y} = r_k \cos t' + \int_{-\pi}^{t'} \alpha \cos[\tfrac{1}{6} r_k t'^3 + (\nu - r_k)t' + \gamma_k]\, dt'. \tag{2.3.2}$$

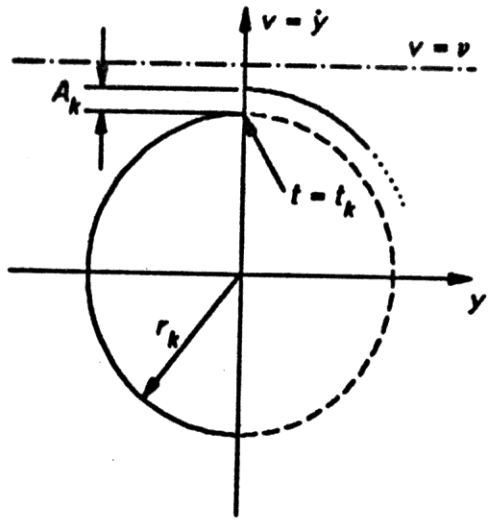

Figure 2.3.1. Illustration of the kick, A_k, received by the ion when $r < \nu$ (Case I).

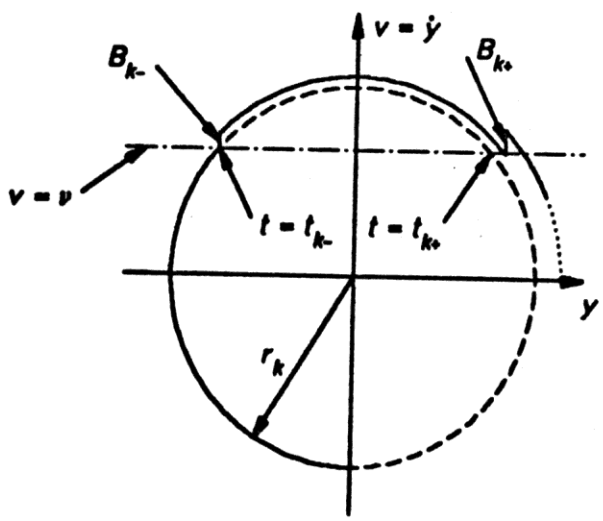

Figure 2.3.2. Illustration of the kicks, $B_{k\pm}$, received by the ion when $r > \nu$ (Case II).

The argument of the cosine is most slowly varying (for $\nu - r_k \geq 0$) at $t' = 0$. Thus the largest contribution to the integral comes close to $t' = 0$ and we may approximate the integrand in (2.3.2) by $A_k\,\delta(t')$ where

$$A_k = \int_{-\infty}^{\infty} \alpha \cos[\tfrac{1}{6} r_k t'^3 + (\nu - r_k)t' + \gamma_k]\,dt'$$

$$= 2\pi\alpha \cos\gamma_k\,(r_k/2)^{-1/3}\,\mathrm{Ai}[(r_k/2)^{-1/3}(\nu - r_k)]. \tag{2.3.3}$$

where Ai is the Airy function and we have used eq. 10.4.32 of Abramowitz and Stegun (1964). Thus before the collision with the field ($t' < 0$) the orbit is given by (2.2.15), and after the collision ($t' > 0$) by

$$x = (r_k + A_k)\cos t', \quad y = (r_k + A_k)\sin t'. \tag{2.3.4}$$

We use (2.3.4) to compute the $(k+1)^{\text{th}}$ orbit variables, (2.2.17),

$$r_{k+1} = r_k + A_k, \tag{2.3.5}$$

$$\gamma_{k+1} = (\gamma_k + 2\pi\nu)_{\text{mod } 2\pi}. \tag{2.3.6}$$

For Case II, we take $r_k > \nu$ (Fig. 2.3.2) so that the particle is in resonance with the wave twice every cyclotron orbit. Again chosing the time origin as in (2.2.14), the particle collides with the wave at

$$t' = t'_{k\pm} = \pm\cos^{-1}(\nu/r_k). \tag{2.3.7}$$

Taylor expanding the unperturbed orbit $y_0(t')$ about $t'_{k\pm}$ and substituting into the expression (2.2.16) for the force due to the electric field we see that

$$f(t') \approx \alpha\cos\{\pm(r_k^2 - \nu^2)^{1/2}[1 - \tfrac{1}{2}(t' - t'_{k\pm})^2] - \nu t'_{k\pm} - \gamma_k\}, \tag{2.3.8}$$

near $t' = t'_{k\pm}$. The stationary phase points in (2.3.8) are at $t' = t'_{k\pm}$; so as in Case I we approximate this force by $B_{k\pm}\delta(t' - t'_{k\pm})$, where

$$B_{k\pm} = \int_{-\infty}^{\infty} \alpha \cos[\pm(r_k^2 - \nu^2)^{1/2}(1 - \tfrac{1}{2}t'^2) - \nu t'_{k\pm} - \gamma_k]$$

$$= \sqrt{2\pi}\,\alpha(r_k^2 - \nu^2)^{-1/4}\cos[(r_k^2 - \nu^2)^{1/2} - \tfrac{1}{4}\pi \mp (\nu t'_{k\pm} + \gamma_k)]. \tag{2.3.9}$$

The differential equation describing the ion's orbit becomes

$$\ddot{y} + y = B_{k-}\delta(t' - t'_{k+}) + B_{k+}\delta(t' - t'_{k+}), \tag{2.3.10}$$

with initial conditions that for $t' < t'_{k-}$

$$\dot{y}(t') = r_k \cos t', \quad y(t') = r_k \sin t'. \tag{2.3.11}$$

Equation (2.3.10) is readily integrated to give for $t > t_{k+}$

$$y = r_{k+1}\sin(t - t_{k+1}), \tag{2.3.12}$$

where we use the subscript $k + 1$, because the electric field has no further effect on the ion until the $(k + 1)^{\text{th}}$ orbit, and where for small α

$$t_{k+1} = t_k + 2\pi + \frac{(r_k^2 - \nu^2)^{1/2}}{r_k^2}(B_{k+} - B_{k-}) \tag{2.3.13}$$

and the new orbit is defined by

$$r_{k+1} = r_k + \frac{\nu}{r_k}(B_{k+} + B_{k-}), \tag{2.3.14}$$

$$\gamma_{k+1} = [\gamma_k + 2\pi\nu + \frac{(r_k^2 - \nu^2)^{1/2}}{r_k^2}\nu(B_{k+} - B_{k-})]_{\text{mod } 2\pi}, \tag{2.3.15}$$

where from (2.3.9)

$$B_{k+} \pm B_{k-} = 2\sqrt{2\pi}\frac{\alpha}{(r_k^2 - \nu^2)^{1/4}} \begin{matrix}\cos\\ \sin\end{matrix}(\gamma_k) \begin{matrix}\cos\\ \sin\end{matrix}\left[(r_k^2 - \nu^2)^{1/2} - \nu\cos^{-1}\left(\frac{\nu}{r_k}\right) - \tfrac{1}{4}\pi\right]. \qquad (2.3.16)$$

It is readily confirmed that (2.3.14) in the limit $r_k - \nu \ll \nu$ agrees with (2.3.5) in the limit of $1 \ll r_k - \nu \ll \nu$ [the asymptotic expansion of Ai (eq. 10.4.60, Abramowitz and Stegun, 1964) is needed]. Furthermore by expanding in Bessel function in (2.2.31) in the limits $r_k \sim \nu$ and $r_k \gg \nu$ (equations 9.3.23 and 9.2.1, Abramowitz and Stegun, 1964), we can recover (2.3.5) and (2.3.14). From (2.2.32) we can recover (2.3.15) but not (2.3.6); in order for Case I to give (2.2.32) we would have to approximate the force by an impulse at $t' \neq 0$.

We can now appreciate the dependence of (2.2.31) and (2.2.32) on r_k (Fig. 2.3.3). For $r_k > \nu$ there is an oscillatory dependence through the Bessel functions. This is due to the fact that the particle passes *twice* through the resonance region $v = \nu$, sampling different phases of the wave. By the beating of the kicks the particle receives we can explain the oscillatory nature of (2.2.31) and (2.2.32). Aside from the oscillatory behaviour there is an overall $r_k^{-3/2}$ dependence for $r_k > \nu$. A factor, $r_k^{-1/2}$, enters through the Bessel functions, and describes the reduction in the kicks, $B_{k\pm}$, that the particle experiences as r_k increases, because it spends less time close to resonance. An additional factor, r_k^{-1}, is geometrical in origin; as r_k is increased, it enters (2.2.31) because the kicks are closer to being perpendicular to the particle's velocity and it enters (2.2.32) because they change the direction of the velocity less. For $r_k \approx \nu$ the particle spends the maximum time close to resonance corresponding to the maxima of the Bessel functions. For $r_k < \nu$ the particle never passes through resonance, and the exchange energy between the particle and the wave is very small, as witnessed by the exponential decay of the Bessel functions when their argument in less than their order. We will concentrate therefore on the regimes $r_k \approx \nu$ and $r_k > \nu$.

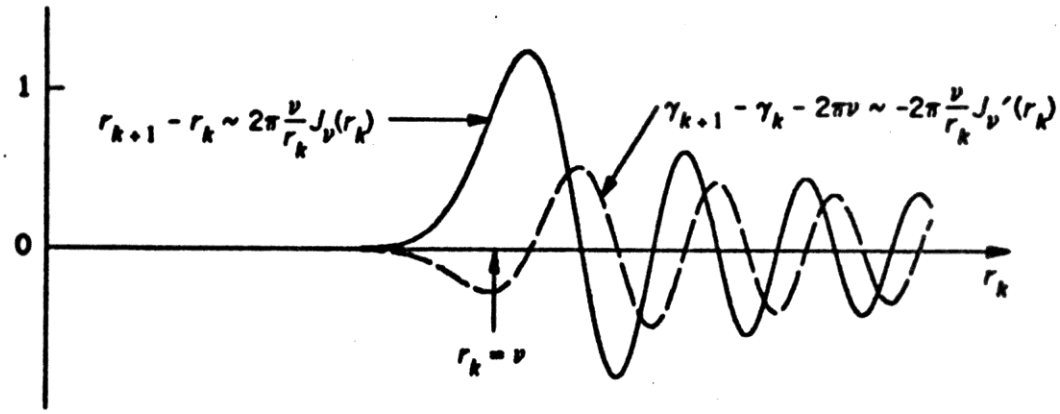

Figure 2.3.3. The field dependent contributions to the change in the particles velocity and phase [see (2.2.31) and (2.2.32)]. The phase factors have been omitted.

Section 2.4. Iteration of Linear Solutions.

We pass now on to the solution of the difference equations

$$r_{k+1} = r_k + 2\pi\alpha\frac{\nu}{r_k}\cos\gamma_k J_\nu(r_k), \tag{2.2.31}$$

$$\gamma_{k+1} = [\gamma_k + 2\pi\nu - 2\pi\alpha\frac{\nu}{r_k}\sin\gamma_k J_\nu'(r_k)]_{\text{mod } 2\pi}. \tag{2.2.32}$$

Firstly we will see how the "true" linear solution (2.2.8) may be recovered. To do this we must integrate along the original unperturbed orbits for all time, instead correcting the unperturbed orbits each cyclotron orbit as is implied by (2.2.31) and (2.2.32). The unperturbed orbits are found by solving the difference equations with $\alpha = 0$, in which case

$$r_{k,0} = r_0, \quad \gamma_{k,0} = (\gamma_0 + 2\pi k\delta)_{\text{mod } 2\pi}, \tag{2.4.1}$$

where

$$\nu = n + \delta \ (n, \text{ an integer}, |\delta| \le \tfrac{1}{2}), \tag{2.4.2}$$

and where the second subscript 0 denotes a true unperturbed orbit. These are plugged into the term proportional to α in (2.2.31) to give

$$r_{k+1} - r_k = 2\pi\alpha\cos\gamma_{k,0}\frac{\nu}{r_0}J_\nu(r_0); \tag{2.4.3}$$

thus

$$r_k - r_0 = \sum_{m=0}^{k-1} r_{m+1} - r_m = 2\pi\alpha\frac{\nu}{r_0}J_\nu(r_0)\sum_{m=0}^{k-1}\cos\gamma_{m,0}. \tag{2.4.4}$$

We can perform the sum in (2.4.4) obtaining

$$\sum_{m=0}^{k-1}\cos\gamma_{k,0} = \begin{cases} k\cos\gamma_0 & \text{for } \delta = 0 \\ \mathfrak{Re}\,[e^{i\gamma_0}(1 - e^{i2\pi\delta k})/(1 - e^{i2\pi\delta})] & \text{for } \delta \ne 0 \end{cases}. \tag{2.4.5}$$

This illustrates the origin of the secular growth in the velocity of the ion for $\delta = 0$, that we observed in (2.2.8). It arises because during each cyclotron orbit the particle sees the wave in exactly the same phase (γ_k = constant). Thus all the kicks the particle receives are in phase and equal, leading to a linear growth (or reduction) of the particle's orbit. For $\delta \neq 0$, $r_k - r_0$ oscillates about some mean value with the amplitude of oscillation being

$$\left|\alpha \frac{\nu}{r_0} J_\nu(r_0) \frac{\pi}{\sin(\pi\delta)}\right|. \tag{2.4.6}$$

This results, of course, in no time-averaged energy trasnfer.

These results we useful because they enable us to understand the estimates given by Sigmar and Callen (1971) for the breakdown of linear theory. Linear theory consists of integrating the particle's motion along its unperturbed orbit. It is inaccurate, therefore, if the force computed along the unperturbed orbit differs substantially from that along the true orbit. Since we do not know the true orbit of the particle we will instead compare the true linear equation (2.4.3) with the interated linear equation (2.2.31). Two things can happen to make these two equations give different results. Firstly $J_\nu(r_k)$ can become significantly different from $J_\nu(r_0)$ (e.g. it can have the opposite sign). The amount r_k has to change by in order to make a difference is roughly $J_\nu(r_0)/J_\nu'(r_0)$; thus linear theory breaks down if the magnitude of the oscillations in r_k predicted by linear theory (2.4.6) exceeds this amount, i.e.

$$\alpha > \left|\frac{r}{\nu J_\nu'(r)} \frac{\sin(\pi\delta)}{\pi}\right|. \tag{2.4.7}$$

The result quoted by Sigmar and Callen (1971) differs from (2.4.7) in that J_ν appears in place of J_ν'. This is because they estimated the scale length for J_ν to be unity rather than our more accurate expression, J_ν/J_ν'.

The second possibility is that γ_k can differ sufficiently from $\gamma_{k,0}$ in which case the oscillatory nature of the sum in (2.4.4) is destroyed. This is possible if the electric field is

sufficient to make $\gamma_{k+1} = \gamma_k$, for then successive kicks given the particle could be in phase, leading to a similar secular behaviour as is seen when $\delta = 0$. From (2.2.32) the condition for this to happen is (taking the $\sin\gamma_k$ term to have a magnitude of 1)

$$\alpha > \left|\frac{r}{\nu J_\nu'(r)}\delta\right|, \tag{2.4.8}$$

the same as (2.4.7) in the limit $\delta \ll 1$, and approximately the same as (2.4.7) for all δ ($\leq \frac{1}{2}$).

The major defect of the linear theory is that it uses information (embodied in the unperturbed orbit) which becomes progressively more and more out of date, as the particle is driven away from its unperturbed orbit by the field. This defect is corrected by the difference equations (2.2.31) and (2.2.32). Here we only continue the integration along an unperturbed orbit for one cyclotron period, before computing a new "unperturbed" orbit. Figures 2.4.1-4 give the results of numerically solving the difference equations for $\nu = 30.23$ and various α. The initial conditions r_0, γ_0 are the same in all these figures. (Note that $r_0 > \nu$, so that we are in the region where the Bessel functions oscillate.) For $\alpha = 0$, the orbit lies on the line $r_k = r_0$. The phase, γ_k, increases by $2\pi\delta$ each orbit. For low α (Fig. 2.4.1), the dominant effect is still the increase of γ_k by $2\pi\delta$; however now the velocity of the particle keeps changing until its velocity is such that $J_\nu(r = j_{\nu,m}) = 0$ (at which point $r_{k+1} = r_k$). ($j_{\nu,m}$ is the mth zero of J_ν.) These velocities, $j_{\nu,m}$, constitute the *stable* orbits for the difference equations, since if the velocity is perturbed slightly from one of these values it will drop back to it. In fact r_{k+1} will only be closer to $j_{\nu,m}$ than r_k if $\cos\gamma_k J_\nu'(j_{\nu,m}) < 0$, which is only true for half of the possible values of γ_k ($\frac{1}{2}\pi < \gamma_k < \frac{3}{2}\pi$ in Fig. 2.4.1). However since γ_k is continually changing the particle never samples the unstable regions of γ_k long enough for the orbit to be unstable. These orbits remain stable until the field given in (2.4.8). Figure 2.4.2 shows the picture at $\alpha = 3.2$ [the right hand side of (2.4.8) equals 3.07, for the revelent zero of the Bessel function]. What has happened here is that the difference equations have developed two *fixed points* ($r_{k+1} = r_k$, $\gamma_{k+1} = \gamma_k$), shown in the figure. [Recall that (2.4.8) was derived by requiring that $\gamma_{k+1} = \gamma_k$.] In principle a particle starting at one of these

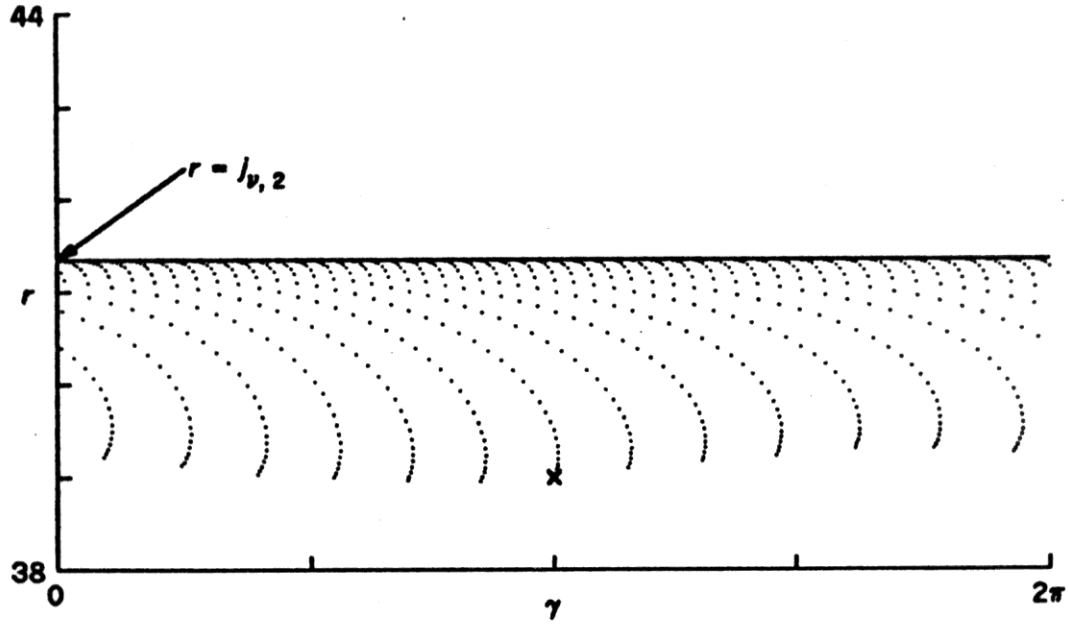

Figure 2.4.1. Iterations of the difference equations (2.2.31) and (2.2.32) for a particle initially at $r = r_0 = 39$ and $\gamma = \gamma_0 = \pi$ [marked by a cross (x)]. In this plot $\nu = 30.23$, $\alpha = 0.3$, and the particle is followed for 1500 orbits.

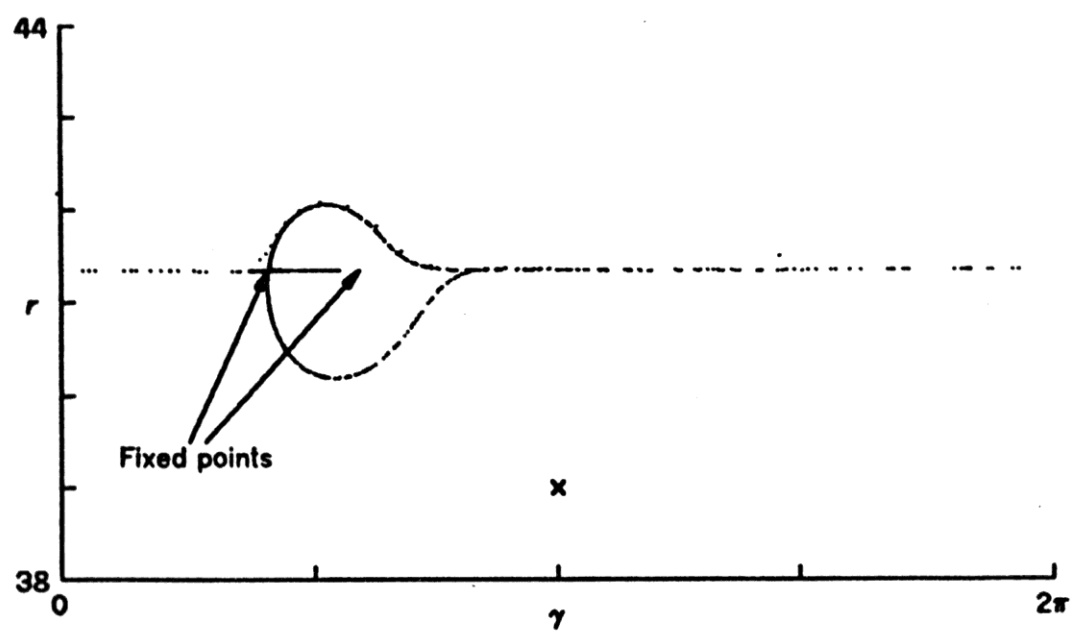

Figure 2.4.2. Same as Fig. 2.4.1, but $\alpha = 3.2$.

fixed points remains there forever. However one of these fixed points (the left one in this case) is always in the range of γ_k, which is unstable to perturbations in r_k, and now the particle remains long enough in the unstable range for the instability to take effect and for r_k to drift away from $j_{\nu,m}$ as is evident in the figure. (The other fixed point is also unstable, but to perturbations in γ_k rather than r_k.) The particle eventually is carried into the stable range of γ_k, so that it recovers from the instability and the orbit forms a "loop" which falls back to $j_{\nu,m}$. Particles with different initial positions form loops either at the same place as shown in the figure or at some other $j_{\nu,m}$, and the loop will enclose $\gamma = \frac{1}{2}\pi$ or $\frac{3}{2}\pi$, depending on whether $J_\nu'(j_{\nu,m})$ is positive or negative. Figure 2.4.3 gives the picture at a slightly larger field. The loop has grown substantially. At $\alpha = 4.5$ (Fig. 2.4.4) the loop has grown to such an extent that it has "collided" with the neighbouring loops at $j_{\nu,1}$ and $j_{\nu,3}$. Whereas at lower fields the particle couldn't leave its loop, it can now be temporarily captured by other loops allowing it to hop between loops and to move much larger distances in velocity space. In this case, it eventually wanders down to $r < \nu$, where the Bessel functions are exponentially small, where it gets "stuck."

Obviously the field at which the loops collide is significant in that it gives the field at which there can be significant energy exchanged between the particle and the wave. It is of interest then to determine how this field varies with the various parameters in the problem. As long as we keep to $r > \nu$ the Bessel functions in (2.2.31) and (2.2.32) are oscillatory with a slowly varying amplitude. In order to proceed further we need an approximation to the Bessel functions valid in this region. Surprisingly enough, we have already derived such an approximation in Sec. 2.3. There we derived approximate formulas for the change in r_k and γ_k when the exact formulas were in terms of Bessel functions. Comparing (2.3.14), (2.3.15), and (2.3.16) with (2.2.31) and (2.2.32) we see that

$$J_\nu(r) \approx \sqrt{2/\pi}\,(r^2 - \nu^2)^{-1/4}\cos[(r^2 - \nu^2)^{1/2} - \nu\cos^{-1}(\nu/r) - \tfrac{1}{4}\pi]. \tag{2.4.9}$$

$$J_\nu'(r) \approx \sqrt{2/\pi}\,[(r^2 - \nu^2)^{1/4}/r]\sin[(r^2 - \nu^2)^{1/2} - \nu\cos^{-1}(\nu/r) - \tfrac{1}{4}\pi]. \tag{2.4.10}$$

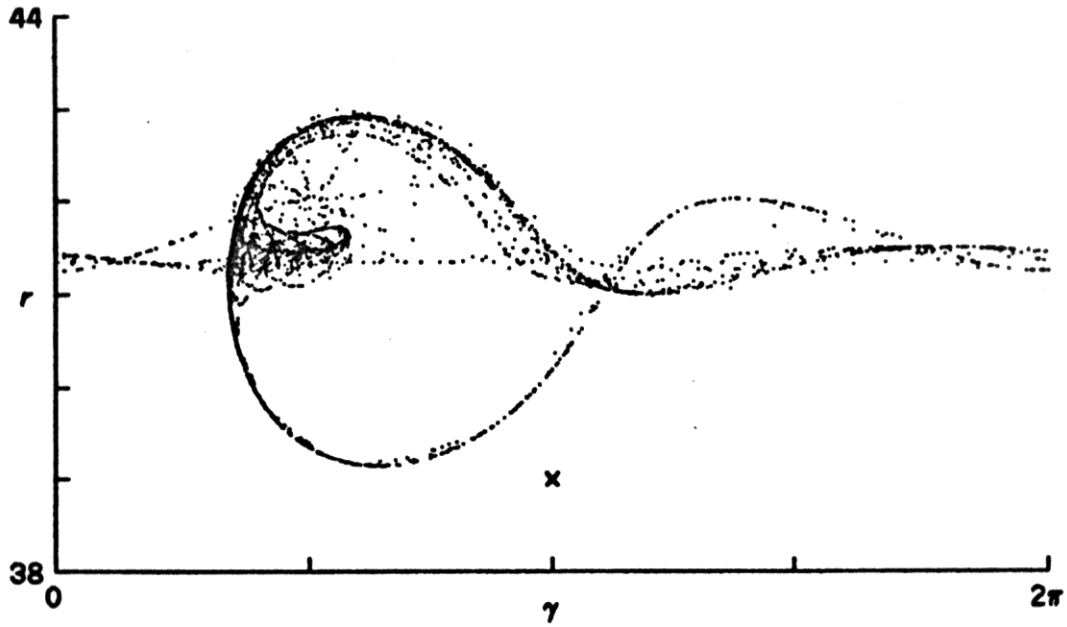

Figure 2.4.3. Same as Fig. 2.4.1, but $\alpha = 3.5$ and the particle is followed for 10 000 orbits.

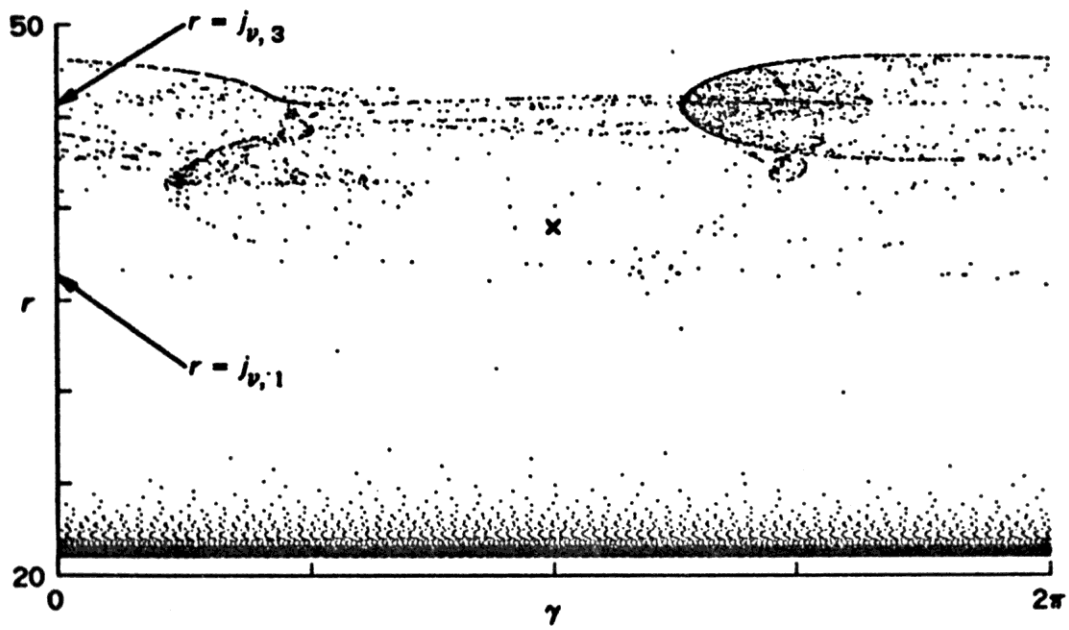

Figure 2.4.4. Same as Fig. 2.4.3, but $\alpha = 4.5$.

Now the size of the loops before they overlap is of the order of or less than the period of oscillation of the Bessel function. Over this scale length the slow variation of the amplitude of the Bessel function is not felt. Thus if we are interested in the field at which the loops overlap, we may neglect the r variation in all but the trigonometric terms above. Thus we define

$$r' = (r^2 - \nu^2)^{1/2} - \nu\cos^{-1}(\nu/r) - \tfrac{1}{4}\pi, \tag{2.4.11}$$

and observe that

$$r_{k+1} - r_k \approx (r'_{k+1} - r'_k)/(\partial r'/\partial r), \tag{2.4.12}$$

as long as $r_{k+1} - r_k \ll r_k$, which is true before the loops overlap. Thus we can rewrite (2.2.31) and (2.2.32) as

$$r'_{k+1} = r'_k + 2\pi A(r, \nu)\cos\gamma_k \cos r'_k, \tag{2.4.13}$$

$$\gamma_{k+1} = [\gamma_k + 2\pi\delta - 2\pi A(r, \nu)\sin\gamma_k \sin r'_k]_{\text{mod } 2\pi}. \tag{2.4.14}$$

where $A(r, \nu)$ is a slowly varying function giving by

$$A(r, \nu) = \alpha\nu|J_\nu'(r)|/r = \alpha\sqrt{2/\pi}\,\nu(r^2 - \nu^2)^{1/4}/r^2, \tag{2.4.15}$$

which we regard as a constant while iterating (2.4.13) and (2.4.14). [By $|J_\nu'(r)|$ we mean the amplitude factor in (2.4.10).] Thus the problem now just depends on two parameters, δ, which measures how close we are to a cyclotron harmonic, and A, which is proportional to α. By numerically iterating these difference equations we can determine and plot (Fig. 2.4.5) the value of A, $A = Q(\delta)$, at which the loops overlap. With these equations, once the loops overlap the ion's motion is unbounded in r'. We have plotted only the interval of δ from 0 to $\frac{1}{2}$; the interval from 0 to $-\frac{1}{2}$ can be mapped into this interval by shifting γ by π; therfore Q is an even function of δ. The region where $Q(\delta)$ is multi-valued appears to be a real feature of (2.4.13) and (2.4.14),

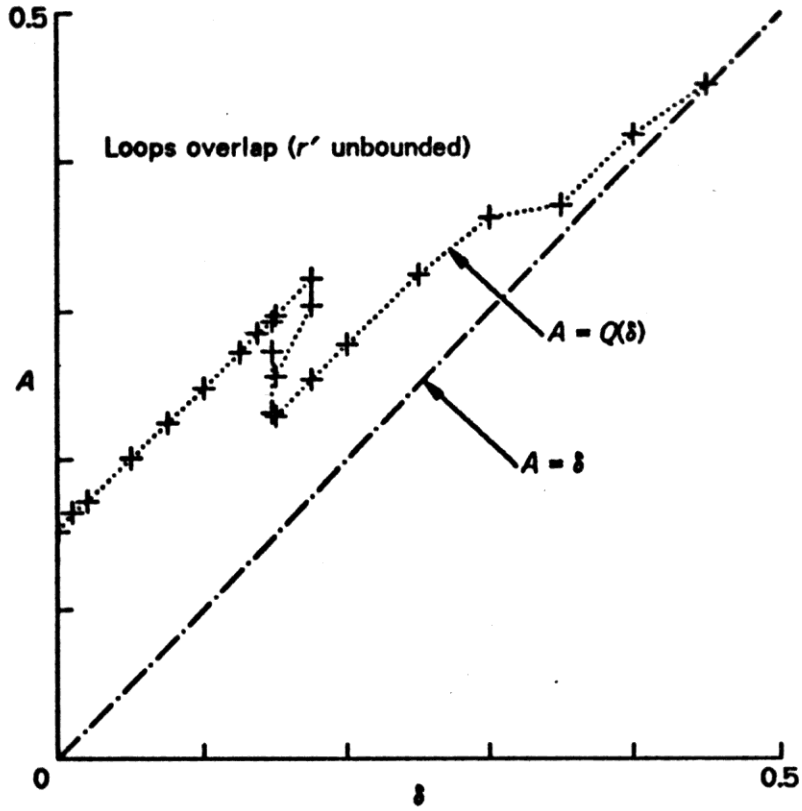

Figure 2.4.5. Threshold for overlap of loops as given by iterating (2.4.13) and (2.4.14), shown with plusses (+).

although we have no explanation for it. Apart from this mysterious multi-valued part Q is an increasing function of $|\delta|$. Thus the overlap condition is $A > Q(\delta)$ or substituting (2.4.15)

$$\alpha > \left|\frac{Q(\delta)r}{\nu J_\nu{}'(r)}\right| = \frac{\sqrt{\pi/2}\,Q(\delta)r^2}{\nu(r^2-\nu^2)^{1/4}}, \tag{2.4.16}$$

for $r > \nu$. The dashed line, $A = \delta$, is the same as the Sigmar and Callen (1971) result, (2.4.9), the field at which the loops first form. Note that, for small δ, $Q(\delta)$ is constant to lowest order in contrast with (2.4.9) which varies as δ.

The equations (2.2.31) and (2.2.32) predict heating of the ions, if the field exceeds that plotted in Fig. 2.4.5. There are features of these equations which are not exhibited by the orbit equation, (2.1.10). The most problematical is that (2.2.31) and (2.2.32) are not time-reversible; e.g. $r_{k+1} - r_k$ is given in terms of r_k, but not r_{k+1}. For instance the fact that for low α all particles drop onto $r = j_{\nu,m}$ (Fig. 2.4.1) and that at higher α they can become stuck at $r < \nu$ (Fig. 2.4.4) are consequences of this irreversibility. This is in contrast to the orbit equations (2.1.9) and (2.1.10), which are reversible. This time reversibility of the single particle equations does not exclude the irreversible phenomenon of heating which is a statistical effect requiring many particles. However we are hestitant to use the results of solving the difference equations, (2.2.31) and (2.2.32), to predict heating for a particle obeying the orbit equation. For this reason, we are lead to attempt to duplicate the results of this section by numerically solving the orbit equations.

Chapter 3. NUMERICAL SOLUTION OF ORBIT EQUATIONS.

Section 3.1. Observation of Trapping.

In this chapter we present the results of numerically integrating the equations of motion, (2.1.9) and (2.1.10). (The details of the numerical integration are given in Appendix A.) These results played an important role in developing our understanding of the motion of the ion. The effects of trapping and stochasticity were first noticed by this means, and the subsequent analysis was to a large extent guided by the numerical results.

We begin by presenting the phenomenon of trapping. To do this we show plots of single cyclotron orbits. Figures 3.1.1 and 3.1.2 show the velocity and configuration space plots of the orbits for $\alpha = 20$, $\phi = 0$, $\nu = 30.23$, and initial velocities, $r_0 = 24$ and 25. We note that a small increase in the initial speed of the ion, results in a dramatic increase in the amount of energy gained by the ion. We explain this by recognizing that for short times (less than a cyclotron period) the ion does not know that it is in a magnetic field. Thus we interpret the energy gained in Fig. 3.1.2 as being the result of the particle's being *trapped*. In the absence of a magnetic field the condition for a particle to be trapped by a wave propagating in the y direction is

$$|\dot{y} - \omega/k| < v_{tr}, \tag{3.1.1}$$

where

$$v_{tr} = \sqrt{qE_0/mk}\,. \tag{3.1.2}$$

In normalized terms (see Sec. 2.1), (3.1.1) reads

$$|\dot{y} - \nu| < \sqrt{\alpha}\,. \tag{3.1.3}$$

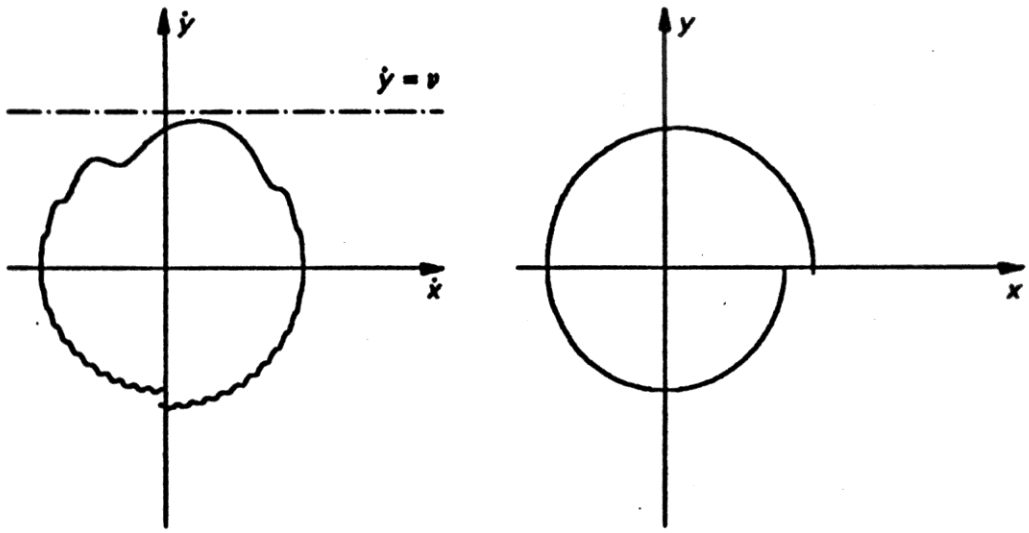

Figure 3.1.1. Ion orbits obtained by numerically integrating the orbit equations from $t = 0$, where $\dot{x} = 0$ and $\dot{y} < 0$, to 2π. The parameters in this plot are: $\nu = 30.23$, $\alpha = 20$, $\phi = 0$, *and* $r_0 = 24$.

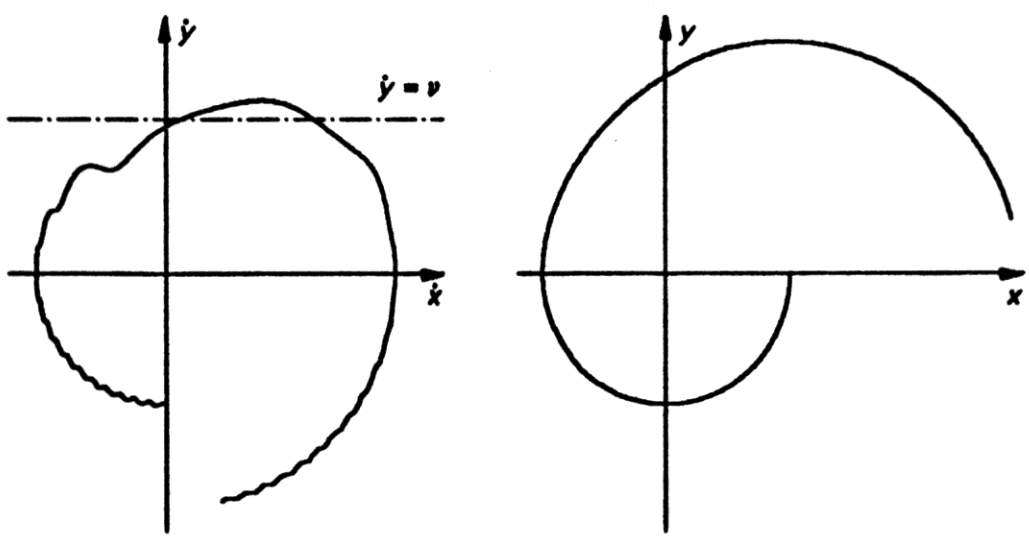

Figure 3.1.2. Same as Fig. 3.1.1, except that $r_0 = 25$.

When considering an ion in a magnetic field, the trapping condition need only be satisfied at some point along the orbit. Thus (3.1.3) becomes

$$r > \nu - \sqrt{\alpha} \equiv r_{tr}, \tag{3.1.4}$$

where r is the initial perpendicular velocity of the particle. With the parameters of Figs. 3.1.1 and 3.1.2 this predicts a value of 25.8 for r_{tr}, which is close to observed threshold.

Equation (3.1.4) is the condition under which a the particle exchanges some energy with the wave. We have yet to determine how much it gains. By integrating the orbit equations for constant ν and α, but different values of r_0 and ϕ (the electric field phase), we can generate a plot of $\langle \Delta\mathcal{E} \rangle$, the phase average energy gain per particle over one cyclotron orbit, against r_0. Such a plot is shown in Fig. 3.1.3, for ν and α the same as Fig. 3.1.1. We notice a sharp threshold to the energy gain close to r_{tr}. The curve peaks close to the threshold and drops off at higher velocities. Since the maximum occurs close to the threshold it suggests that the maximum is given by

$$\langle \Delta\mathcal{E} \rangle_{max} = \tfrac{1}{2}[(\nu + \sqrt{\alpha})^2 - (\nu - \sqrt{\alpha})^2] = 2\nu\sqrt{\alpha}, \tag{3.1.5}$$

or in unnormalized terms

$$\langle \Delta\mathcal{E} \rangle_{max} = 2m(\omega/k)v_{tr}. \tag{3.1.6}$$

This just says that a particle that is just trapped will bounce once in the potential well of the field and come out with a velocity $(\omega/k + v_{tr})$. We see from Fig. 3.1.3 that this is an accurate estimate.

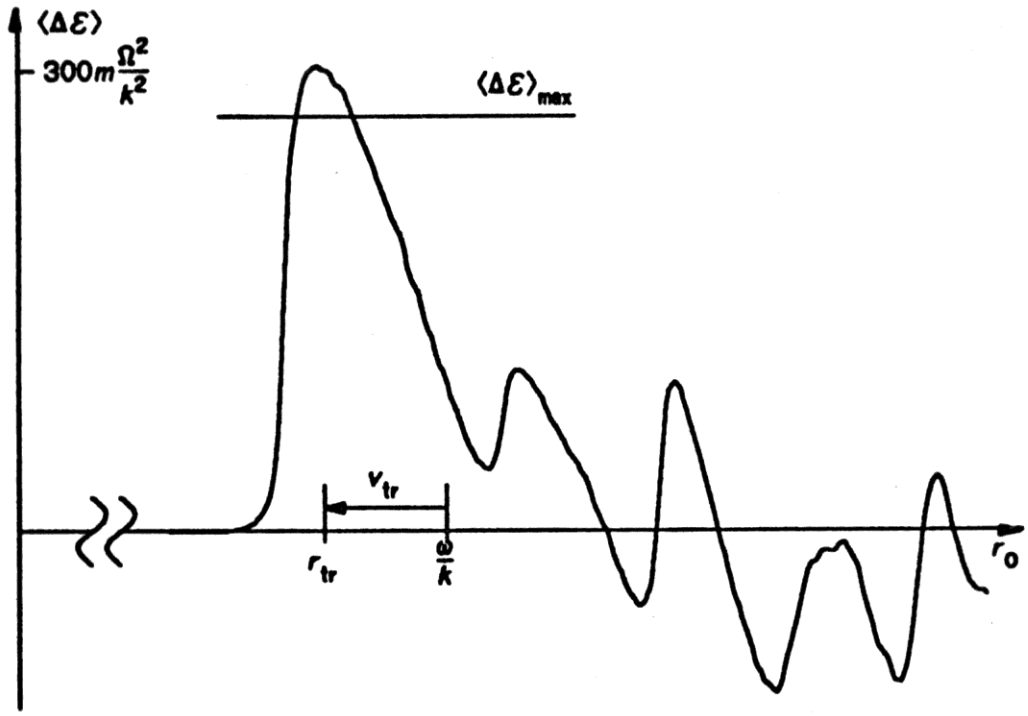

Figure 3.1.3. Plot of the phase averaged energy gain per ion over one cylcotron orbit, $\langle\Delta\mathcal{E}\rangle$, against ion velocity, r_0, for $\nu = 30.23$ and $\alpha = 20$. The phase average was obtained by integrating the orbits equations for 50 particles with evenly distributed phases in $(0, 2\pi)$. The integrations were begun and ended at $\dot{x} = 0$ and $\dot{y} < 0$. $\langle\Delta\mathcal{E}\rangle_{max}$ is defined in (3.1.6).

Section 3.2. Observation of Stochasticity.

In this section we seek to determine whether the trapping observed in the previous section leads to real heating. Also we wish to see whether the large energy exchanges that we observed in Sec. 2.4 when iterating the linear equations (2.2.31) and (2.2.32) are exhibited by the nonlinear equations. To do this we must look at the *long* time behaviour of the orbit equations, (2.1.9) and (2.1.10). Thus we will integrate the equations over many cyclotron orbits, in contrast to the single cyclotron orbit integrations presented in the previous section. The problem that we are faced with is that of finding a suitable way of presenting the results. Clearly plots like Figs. (3.1.1) and (3.1.2) are useless for more than a few cyclotron periods.

The state of a particle whose motion is described by the orbit equation (2.1.10) is completely given by the three variables: the speed of the ion, r, the angle of the velocity vector, $w_1 = \tan^{-1}(y/\dot{y})$, and the phase of the wave, $w_2 = (\nu t + \phi)_{\text{mod } 2\pi}$. [That these variables are sufficient is easily seen by recognizing that they provide sufficient information to begin the integration of (2.1.10).] A complete description of the system is given by the trajectory of the particle in (r, w_1, w_2) space. Since two of these coordinates are angles it is convenient to visualize the trajectory in toroidal coordinates, Fig. 3.2.1. In the limit $\alpha = 0$ the ion spirals around the surface of a torus with constant minor radius, r, going ν times round the short way (w_2 increasing) for once around the long way (w_1 increasing); in the process the ion will map out the entire surface of the torus, except for rational values of ν (a set of measure zero). Rather than displaying the ion's trajectory in this way, we plot only a *cross-section* of its trajectory. We choose the cross-section defined by $w_1 = \pi$, the ion travelling in the $-y$ direction. This particular choice of w_1 is motivated by observing that the interaction between the wave and the ion is minimum when they are travelling in opposite directions. Such a cross-section is commonly referred to as a *surface of section*. For brevity we will use Σ to denote the $w_1 = \pi$ surface of section. In plotting this cross-section we will plot r and w_2 as cartesian rather than polar coordinates, since in practice we will only be interested in a small range of r.

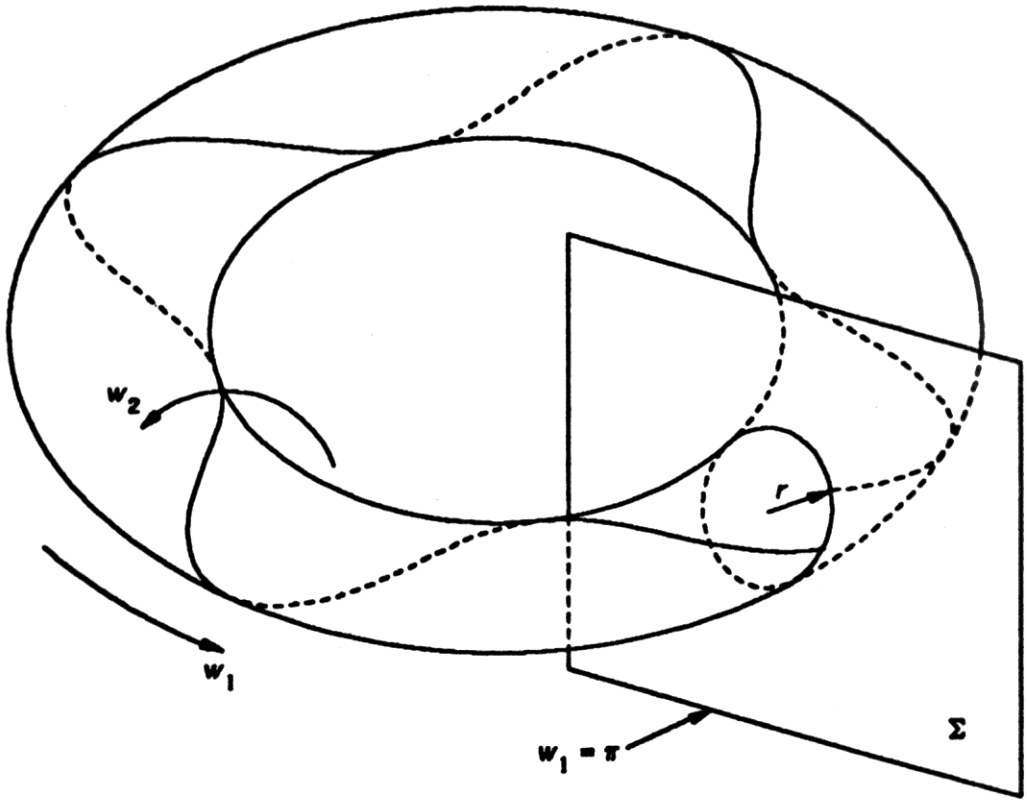

Figure 3.2.1. A particle's trajectory in the space given by the magnitude of its velocity, r, the angle of its velocity vector, w_1, and the phase of the wave, $w_2 = \nu t + \phi$. The trajectory is shown in the limit $\alpha \to 0$, when the trajectory maps out the surface of a torus [assuming ν ($= \dot{w}_2/\dot{w}_1$) is irrational]. The surface of section, Σ, defined by $w_1 = \pi$ is also shown.

Figs. 3.2.2, 3.2.3, and 3.2.4 show the cross-sections for $\nu = 30.23$ and various α. In each case the trajectories of a number of particles is given and a small region of velocity space with $r > \nu$ is plotted. As in Sec. 2.4 we will concentrate on the regions $r \approx \nu$ and $r > \nu$. We will not consider the case $r \ll \nu$, where the wave particle interaction is negligible. If $\alpha \to 0$, then it would take the particle exactly a cyclotron period, 2π, to come back to the $w_1 = \pi$ plane, in which case w_2 will have increased by $2\pi\nu$; the velocity of the particle, r, will remain unchanged. Thus the crossings of a particular particle will all lie on a straight line r = constant.

In Fig. 3.2.2 $\alpha = 1$ and we see that the straight lines in $\alpha = 0$ case have become curved. However the points still do lie on lines. Such lines can, in principle, be written in the form

$$\tilde{\gamma}_1(r, w_2) = \text{const}, \tag{3.2.1}$$

where the constant depends on the starting position of the particle. (This choice of notation is made because, as we will see in Sec. 4.2, $\tilde{\gamma}_1$ is a perturbed action.) This indicates that there exists a constant of the motion such that the motion is completely integrable. A consequence of this integrability is that there can be no time averaged energy exchange between the particle and the wave; the particle's energy will just oscillate about some average value. We will also speak of motion of this type as being coherent. The presence of smooth lines in Σ indicates that the motion in the phase space illustrated in Fig. 3.2.1 is still constrained to lie on a surface. This surface lies close to the $\alpha = 0$ torus shown in that figure, because r is nearly constant in Fig. 3.2.2.

Figure 3.2.3 shows the picture when α has been increased to 2.2. Again there are trajectories that lie on smooth curves spanning all w_2, indicating integrability of the motion. However we see two new features. Firstly there are some trajectories which lie on *islands*. Each chain of islands is generated by a single particle trajectory. Two of the chains of islands are numbered in Fig. 3.2.3, the numbers indicating the order in which the islands are visited. The

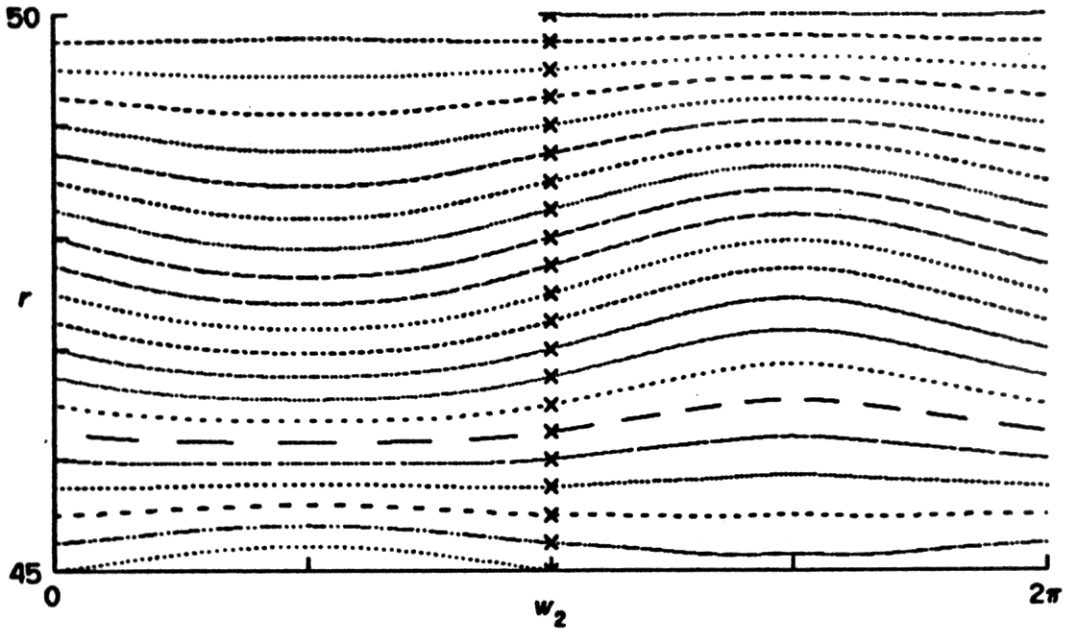

Figure 3.2.2. The surface of section, Σ, for $\nu = 30.23$ and $\alpha = 1$. Crosses (x) denote the initial positions of the particles and dots (·) subsequent crossings. The particles are followed for 300 crossings of the $w_1 = \pi$ plane.

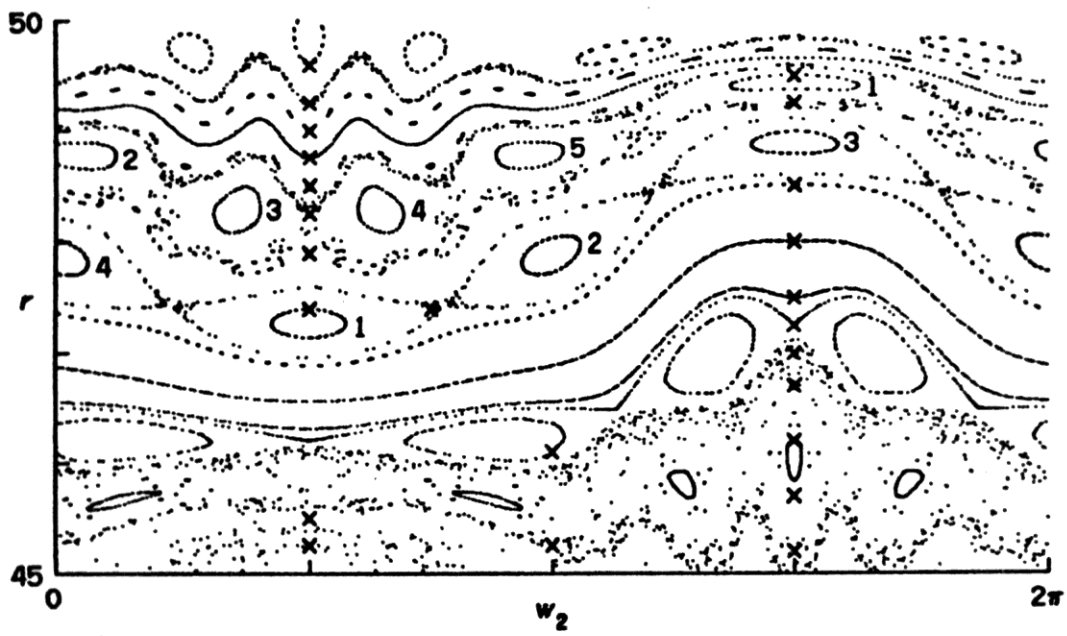

Figure 3.2.3. Σ for $\nu = 30.23$ and $\alpha = 2.2$.

order of a chain of islands is the number of islands in a chain, and gives the number of cyclotron orbits it takes for a particle to return to a given island. Thus 4th and 5th order chains are visible in Fig. 3.2.3. Since the islands form smooth curves the motion of the corresponding particle is integrable. The second feature is that between the island chains are regions where the motion is *stochastic*. The trajectories no longer lie on smooth lines, but appear to wander freely about a subset of Σ. However the presence of the integrable trajectories prevents the particle's gaining significant energy.

In Fig. 3.3.4 α is 4. In this case the motion is stochastic is nearly all of the portion of Σ we have plotted. This means that particles may be heated through the range of velocity space plotted.

Summarizing the behaviour of these three plots: At small α the motion is coherent over a large range of r. At intermediate values of α the motion in Σ has a very detailed structure, with portions of Σ coherent and portions stochastic. The scale length in r of this structure is typically 2π (we will see in the next chapter that this is related to the period of a Bessel function). For large α this structure is destroyed and Σ is stochastic over a region of r greater than 2π. The value of α at which this happens we term the *stochasticity threshold*. It gives the field at which appreciable heating of the particles can take place.

Figures 3.2.5 and 3.2.6 show Σ for the same parameters as in Fig. 3.2.3, but at lower and higher velocities. We see that at lower velocities the motion is more stochastic than in Fig. 3.2.3 whereas at higher velocities it is less so. This is consistent with the r dependence, exhibited by the coefficient, A (2.4.15), in the difference equations (2.4.13) and (2.4.14).

Finally we show Σ for $\nu = 30$, 30.11 and 30.47 for the same region of velocity space as Figs. 3.2.2-4 illustrating the three regimes of α for these frequencies (Figs. 3.2.7-15). We see that the plots for $\nu = 30$ are unusual, for all $\alpha \neq 0$ there are large islands present that occupy all of Σ.

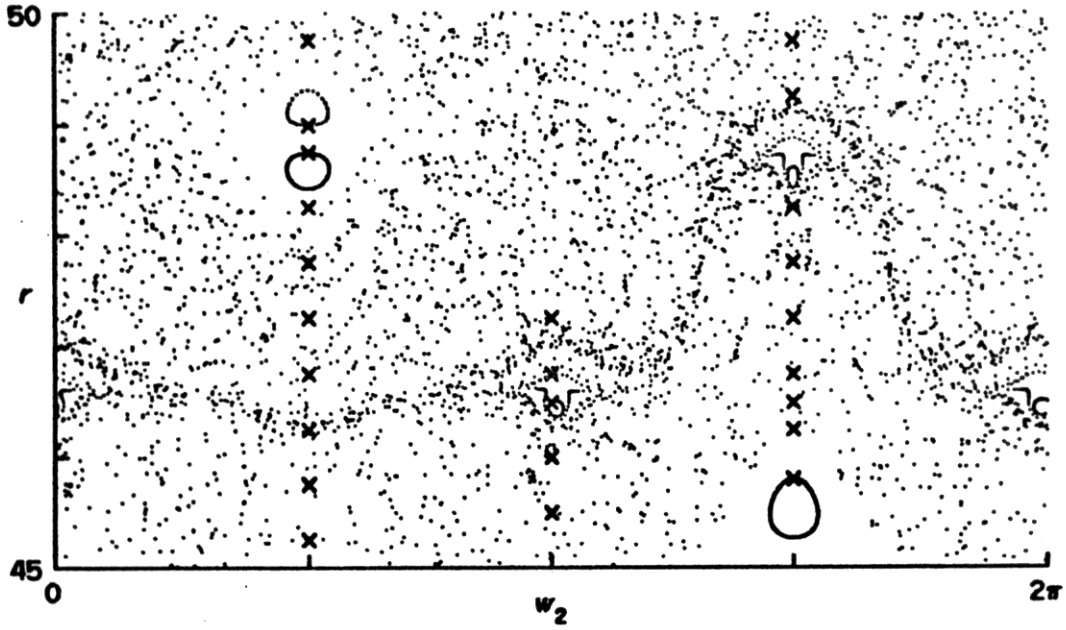

Figure 3.2.4. Σ for $\nu = 30.23$ and $\alpha = 4$.

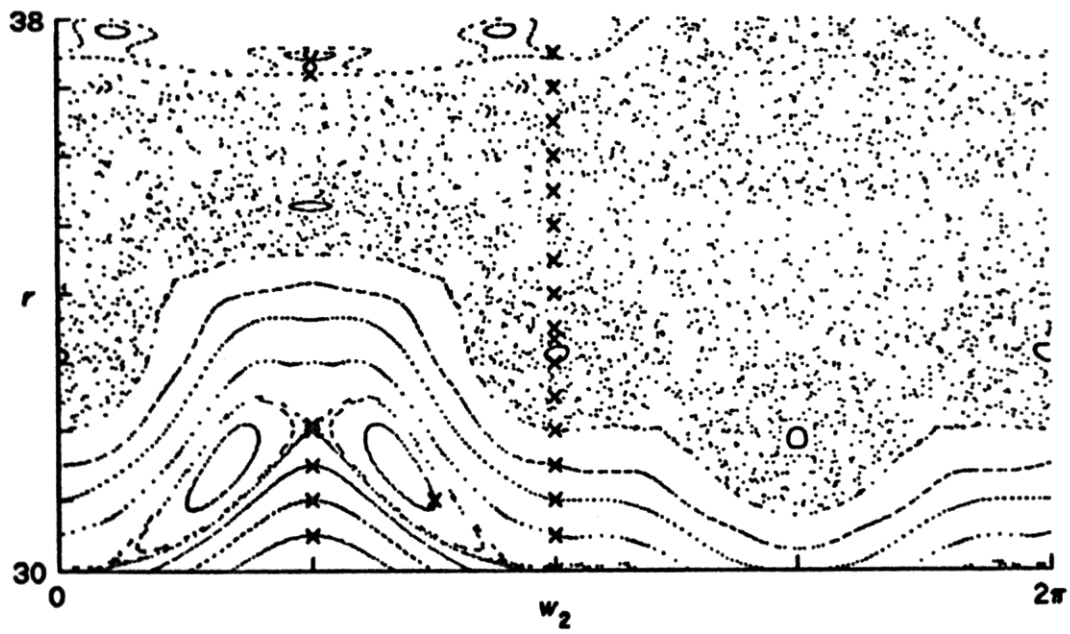

Figure 3.2.5. Σ for $\nu = 30.23$, $\alpha = 2.2$, and r between 30 and 38.

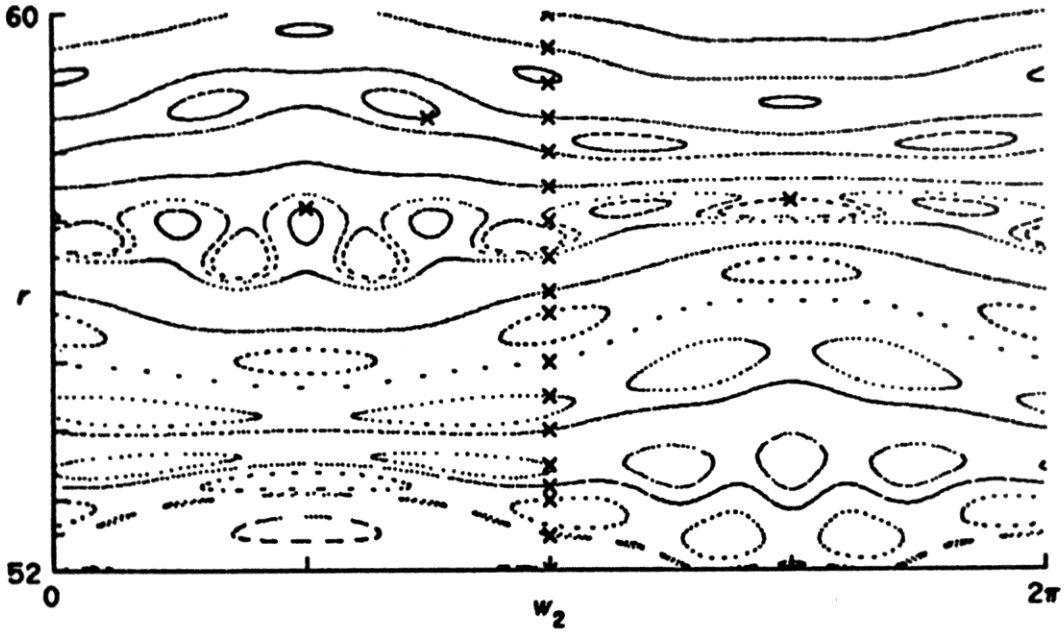

Figure 3.2.6. Σ for $\nu = 30.23$, $\alpha = 2.2$, and r between 52 and 60.

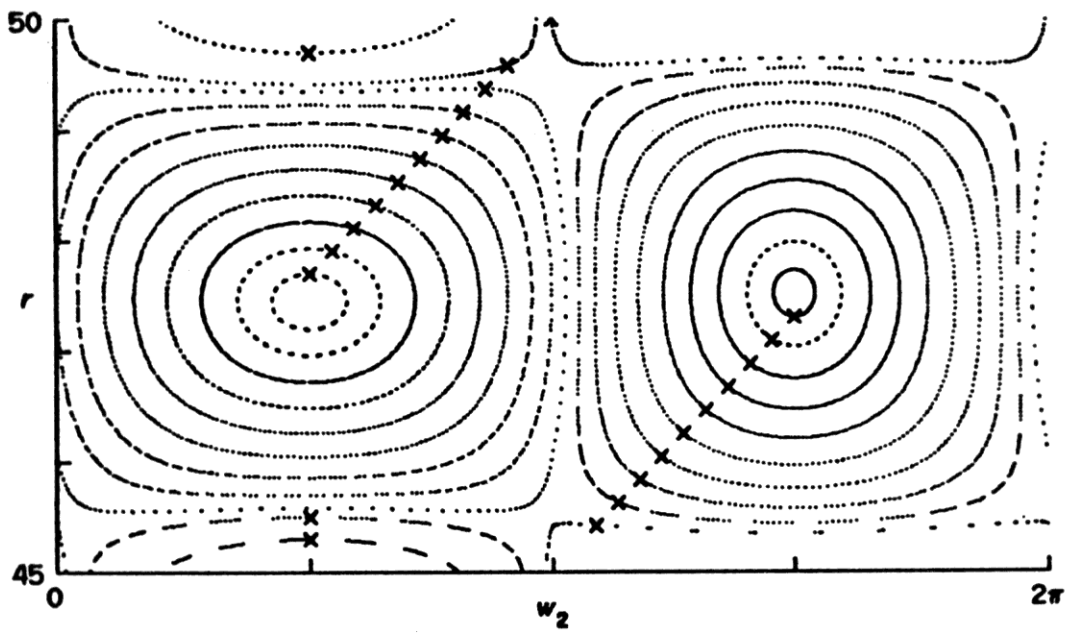

Figure 3.2.7. Σ for $\nu = 30$ and $\alpha = 1$.

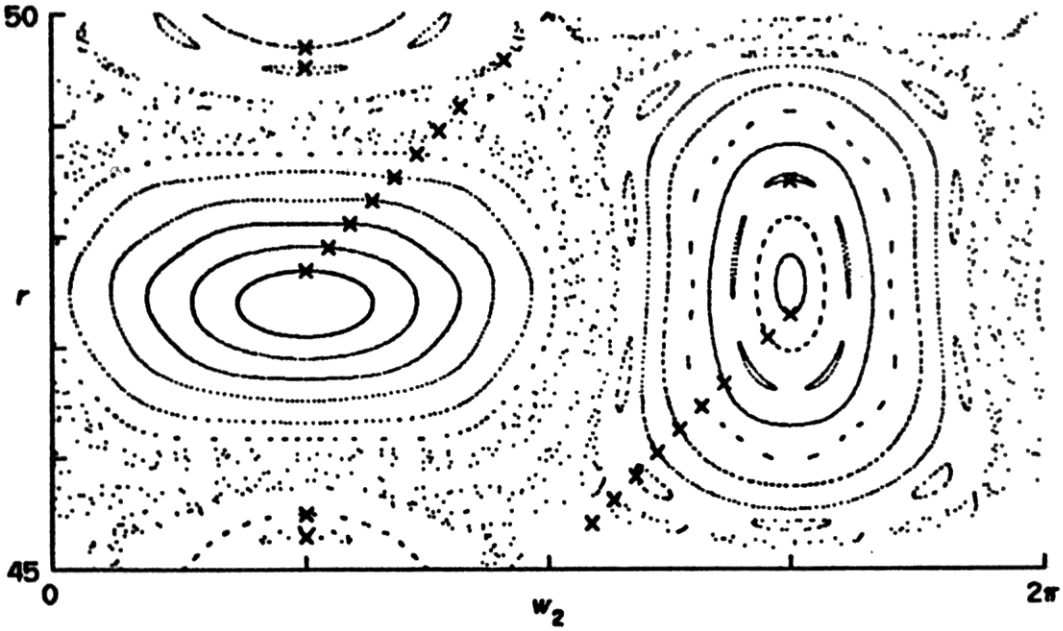

Figure 3.2.8. Σ for $\nu = 30$, $\alpha = 3$.

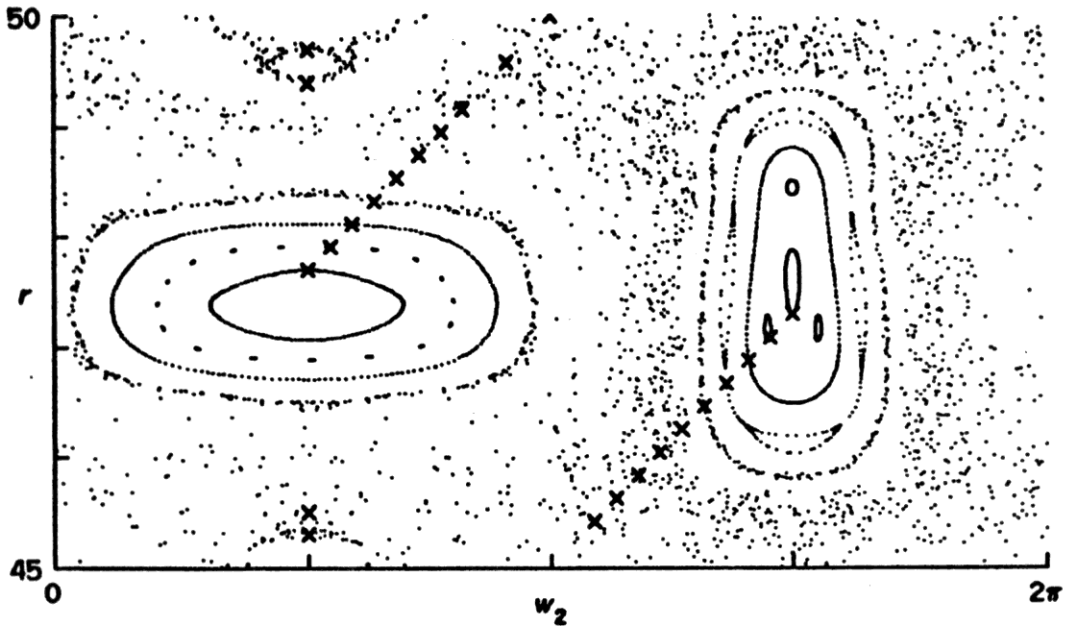

Figure 3.2.9. Σ for $\nu = 30$ and $\alpha = 4.1$.

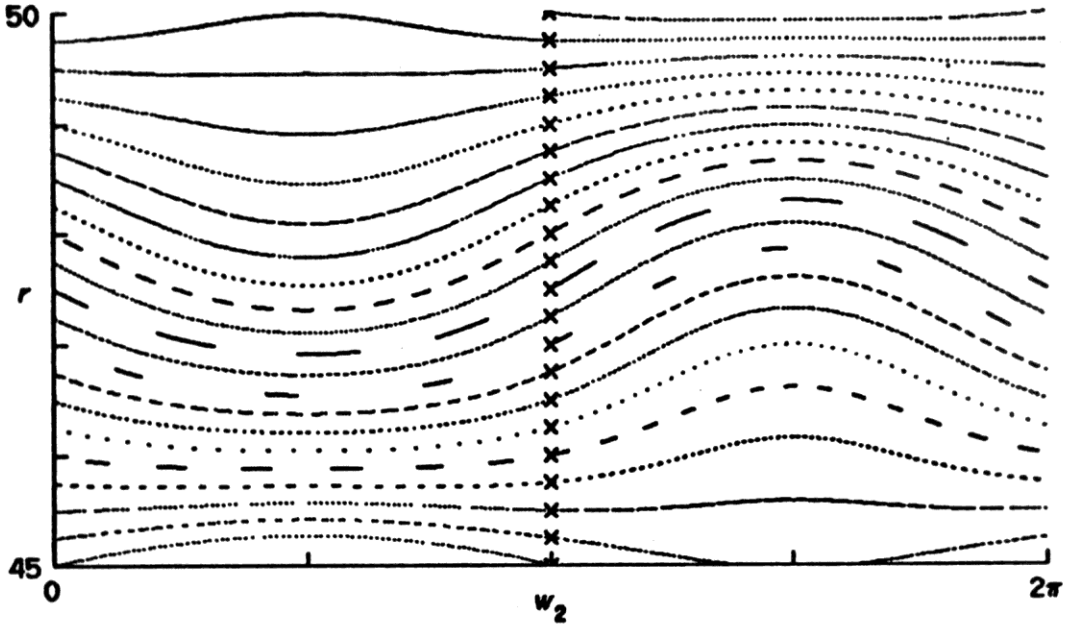

Figure 3.2.10. Σ for $\nu = 30.11$, $\alpha = 1$.

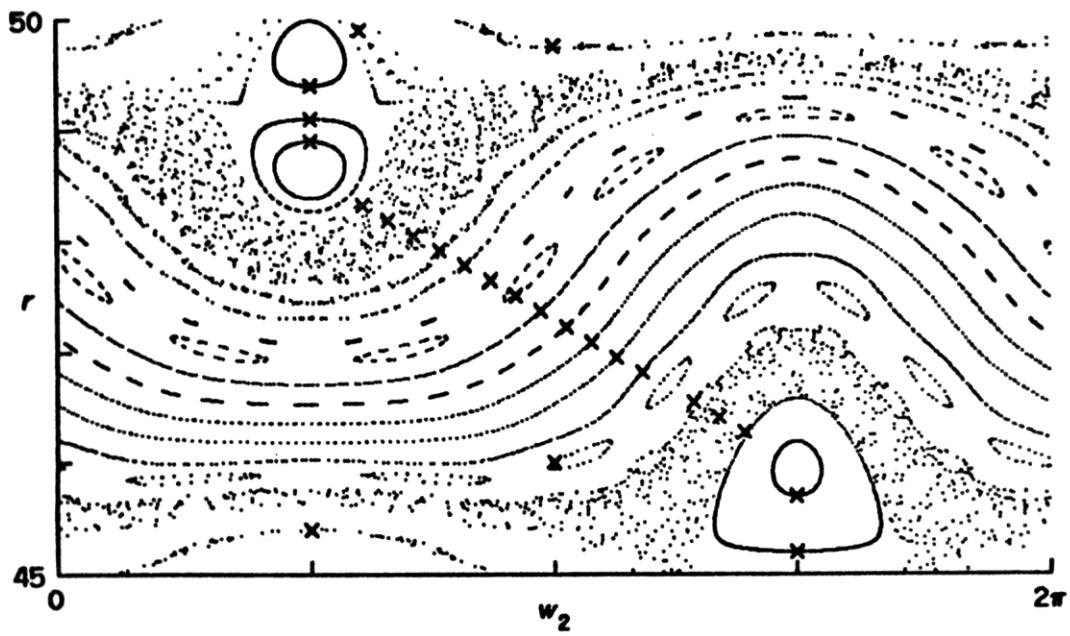

Figure 3.2.11. Σ for $\nu = 30.11$ and $\alpha = 2$.

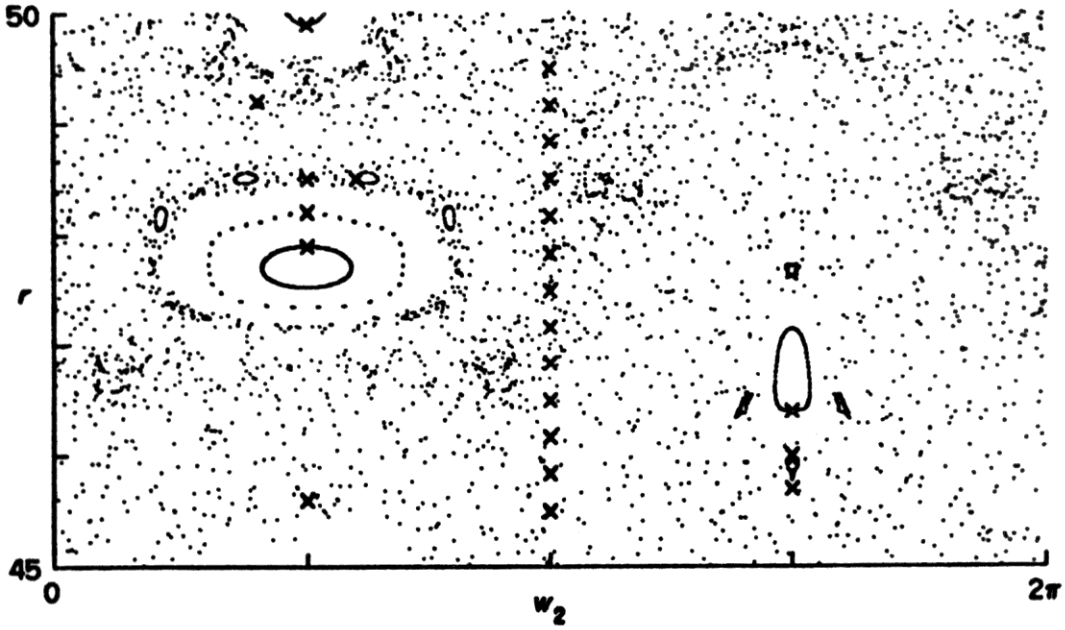

Figure 3.2.12. Σ for $\nu = 30.11$, $\alpha = 4$.

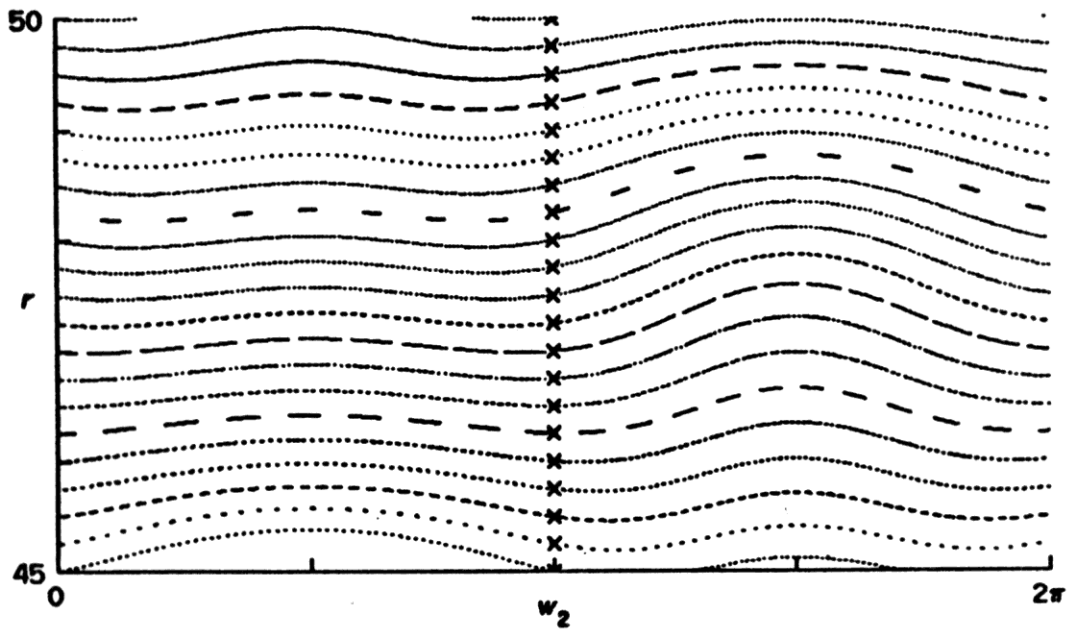

Figure 3.2.13. Σ for $\nu = 30.47$ and $\alpha = 1$.

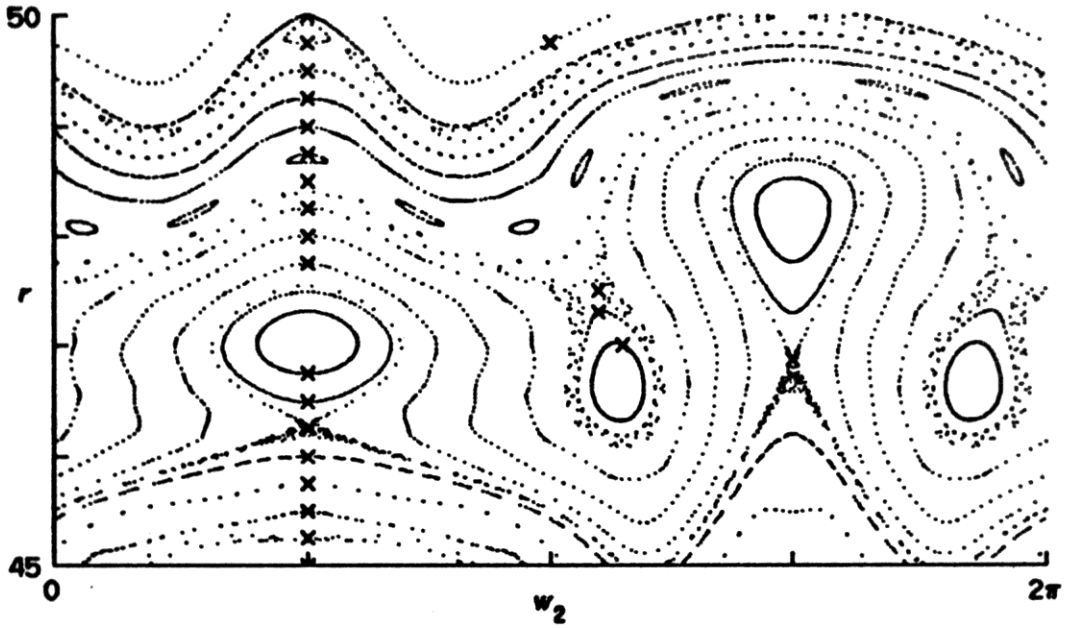

Figure 3.2.14. Σ for $\nu = 30.47$, $\alpha = 2.5$.

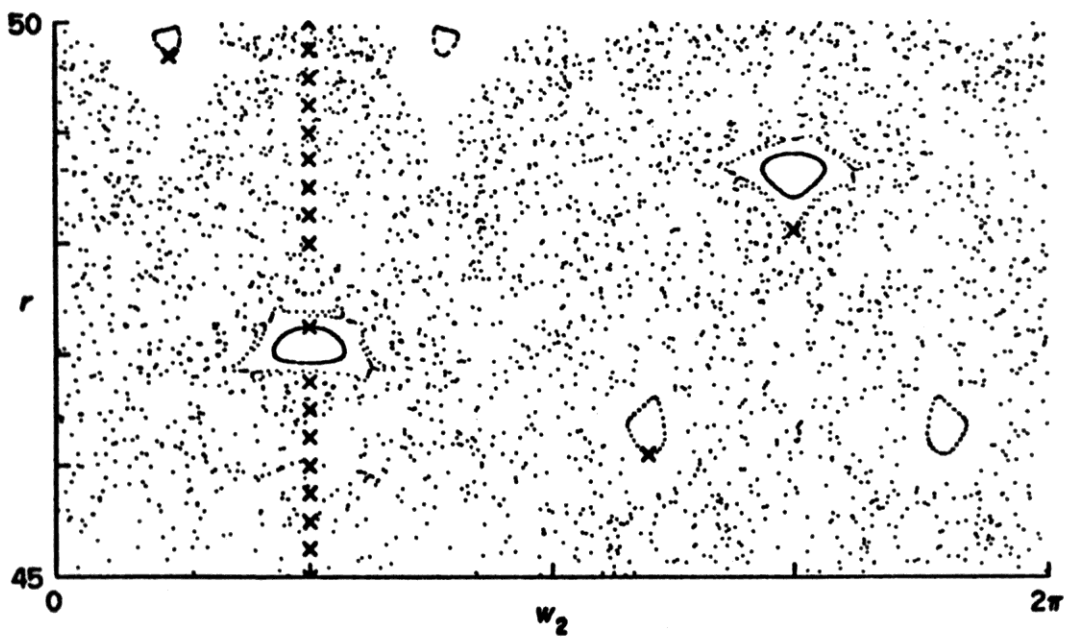

Figure 3.2.15. Σ for $\nu = 30.47$ and $\alpha = 3.5$.

Chapter 4. HAMILTONIAN FORMULATION.

Section 4.1. Formulation in Terms of Hamiltonian.

In this chapter we use the Hamiltonian formulation to look at the motion of the ion described by the orbit equations (2.1.9) and (2.1.10). The advantages of this approach over the linear analysis of the Chapter 2 is two-fold. Firstly by using the Hamiltonian we are able to solve for the frequencies in the problem without having to completely solve for the motion. We shall see in Secs. 4.2 and 4.4 that this enables us to predict the dominant features in the exact numerical calculation of Sec. 3.2). The second advantage is that we are able to make approximations that give good results for long times and obtain a good bound on the accuracy of these results.

We begin by writing down the Hamiltonian for a particle in electric and magnetic fields as (Goldstein, 1951)

$$K = \tfrac{1}{2}(\mathbf{p} - q\mathbf{A})^2/m + q\Phi. \tag{4.1.1}$$

where $\mathbf{B} = \nabla \times \mathbf{A}$ and $\mathbf{E} = -\nabla\Phi - \partial\mathbf{A}/\partial t$. In our problem $\mathbf{B} = B_0\hat{\mathbf{z}}$ and $\mathbf{E} = E_0\hat{\mathbf{y}}\cos(ky - \omega t - \phi)$, giving

$$\mathbf{A} = -B_0 y\hat{\mathbf{x}}, \quad \Phi = -(E_0/k)\sin(ky - \omega t - \phi). \tag{4.1.2}$$

Evaluating the Hamiltonian (4.1.1) we obtain

$$K = \tfrac{1}{2}[(p_x + qB_0 y)^2 + p_y{}^2]/m - (qE_0/k)\sin(ky - \omega t - \phi). \tag{4.1.3}$$

At this stage it is convenient to introduce the normalization first used in Chapter 2. Normalizing K to $m(\Omega/k)^2$ we obtain

$$K = \tfrac{1}{2}[(p_x + y)^2 + p_y{}^2] - \alpha \sin(y - \nu t - \phi). \tag{4.1.4}$$

Since K is independent of x, p_x is a constant. We could then replace p_x by a constant in (4.1.4), thus reducing the number of degrees of freedom in the problem. However we will postpone using this fact, preferring instead to make a canonical transformation to remove the time dependence from the Hamiltonian. We accomplish this, using the notation of Goldstein (1951), by means of the generating function,

$$F_2 = (P_x - \nu t - \phi)x + P_y(y - \nu t - \phi + P_x). \tag{4.1.5}$$

where the new coordinates are denoted by capital letters. Equation (4.1.5) gives the following relations between the new and the old coordinates:

$$X = x + p_y,\ P_x = p_x + \nu t + \phi,\ Y = y + p_x,\ P_y = p_y, \tag{4.1.6}$$

and the new Hamiltonian H is given by

$$H = K - \nu X = \tfrac{1}{2}Y^2 + \tfrac{1}{2}P_y{}^2 - \nu X - \alpha \sin(Y - P_x). \tag{4.1.7}$$

Note that Y differs from y by a constant, p_x, which without loss of generality we may take to be zero (e.g. by choice of the y origin). [This is equivalent to the statement that $\dot{x} = y$ (2.1.9).] Finally we transform (P_y, Y) and (P_x, X) to the action-angle variables (I_1, w_1) and (I_2, w_2) respectively, using the generating function

$$F_1 = \tfrac{1}{2}Y^2 \cot w_1 + X w_2. \tag{4.1.8}$$

This gives

$$P_y = \sqrt{2I_1}\cos w_1,\ Y = \sqrt{2I_1}\sin w_1, \tag{4.1.9}$$

$$X = -I_2, \; P_x = w_2. \tag{4.1.10}$$

Performing the transformation on H we find

$$H = I_1 + \nu I_2 - \alpha \sin[\sqrt{2I_1}\,\sin w_1 - w_2]. \tag{4.1.11}$$

The original position variables, x and y, are given by

$$y = \sqrt{2I_1}\sin w_1, \; x = -I_2 - \sqrt{2I_1}\cos w_1. \tag{4.1.12}$$

Note that the Hamiltonian equation $\dot{w}_2 = \partial H/\partial I_2 = \nu$ is trivially integrated to give $w_2 = \nu t + \phi$. Thus we may interpret (4.1.11) as describing a pair of harmonic oscillators, the ion in a magnetic field described by (I_1, w_1) with frequency 1 (Ω) and the wave described by (I_2, w_2) with frequency ν (ω), coupled by the last term in (4.1.11).

One essential test of the correctness of (4.1.11) is to compute the Hamiltonian equations of motion, and to see if they give the Lorentz force law, (2.1.7) and (2.1.8). The Hamiltonian equations are:

$$\dot{w}_1 = \partial H/\partial I_1 = 1 - \alpha(2I_1)^{-1/2}\sin w_1 \cos[\sqrt{2I_1}\,\sin w_1 - w_2], \tag{4.1.13}$$

$$\dot{w}_2 = \partial H/\partial I_2 = \nu, \tag{4.1.14}$$

$$\dot{I}_1 = -\partial H/\partial w_1 = \alpha(2I_1)^{1/2}\cos w_1 \cos[\sqrt{2I_1}\,\sin w_1 - w_2], \tag{4.1.15}$$

$$\dot{I}_2 = -\partial H/\partial w_2 = -\alpha\cos[\sqrt{2I_1}\,\sin w_1 - w_2]. \tag{4.1.16}$$

Of course (4.1.14) is easily integrated to give

$$w_2 = \nu t + \phi. \tag{4.1.17}$$

From (4.1.13) we form

$$\dot{y} = (2I_1)^{-1/2}\sin w_1\,\dot{I}_1 + (2I_1)^{1/2}\cos w_1\,\dot{w}_1$$

$$= \sqrt{2I_1}\cos w_1. \tag{4.1.18}$$

$$\dot{x} = -\dot{I}_2 - (2I_1)^{-1/2}\cos w_1\,\dot{I}_1 + (2I_1)^{1/2}\sin w_1\,\dot{w}_1$$

$$= \sqrt{2I_1}\sin w_1$$

$$= y. \tag{4.1.19}$$

Taking a further time derivative we obtain

$$\ddot{y} = (2I_1)^{-1/2}\cos w_1\,\dot{I}_1 - (2I_1)^{1/2}\sin w_1\,\dot{w}_1$$

$$= -\sqrt{2I_1}\sin w_1 + \alpha\cos[\sqrt{2I_1}\sin w_1 - w_2]$$

$$= -\dot{x} + \alpha\cos(y - \nu t - \phi), \tag{4.1.20}$$

$$\ddot{x} = \dot{y}, \tag{4.1.21}$$

as required.

We may also mention an alternative derivation of the Hamiltonian, (4.1.11), which avoids ever introducing time into the Hamiltonian. If we transform to the frame of the wave, $\nu\hat{y}$, then all the fields are static. The Hamiltonian in this frame is then numerically equal to the total energy of the ion. A Galilean transformation back to the rest frame gives (4.1.7).

Section 4.2. Integrals of the Motion.

The Hamiltonian in (4.1.11) cannot in general be integrated exactly. However we saw in Sec. 3.2 that at sufficiently small α an additional (approximate) constant of motion does exist, showing that the Hamiltonian is approximately integrable. We are able to derive this constant using standard techniques. We must distinguish two cases: when the unperturbed ($\alpha = 0$) motion is far from any resonances and when it is close to a resonance. What resonances are important may be determined by first treating the non-resonant case, and deducing the presence of resonances from any *resonant denominators* appearing in the analysis. Similar results to the ones given here are derived by Timofeev (1974).

The analysis begins by Fourier transforming the angle dependent term in (4.1.11) giving

$$H = I_1 + \nu I_2 - \alpha \Sigma_m J_m(\sqrt{2I_1}) \sin(m w_1 - w_2), \tag{4.2.1}$$

where we we have used the Fourier expansion, eq. 9.1.41, of Abramowitz and Stegun (1964). There is then a standard procedure given by Walker and Ford (1969) for transforming to a new set of coordinates in which the Hamiltonian is cyclic to order α^2. This consists of introducing the new set of coordinates $(\tilde{I}_1, \tilde{w}_1)$ and $(\tilde{I}_2, \tilde{w}_2)$ using the generating function

$$F_3 = -I_1\tilde{w}_1 - I_2\tilde{w}_2 - \alpha \Sigma_m J_m(\sqrt{2I_1}) \cos(m\tilde{w}_1 - \tilde{w}_2)/(m - \nu). \tag{4.2.2}$$

The old and new coordinates are then related by

$$w_1 = \tilde{w}_1 + \alpha \Sigma_m (\partial/\partial I_1) J_m(\sqrt{2I_1}) \cos(m\tilde{w}_1 - \tilde{w}_2)/(m - \nu), \tag{4.2.3}$$

$$w_2 = \tilde{w}_2, \tag{4.2.4}$$

$$\tilde{I}_1 = I_1 - \alpha \Sigma_m m J_m(\sqrt{2I_1}) \sin(m\tilde{w}_1 - \tilde{w}_2)/(m - \nu), \tag{4.2.5}$$

$$\tilde{I}_2 = I_2 + \alpha \Sigma_m J_m(\sqrt{2I_1}) \sin(m\tilde{w}_1 - \tilde{w}_2)/(m - \nu). \tag{4.2.6}$$

The new Hamiltonian is then

$$\tilde{H} = \tilde{I}_1 + \nu\tilde{I}_2 + \alpha \Sigma_m J_m(\sqrt{2I_1})[\sin(m\tilde{w}_1 - \tilde{w}_2) - \sin(mw_1 - \tilde{w}_2)], \tag{4.2.7}$$

although this is not in the proper form until we have eliminated the variables I_1 and w_1. As long as $(m - \nu)$ is not small for any m [we require $(m - \nu) \gg O(\alpha)$, so that the terms proportional to α in (4.2.3-6) are small] then the transformation given by (4.2.2) is an infinitesimal one (for infinitesimal α) and specifically (4.2.3) tells us that w_1 and $\tilde{w}_1$ differ by $O(\alpha)$. Thus if we substitute (4.2.3) into (4.2.7) we obtain

$$\tilde{H} = \tilde{I}_1 + \nu\tilde{I}_2 + O(\alpha^2). \tag{4.2.8}$$

To order $O(\alpha^2)$, $\tilde{I}_1$ and $\tilde{I}_2$ are constants since $\tilde{H}$ is cyclic in the angle variables and so sufficient integrals of the motion are known to completely specify the motion. By computing surfaces of constant $\tilde{I}_1$ we can display the motion and compare it with that given by the numerical solution in Chapter 3. Substituting (4.2.3) and (4.2.4) into (4.2.5) we have

$$\tilde{I}_1 = I_1 - \alpha \Sigma_m mJ_m(\sqrt{2I_1}) \sin(mw_1 - w_2)/(m - \nu) + O(\alpha^2) = \text{const} + O(\alpha^2). \tag{4.2.9}$$

In the analysis above we had to exclude the case $\nu \approx n$, an integer, because of the presence of $(m - \nu)$ in the generating function (4.2.2). The problem arises because if $\nu \approx n$, then the $m = n$ term in the sum in (4.2.1) drives the zeroth order terms resonantly, so that there will be large deviations in motion from the unperturbed motion and an infinitesimal transformation given by (4.2.2) breaks down. We may still derive additional constants of the motion, by utilizing a transformation to a rotating frame described by Jaeger and Lichtenberg (1972). The generating function for this transformation is

$$F_2 = \hat{I}_1(nw_1 - w_2) + \hat{I}_2 w_2. \tag{4.2.10}$$

Then the old coordinates may be expressed as

$$I_1 = n\hat{I}_1,\ I_2 = \hat{I}_2 - \hat{I}_1,\ w_1 = (\hat{w}_1 + \hat{w}_2)/n,\ w_2 = \hat{w}_2, \tag{4.2.11}$$

and the Hamiltonian (4.2.1) becomes

$$\hat{H} = (n - \nu)\hat{I}_1 + \nu\hat{I}_2 - \alpha\, \Sigma_m\, J_m[(2n\hat{I}_1)^{1/2}]\sin[m\hat{w}_1/n - (1 - m/n)\hat{w}_2]. \tag{4.2.12}$$

Note that $\hat{w}_1 = nw_1 - w_2$ is slowly varying, whereas $\hat{w}_2 = w_2$, the wave phase, is still rapidly varying. The dominant contributions to the behaviour of the ion are given by the slowly varying components of $\hat{H}$ only (Bogoliubov and Mitropolsky, 1961), thus we may average over a period of w_2 to give

$$\langle\hat{H}\rangle = (n - \nu)\hat{I}_1 + \nu\hat{I}_2 - \alpha\, J_n[(2n\hat{I}_1)^{1/2}]\sin\hat{w}_1. \tag{4.2.13}$$

Since $\langle\hat{H}\rangle$ is cyclic in $\hat{w}_2$, $\hat{I}_2$ is constant to order α^2, as is $\langle\hat{H}\rangle - \nu\hat{I}_2$. Expressing this latter quantity in the original coordinates using (4.2.11) and (4.2.13) we obtain to order α^2

$$\langle\hat{H}\rangle - \nu\hat{I}_2 = (n - \nu)I_1/n - \alpha\, J_n(\sqrt{2I_1})\sin(nw_1 - w_2) = \text{const}. \tag{4.2.14}$$

Remarkably, the motion derived in the non-resonant case as given by (4.2.9) agrees with (4.2.14), because in the limit $(n - \nu) \to 0$, only the $m = n$ term contributes in the sum in (4.2.9) and so (4.2.9) reduces to (4.2.14). We may therefore use (4.2.9) to determine the motion for all ν. On Σ (the cross-section $w_1 = \pi$, Fig. 3.2.1), (4.2.9) becomes to order α^2

$$\tilde{I}_1 = I_1 + \alpha\, \Sigma_m\, m(-1)^m J_m(\sqrt{2I_1})\sin w_2/(m - \nu) = \text{const}. \tag{4.2.15}$$

From (4.1.18) and (4.1.19) the magnitude of the velocity, r, is given by

$$I_1 = \tfrac{1}{2}r^2. \tag{4.2.16}$$

In Figs. 4.2.1-10 we have plotted the curves of constant $\tilde{I}_1$ at the $w_1 = \pi$ plane for the same values as in the numerical computations shown in Figs. 3.2.2-4 and 3.2.7-15. Note that for $\nu = 30$ the motion in Σ is independent of α; in this case α only determines the time scale of the motion. Comparing these figures with those of Sec. 3.2, we see that (4.2.16) gives the coherent motion at low α accurately. It also predicts the location and size of the *first* order islands. Islands of higher orders are not predicted, nor, of course, is the stochastic motion seen in Sec. 3.2.

Section 4.3. Origin of Stochasticity.

Two important features were observed in the exact numerical computations in Sec. 3.2, but are not predicted by the approximate integral of the motion, $\tilde{I}_1$ (4.2.15). They are the higher (than first) order islands and the stochastic motion. The stochasitc motion is of course of principle interest for RF heating. However the appearance of islands is intimately related to onset of stochasticity. We will trace the connection in this section, for it is on the basis of that connection that we are able to derive an analytic expression for the stochasticity threshold in Sec. 4.4. A more complete description of the subject can be found in Ford (1975), and more mathematical treatments are given by Arnold and Avez (1968) and Moser (1973). In this discussion we will find it helpful to refer the the surface of section plots of Sec. 3.2.

In Sec. 3.2 we defined a surface of section by $w_1 = \pi$, and we plotted r *vs.* w_2. [We argued that specifying w_1, w_2, and r is sufficient to begin the integration of the orbit equation (2.1.10).] Unfortunately this surface of section, which was arrived at from studying the orbit equation, differs somewhat from that defined by other authors, who consider the problem more in terms of the Hamiltonian. We can, however, establish a connection between our surface of section and the more usual one. If we followed the conventions of Arnold and Avez (1968), for instance, we

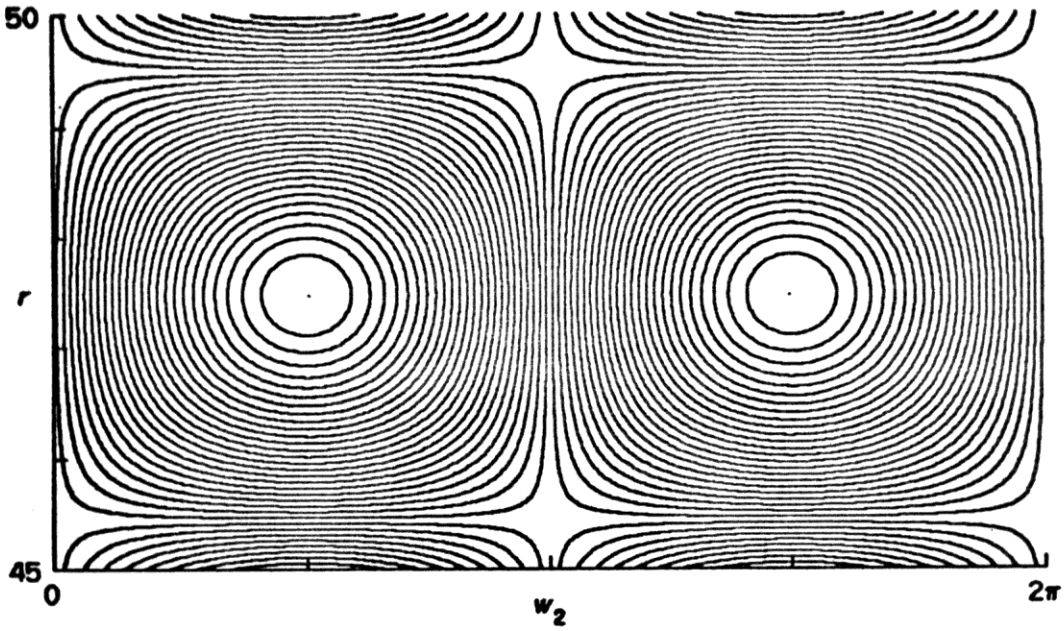

Figure 4.2.1. Line of constant $\tilde{\gamma}_1$ (4.2.15) on the surface of section, Σ, for $\nu = 30$ and all nonzero α. (Cf. Figs. 3.2.7 to 3.2.9.)

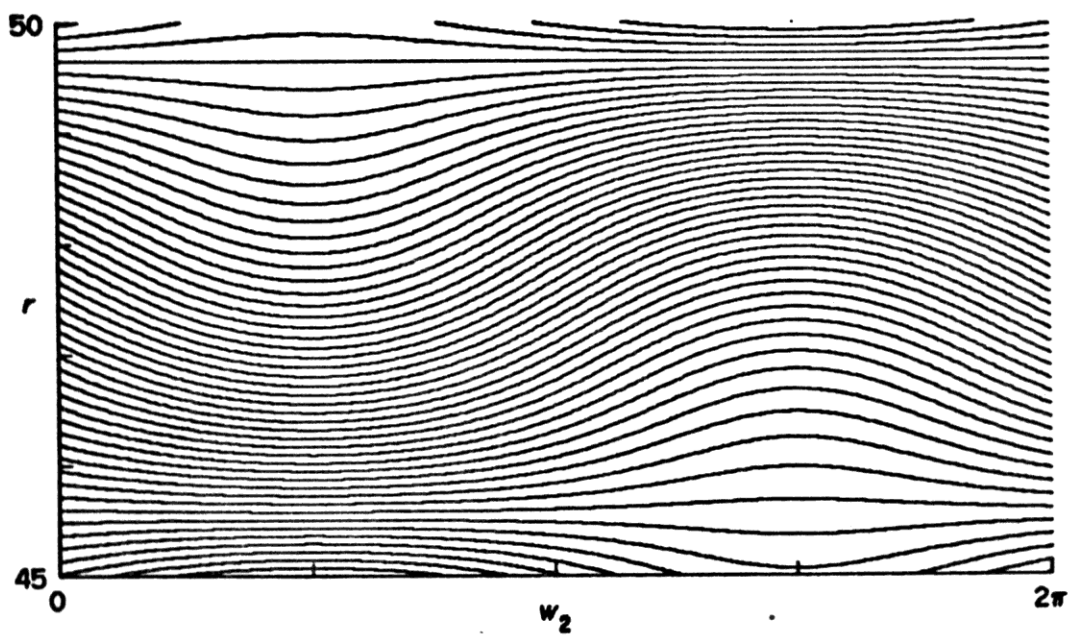

Figure 4.2.2. Same as Fig. 4.2.1, but $\nu = 30.11$ and $\alpha = 1$. (Cf. Fig. 3.2.10.)

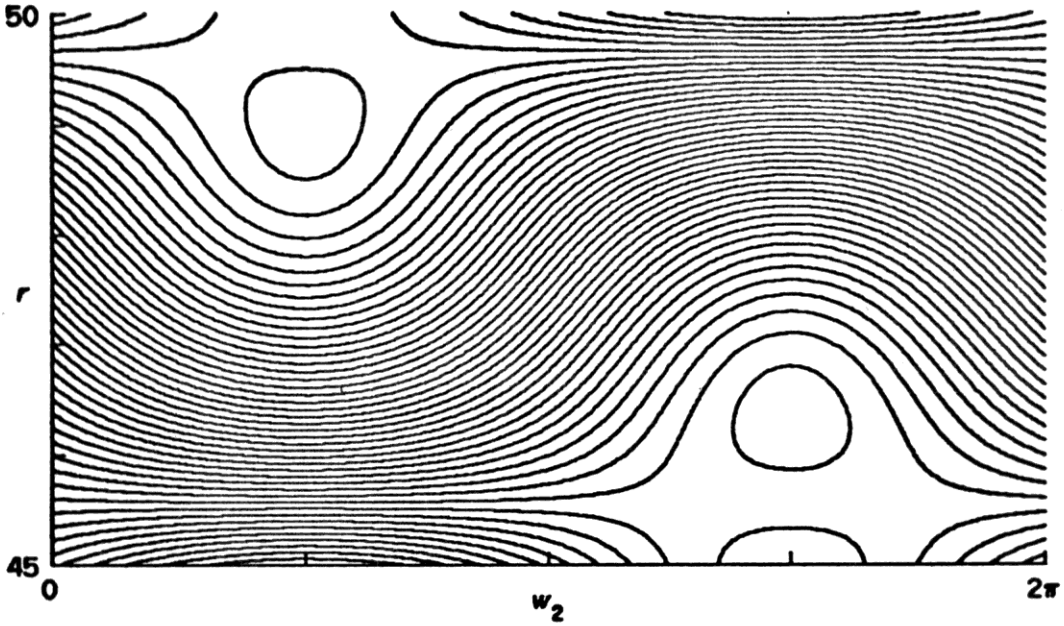

Figure 4.2.3. Same as Fig. 4.2.1, but $\nu = 30.11$ and $\alpha = 2$. (Cf. Fig. 3.2.11.)

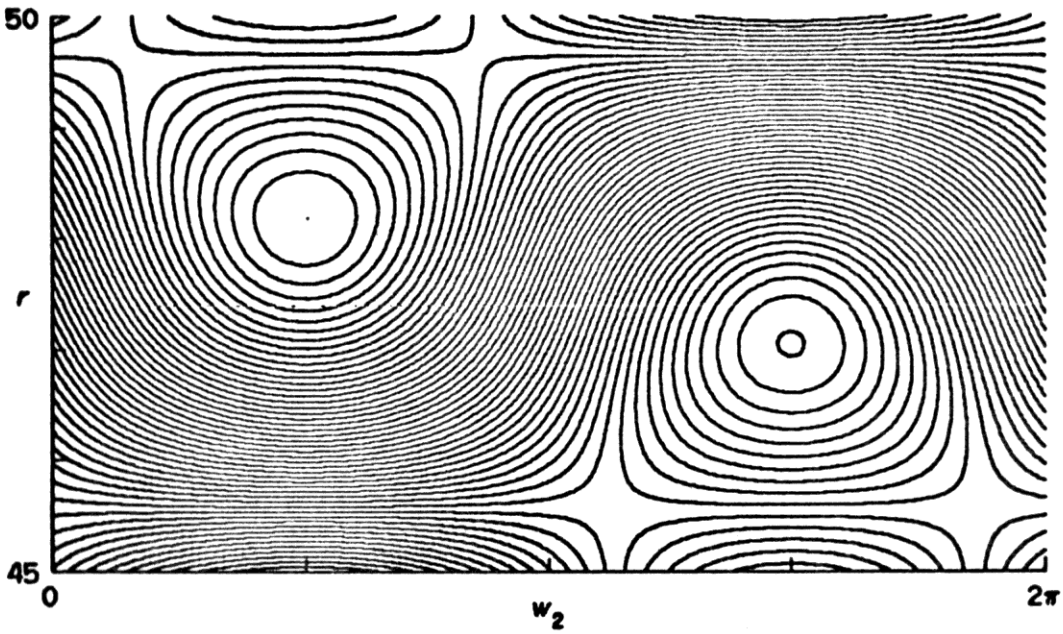

Figure 4.2.4. Same as Fig. 4.2.1, but $\nu = 30.11$ and $\alpha = 4$. (Cf. Fig. 3.2.12.)

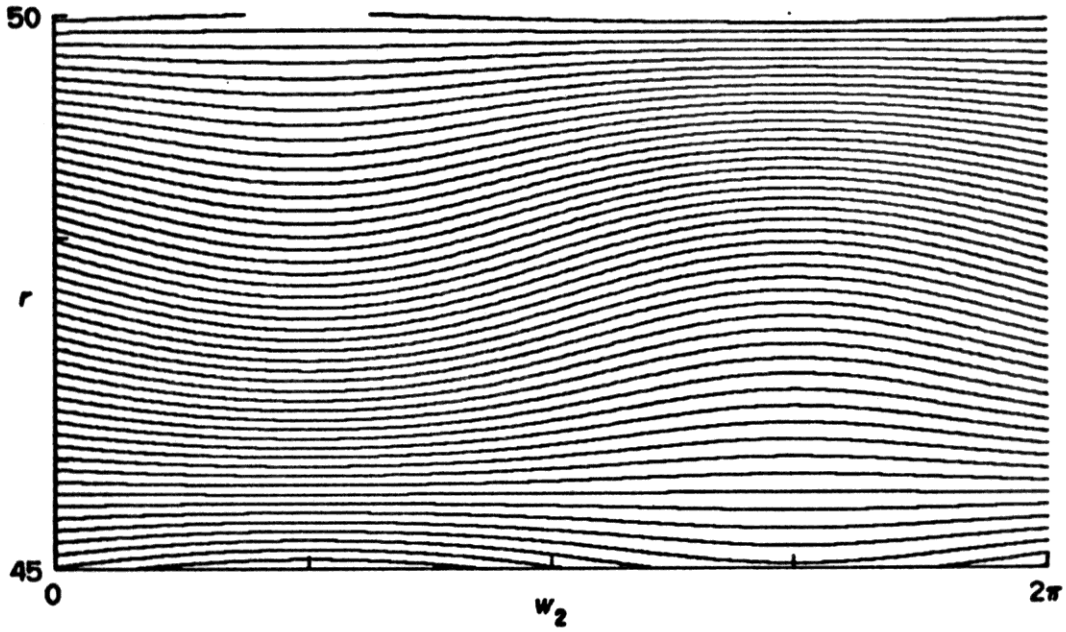

Figure 4.2.5. Same as Fig. 4.2.1, but $\nu = 30.23$ and $\alpha = 1$. (Cf. Fig. 3.2.2.)

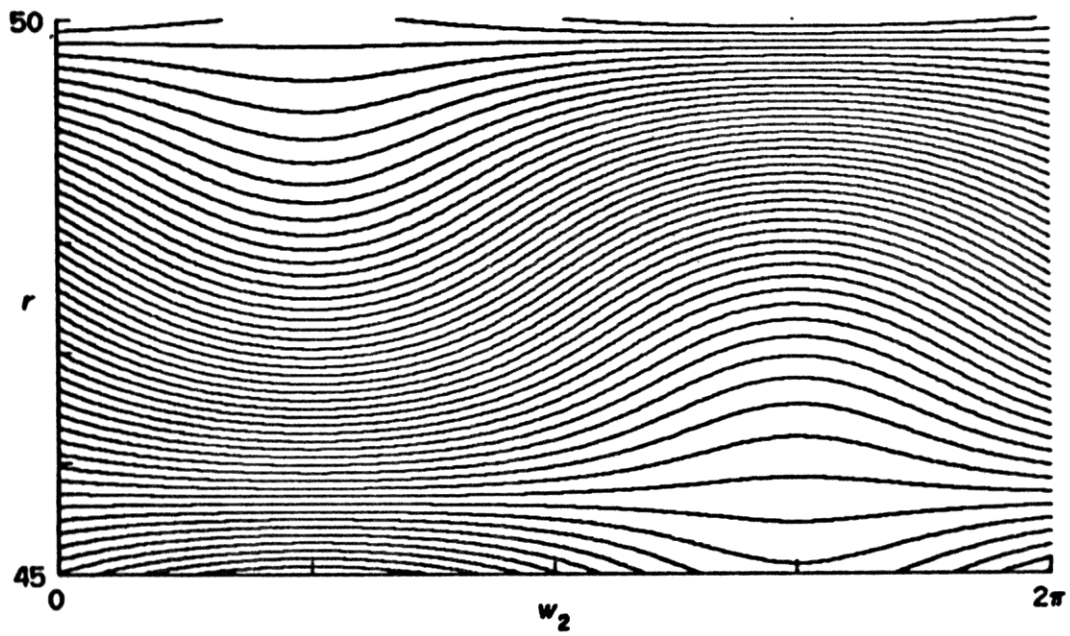

Figure 4.2.6. Same as Fig. 4.2.1, but $\nu = 30.23$ and $\alpha = 2.2$. (Cf. Fig. 3.2.3.)

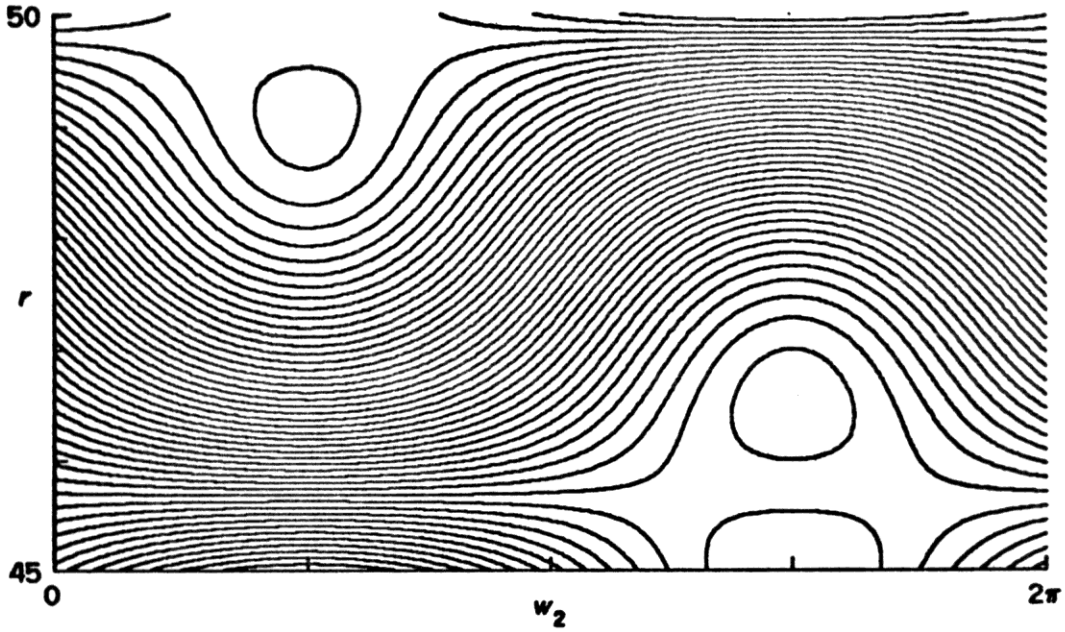

Figure 4.2.7. Same as Fig. 4.2.1, but $\nu = 30.23$ and $\alpha = 4$. (Cf. Fig. 3.2.4.)

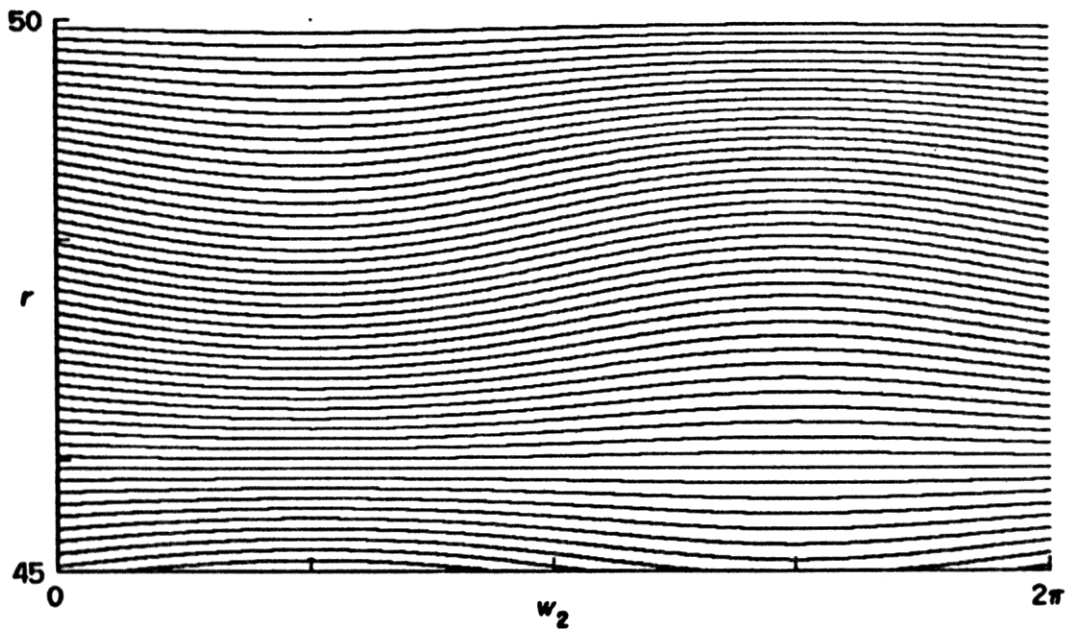

Figure 4.2.8. Same as Fig. 4.2.1, but $\nu = 30.47$ and $\alpha = 1$. (Cf. Fig. 3.2.13.)

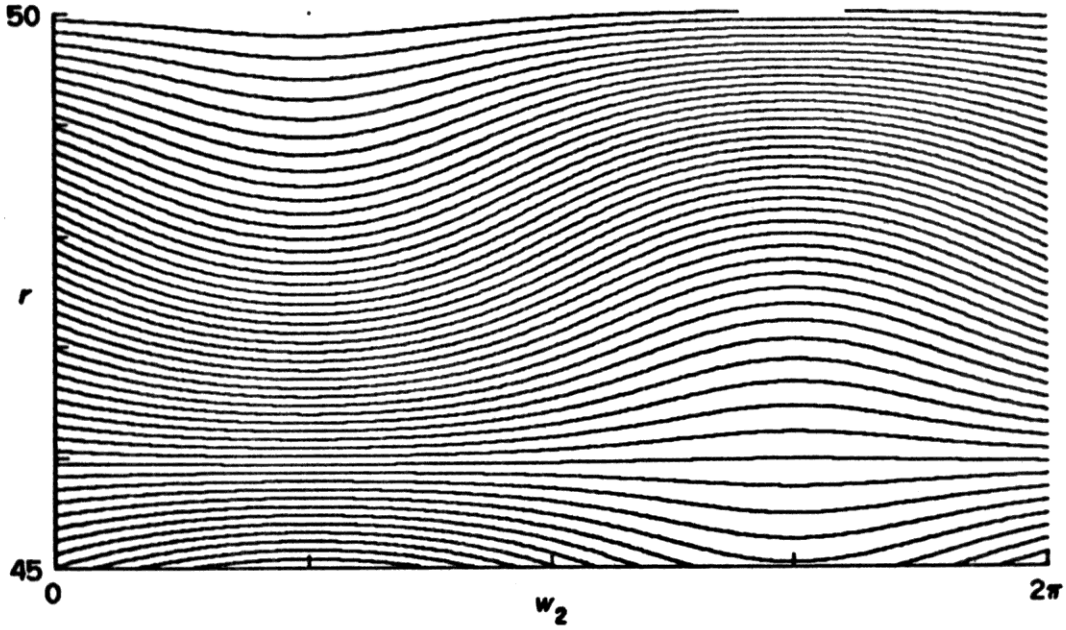

Figure 4.2.9. Same as Fig. 4.2.1, but $\nu = 30.47$ and $\alpha = 2.5$. (Cf. Fig. 3.2.14.)

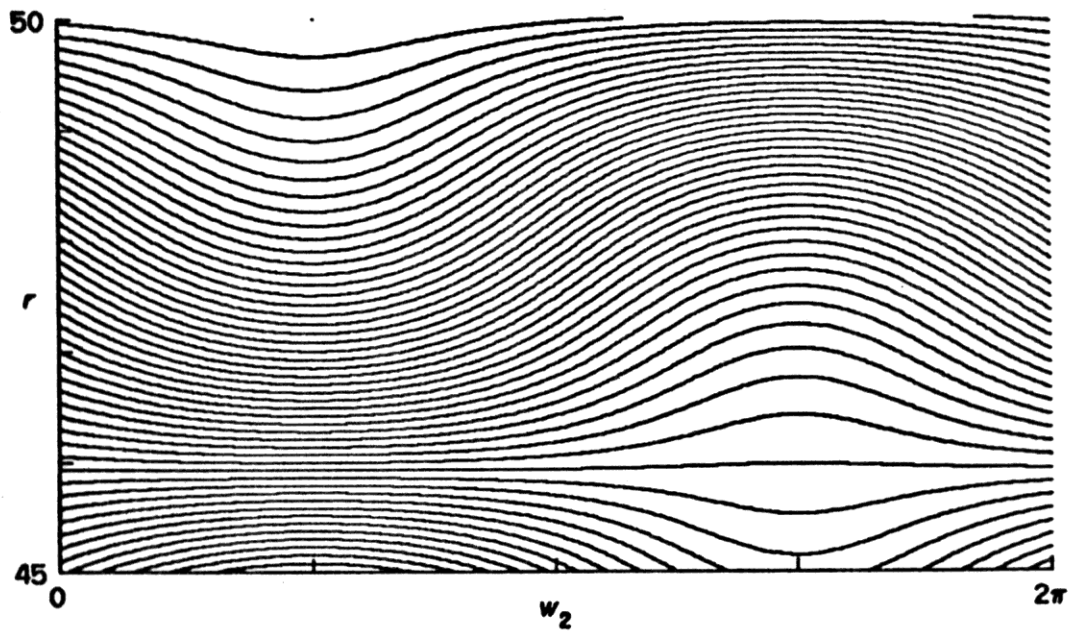

Figure 4.2.10. Same as Fig. 4.2.1, but $\nu = 30.47$ and $\alpha = 3.5$. (Cf. Fig. 3.2.15.)

would consider particles with a constant $H = h$ and at a constant w_1 ($= \pi$, in our case), and we would plot the conjugate coordinates, I_2 and w_2. Again the specification of H, w_1, w_2, and I_2 is enough to fully specify the state of the particle, since we can solve for I_1 from the equation for the Hamiltonian (4.1.11). It seems at first sight that requiring H to be a constant for all particles in the surface of section plot would overly restrict the class of particles we could study. However from (4.1.6) and (4.1.10) we have $I_2 = -(x + p_y)$, and so the value of the Hamiltonian in (4.1.11) can always be adjusted to a constant value, h, by suitably chosing the origin for x (a choice which merely results in a spatial translation of the entire trajectory). We may think of the Hamiltonian equations of motion as defining a mapping, T, of the (I_2, w_2) plane into itself over a period of w_1. Arnold and Avez (1968) prove that this mapping is *area-preserving*, i.e. that

$$\oint_\gamma I_2 dw_2 = \oint_{T\gamma} I_2 dw_2. \tag{4.3.1}$$

where γ is a closed curve in the (I_2, w_2) plane and $T\gamma$ is the result of mapping it. We may use (4.3.1) to determine the corresponding area conservation theorem for the surface of section, (r, w_2), used in Sec. 3.2, since these coordinates are related to (I_2, w_2) by

$$w_2 = w_2, \quad I_2 = (h - \tfrac{1}{2}r^2 - \alpha \sin w_2)/\nu, \tag{4.3.2}$$

where we have used the fact that $H = h$ and $w_2 = \pi$ in (4.1.11). The Jacobian for this transformation is $\partial I_2/\partial r = -r/\nu$; so (4.3.1) becomes

$$\oint_\gamma \tfrac{1}{2}r^2 dw_2 = \oint_{T\gamma} \tfrac{1}{2}r^2 dw_2. \tag{4.3.3}$$

We note the integrals express the area of a closed curve when r and w_2 are plotted in polar coordinates.

The study of the Hamiltonian equations is equivalent to the study of the area-preserving mapping, T, of Σ. We will begin by discussing the case where ν is not close to an integer. In the

limit $\alpha \to 0$ the T is given by

$$r \leftarrow r, \quad w_2 \leftarrow w_2 + 2\pi\nu, \tag{4.3.4}$$

i.e. Σ (plotted in polar coordinates) is rotated by $2\pi\nu$. The angle of advance of w_2 is independent of r, because, in the limit of $\alpha \to 0$, the Hamiltonian (4.1.11) describes two harmonic oscillators. A circle is an invariant curve under the mapping (i.e. r is a constant of the motion); however, unless ν is rational (a set of measure zero), there are no *fixed points* of the mapping; that is there are no points for which $T^p(r, w_2) = (r, w_2)$, where p is an integer. (Of course the point $r = 0$ is a fixed point in this case; however we will omit this from the discussion.)

As α is increased to a finite value the mapping (4.3.4) is perturbed. If α is small enough, there are still curves that are mapped into themselves, and the curves are close to circles (see Figs. 3.2.2, 3.2.10, and 3.2.13, but remember that these are plotted in cartesian rather than polar coordinates). The new invariant curves are described by the perturbed action $\tilde{I}_1$ (4.2.15). In addition, the angle by which the invariant curves are rotated upon applying T is perturbed, and becomes a function of r. As we will see later this arises from a nonlinear shift in the cyclotron frequency, $\dot{w}_1$, in which case the mean angle by which the curve is rotated is $2\pi\nu/\langle\dot{w}_1\rangle$. If $\nu/\langle\dot{w}_1\rangle$ is a rational number, s/p, then to lowest order in α, all of the points on some of the invariant curves become p^{th} order fixed points, so that each point of the curve maps onto itself on applying T^p. Such curves of fixed points are highly susceptible to perturbations. The effect of perturbations is to cause only $2p$ of the points to remain fixed points. Half of them are *elliptic* fixed points around which *islands* form (for instance, see the numbered islands in Fig. 3.2.3), while the other half are *hyberbolic* fixed points, lying on the seperatix between the island chain and the unperturbed invariant curves. In Fig. 4.3.1 we show a typical chain of islands with the fixed points marked. The elliptic and hyberbolic fixed points are also called "O" and "X" points for obvious reasons. Near the elliptic fixed points the mapping, T^p, is stable. On successive aplications of T^p a particle maps an an ellipse with its center at the elliptic fixed point. However

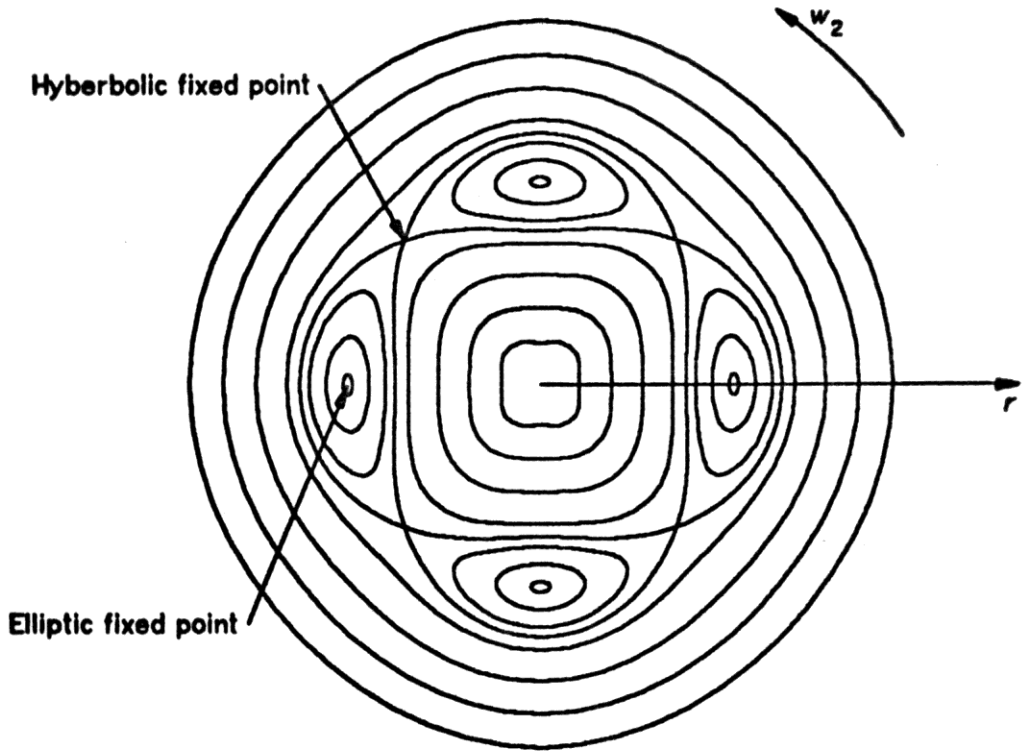

Figure 4.3.1. Schematic diagram showing 4th order islands in Σ and the elliptic and hyberbolic fixed points.

the mapping, T^p, at the hyberbolic fixed points is unstable; particles starting close to the fixed point move away from it on a hyperbolic path whose asymptote is the separatrix bounding the islands. It is clear that the motion of the particle near the separatrix can be grossly changed by a small perturbation; indeed an arbitrarily small perturbation can kick it out of or into the island system. In fact in the presence of perturbations, the motion becomes stochastic in a band centered at the separatrix (again see Figs. 3.2.3, 3.2.11, 3.2.14). The way to picture this is as follows: The motion of the particle under a mapping of T^p is that of an anharmonic oscillator about the elliptic fixed point. The frequency of the oscillator, defined as the mean angle advance around the elliptic point for each application of T^p, decreases as the sepatrix is approached, and is zero on the separatrix (because the separatrix contains fixed points). Now whenever this frequency is a rational number, s'/p', the corresponding island maps onto itself under the mapping $T^{pp'}$. But by the same argument as before such a island will turn into a chain of p' sub-islands. As the separatrix of the main island chain is approached there are infinitely many chains of these sub-islands. The picture repeats itself indefinitely, each sub-island supporting its own set of sub-sub-islands, etc. There are two ways of viewing how this process leads to stochasticity. One is to say that the infinite series of islands chains have an infinite number of hyberbolic fixed points associated with them; these constitute "scatterers" for the motion in phase space, making it a random walk. The other point of view to take is to say that when the sub-islands are too close together (e.g. near the separatrix) they "overlap" destroying their structure and leading to stochasticity. This latter view leads to a method for computing the fraction of phase space that is stochastic. If the size and position of all the sub-islands can be determined, then we can compute where they overlap. The method is of necessity non-rigorous because when we can really only speak of islands before the motion becomes stochastic. The normal procedure is to neglect the influence of neighboring islands when finding the size of a particular chain of islands.

The same mechanism that causes the motion to become stochastic near the separatices, also is reponsible for the gross stochasticity observable in Figs. 3.2.4, 3.2.12, and 3.2.15. As the field

increases, the perturbations, that caused the line of fixed points to turn into a chain of islands, grows, leading to a growth of the islands. (This is not necessarily visible in the surface of section plots, since the stochastic bands about the separatrix also grow, "eating" away at the islands.) The other thing that happens it that more chains of islands appear as $\langle \dot{w}_1 \rangle$ is perturbed more by the wave. At what we define as the "stochasticity threshold" these two phenomena lead to the overlap of the islands. Above this field the motion is stochastic over a large range of velocity space (larger that the period of oscillation of the Bessel functions in Sec. 2.2).

The situation when ω is close to a cyclotron harmonic (ν close to an integer) has been recently treated by Fukuyama *et al.* (1977). It differs in important respects from that presented above. If we look at Fig. 3.2.7 we see that there are large first order islands present, even for small α. These islands occupy most (all, if ν is an integer) of phase space. Furthermore they do not grow to the point where they overlap. Thus the mechanism by which the stochasticity threshold is reached in this case is by the growth and overlap of the sub-islands within the first order islands. Their growth causes a band near the separatrix in Fig. 3.2.7 to become stochastic (see Fig. 3.2.8). Eventually this band grows until a substantial part of the first order islands is stochastic. Since the first order islands constitute such a large fraction of phase space, this allows particles to travel freely throughout most of phase space (see Fig. 3.2.9). In their paper, Fukuyama *et al.* (1977) were able find the size and location the sub-islands in this case, and hence the condition for their overlap and the stocasticity threshold. We have given steps leading to their threshold in Appendix B.

To summarize: When ν is close to an integer, n, there is only one primary resonance in effect $\nu = n\langle \dot{w}_1 \rangle$. This leads to large first order islands. The motion becomes stochastic because the sub-islands within the first order islands overlap, destroying most of the first order islands. If ν is not close to an integer, there are higher order islands of many different orders possible. These are caused by the resonance $\nu/\langle \dot{w}_1 \rangle = s/p$. The motion becomes stochastic when enough of these islands appear, and when they have sufficient size, to cause them to overlap each other.

In the next section we will present the calculation of the threshold for and location of the higher order islands in the case where ν is not close to an integer. It turns out that the nonlinear shift in $\langle \dot{w}_1 \rangle$ which leads to the fixed points is $O(\alpha^2)$. The perturbation that gives the islands themselves is higher order in the field. Thus we do not compute the size of the islands. So the analysis we present is only part of what is required to find the stochasticity threshold analytically. We will turn to the numerical simulations to complement the analysis we have done, and the combination enables us to find an analytic form for the stochasticity threshold.

Section 4.4. Derivation of Island and Stochasticity Thresholds.

In order to find the pth order islands, we must find the pth order fixed points. These in turn are found by setting

$$\langle \dot{w}_1 \rangle / \langle \dot{w}_2 \rangle = \langle \dot{w}_1 \rangle / \nu = p/s, \tag{4.4.1}$$

where s and p are integers and the (time) average is performed over p cyclotron orbits (or, equivalently, s wave periods). We have also noted that $w_2 = \nu t + \phi$ (4.1.17). A particle satisfiying (4.4.1) will complete s wave periods (the short way round the torus in Fig. 3.2.1) in exactly p cyclotron orbits (the long way round), and so its trajectory is a fixed point of T^p. (We use the term "cyclotron orbits" to denote the time it takes the ion to complete a cyclotron orbit. The term "cyclotron period" bears with it the connotation of the constant time 2π.)

We begin by looking at the first order fixed points for which $p = 1$ and $s = n$. These may be derived directly from the Hamiltonian $\hat{H}$ (4.2.12) by noting that (4.4.1) implies that $\langle \dot{\hat{w}}_1 \rangle = 0$. We take an equivalent route here and derive the threshold from the Hamiltonian H (4.2.1). We chose this procedure because it is somewhat easier to extend it to the derivation of higher order islands. We computing $\dot{w}_1$ from $\partial H / \partial I_1$ so that

$$\dot{w}_1 = 1 - \alpha \Sigma_m (\partial/\partial I_1) J_m(\sqrt{2I_1}) \sin(mw_1 - w_2). \tag{4.4.2}$$

In order to compute the average of (4.4.2), we begin by assuming that I_1 is constant and that $n\dot{w}_1 = \dot{w}_2 = \nu$ (we will check these assumptions *a posteriori*). The average commutes with the Bessel function, and we have

$$\langle \sin(mw_1 - w_2) \rangle = \sin(nw_1 - w_2)\, \delta_{mn}, \tag{4.4.3}$$

Taking the average of (4.4.2) we obtain

$$\langle \dot{w}_1 \rangle = 1 - \alpha (\partial/\partial I_1) J_n(\sqrt{2I_1}) \sin(nw_1 - w_2). \tag{4.4.4}$$

In order to find the threshold for first order islands, we substitute (4.4.4) into (4.4.1) and take $\sin(nw_1 - w_2) = \pm 1$. Solving for α gives

$$\alpha = \left| \frac{r}{nJ_n'(r)} \delta \right|. \tag{4.4.5}$$

where as before $\delta = \nu - n$ (2.4.2) and $r = \sqrt{2I_1}$ (4.2.16). This is of course the same as the result of Sigmar and Callen (1971) given in (2.4.8), with the replacement of ν by n. Indeed this is just to be expected, for each gives the condition for there to be an integral number, n, of wave periods per cyclotron orbit. Equation (4.4.5) tells us the location of the islands. The threshold is minimized by chosing r at an extremum of $J_n'(r)/r$. To check the assumptions we made, we note that in fact $I_1 = \text{const} + O(\alpha)$ and $n\dot{w}_1 = n + O(\alpha) = \nu + O(\alpha)$, where the latter equality results from $\delta = O(\alpha)$ (4.4.5). Thus the assumptions we made are shown to be justified and terms missing in (4.4.4) are $O(\alpha^2)$ and may be neglected.

An alternative derivation of the threshold for first order islands is to observe that they must always form around the extrema of $\tilde{I}_1$, (4.2.15), in the (I_1, w_2) plots of Sec. 4.2. Setting $\partial\tilde{I}_1/\partial I_1 = \partial\tilde{I}_1/\partial w_2 = 0$ in (4.2.15) we obtain $\cos w_2 = 0$ [there are other roots for w_2 but these

correspond to the saddle points of (4.2.15)], and then α is given by

$$\alpha = |\Sigma_m (m/r)(-1)^m J_m'(r)/(m - \nu)|^{-1}. \tag{4.4.6}$$

For ν close to an integer n, only the $m = n$ term contributes in (4.4.6), and (4.4.6) reduces to (4.4.5). It is clear the (4.2.15) also tells the *size* of the first order islands, as can be readily seen from the plots of Sec. 4.2.

We have a problem when trying to find the higher ($p > 1$) order islands, because the sum in (4.2.1) contains no terms that don't average to zero for the higher order islands. This problem is resolved by making the canonical transformation given by (4.2.2), for by computing the Hamiltonian correct to $O(\alpha^2)$ we will find that there is a angle *independent* term proportional to α^2 (which obviously survives the averaging process). We begin with the form of $\tilde{H}$ given in (4.2.7) which, although exact, is not in the proper form. To put it in the proper form we substitute for w_1 using (4.2.3) so that to order α^2

$$\tilde{H} = \tilde{I}_1 + \nu\tilde{I}_2 - \alpha^2 \sum_{m,k} \frac{J_k'[(2\tilde{I}_1)^{1/2}]J_m[(2\tilde{I}_1)^{1/2}]}{(2\tilde{I}_1)^{1/2}} \frac{m}{k - \nu} \cos(m\tilde{w}_1 - \tilde{w}_2)\cos(k\tilde{w}_1 - \tilde{w}_2). \tag{4.4.7}$$

Here we have assumed that $I_1 = \tilde{I}_1 + O(\alpha)$ and similarly for w_1. These assumptions break down for first order islands because of the presence of the $(n - \nu)$ denominators in (4.2.3) and (4.2.5) which, from (4.4.5), are of order α for first order islands. To find the threshold for higher order islands we compute $\langle \dot{w}_1 \rangle$ using $\langle \dot{w}_1 \rangle = \langle \dot{\tilde{w}}_1 \rangle = \langle \partial\tilde{H}/\partial\tilde{I}_1 \rangle$. If $p \neq 2$ then only the $m = k$ terms do not average to zero giving

$$\langle \dot{w}_1 \rangle = 1 - \frac{\alpha^2}{4} \sum_{m=-\infty}^{\infty} \frac{\partial^2 J_m^{\,2}[(2\tilde{I}_1)^{1/2}]}{\partial\tilde{I}_1^{\,2}} \frac{m}{m - \nu}. \tag{4.4.8}$$

(We have managed to write this more compactly by introducing an additional derivative operator.)

For $p = 2$ ($s = 2n + 1$) there are additional contributions to the average from the terms satisfying $m + k = s$ which add

$$-\frac{\alpha^2}{2}\sum_{m=-\infty}^{\infty}\frac{\partial}{\partial\tilde{I}_1}\left[\frac{J_m J_{s-m}'}{(2\tilde{I}_1)^{1/2}}\right]\frac{m}{s-m-\nu}\cos(s\tilde{w}_1-2\tilde{w}_2) \tag{4.4.9}$$

to the right hand side of (4.4.8). [The argument to the Bessel functions is $(2\tilde{I}_1)^{1/2}$.] To find the effect of (4.4.9) on $\langle\dot{w}_1\rangle$, we evaluate it with $\nu \approx n+\frac{1}{2}$ [where we expect the second order ($p=2$) islands to be important] and in the limit of $r \gg \nu$ (in this limit $J_m' \approx J_{m-1} \approx -J_{m+1}$). Keeping only the $m=n$ and $n+1$ terms, which have the smallest denominators, (4.4.9) evaluates to

$$-\frac{\alpha^2}{2}\frac{\partial}{\partial\tilde{I}_1}\left[\frac{J_n^2+J_{n+1}^2}{(2\tilde{I}_1)^{1/2}}\right]2n\cos(s\tilde{w}_1-2\tilde{w}_2). \tag{4.4.10}$$

Now successive Bessel functions behave as either sines or cosines. This means that the numerator in (4.4.10) is approximately constant, having only an overall $1/r$ dependence. (We have checked this point numerically, still keeping only two terms of the sum, but not assuming that $r \gg \nu$, and we find that it is true even when $r \approx \nu$.) Thus, on taking the derivative, we see that (4.4.10) will be reduced by a factor of r; this is to be constrasted with the sum in (4.4.8), which as we will see is not reduced when the derivatives are taken.

To compute the threshold for islands we merely susbtitute (4.4.8) into (4.4.1) to find that

$$\alpha^2 = -\frac{\epsilon}{\nu}\left[\frac{1}{4}\sum_{m=-\infty}^{\infty}\frac{\partial^2 J_m^2[(2\tilde{I}_1)^{1/2}]}{\partial\tilde{I}_1^2}\frac{m}{m-\nu}\right]^{-1}, \tag{4.4.11}$$

where

$$\epsilon = \nu - s/p. \tag{4.4.12}$$

Note that in general $\alpha = o(\delta)$ at the threshold for higher order islands. This checks out with the assumption we made earlier that $\tilde{I}_1$ and $\tilde{w}_1$ differed from the original variables by $O(\alpha)$.

Note that at this stage we are not able to give the size of the higher order islands (with the possible exception of second order islands). For the first order islands, the term which gave the shift in the cyclotron frequency was angle dependent and this was the needed perturbation to

create the islands. However for the higher order islands it is an angle independent term that causes the cyclotron frequency shift. Thus all the points at a given $\tilde{I}_1$ constitute p^{th} order fixed points. What is required is to find the additional perturbation that breaks this line of fixed points up into islands. The form of perturbation necessary has the form $\sin|\cos(s\tilde{w}_1 - p\tilde{w}_2)$. Such a perturbation will yield the size of the higher order islands using a generating function similar to (4.2.10). To order α^2 there are only the angle dependent terms that give the size for first and second order islands. For arbitrary order islands it is not clear to what order we must go in order to obtain the necessary perturbation. Thus while we know at what field arbitrary order islands appear and at what $\tilde{I}_1$ they form at a given field, we have not yet been able to determine their size.

In order to better understand the formulas for the nonlinear cyclotron frequency shift, (4.4.4) and (4.4.8), and the island thresholds, (4.4.5) and (4.4.11), we examine them in various limits. Firstly we expand the Bessel functions in the limit $r \gg \nu$ (eq. 9.2.1, Abramowitz and Stegun, 1964). In this limit the frequency shift giving first order islands, (4.4.4), becomes

$$\langle \dot{w}_1 \rangle = 1 - \alpha\sqrt{2/\pi}\, r^{-3/2} \sin(r - \tfrac{1}{2}\nu\pi - \tfrac{1}{4}\pi)\, \sin(nw_1 - w_2). \tag{4.4.13}$$

The threshold for first order islands derived from this is minimized by letting both sine factors have unit magnitude giving

$$\alpha = \left|\frac{\sqrt{\pi}r^{3/2}}{\sqrt{2}n}\delta\right|. \tag{4.4.14}$$

In order to put (4.4.8) in a simple form we make the additional assumption that $\nu \gg 1$. It is easily verified that

$$\tfrac{1}{4}\partial^2 J_m{}^2[(2\tilde{I}_1)^{1/2}]/\partial\tilde{I}_1{}^2 \approx -\sin(2r)\,(-1)^m/(\pi r^3), \tag{4.4.15}$$

where we have used the fact that $\tilde{I}_1 \approx I_1 = \frac{1}{2}r^2$. The terms left in the sum in (4.4.8) are then

$\Sigma_m (-1)^m m/(m - \nu)$. The major contribution to the sum comes from the terms such that $m \approx \nu$, in which case the factor of m may be replaced by ν, leaving $\Sigma_m (-1)^m/(m - \nu)$. Now this is just the partial fraction expansion of the cosecant function (eq. 4.3.93, Abramowitz and Stegun, 1964). The expression for $\langle \dot{w}_1 \rangle$ becomes

$$\langle \dot{w}_1 \rangle = 1 - \alpha^2 \frac{\sin(2r)}{\sin(\pi\nu)} \frac{\nu}{r^3}. \tag{4.4.16}$$

The island threshold is then

$$\alpha^2 = -\epsilon \frac{\sin(\pi\nu)}{\sin(2r)} \frac{r^3}{\nu^2}. \tag{4.4.17}$$

Unfortunately the asymptotic expansion is only valid for $r/\nu \gg 1$. Since we are interested in $\nu \gg 1$, this places a severe restriction on r. We would like to be able to extend the above results to the region $r > \nu$. To do this we use the approximations (2.4.9) and (2.4.10). Numerically comparing (2.4.9) with the Bessel function indicates that it is an excellent approximation for r larger than the first maxima the Bessel function. From eq. 9.3.23 of Abramowitz and Stegun (1964) the first maxima of the Bessel function of order ν is at $\nu + (\frac{1}{2}\nu)^{1/3}$; so (2.4.9) is valid for $r > \nu + (\frac{1}{2}\nu)^{1/3}$. This approximation is readily incorporated into (4.4.13) and (4.4.14), giving for the threshold

$$\alpha = \left| \frac{\sqrt{\pi} r^2}{\sqrt{2} n (r^2 - n^2)^{1/4}} \delta \right|. \tag{4.4.18}$$

For higher order islands the situation is slightly more complicated. The typical Bessel function term in (4.4.8) now reads

$$\tfrac{1}{4}\partial^2 J_m{}^2[(2\tilde{\gamma}_1)^{1/2}]/\partial\tilde{\gamma}_1{}^2 \approx -\sin\{2[(r^2 - m^2)^{1/2} - m\cos^{-1}(m/r)]\}\,(r^2 - m^2)^{1/2}/(\pi r^4). \tag{4.4.19}$$

The sum is more difficult, reading $\mathfrak{Im}\ \Sigma_m \exp\{2[]\}/(m - \nu)$, where we have brought all the slowly varying functions of ν outside the sum (replacing m by ν), and the phase factor in []'s in (4.4.19) should be placed in the exponential function. The sum may be computed by making a Taylor

series expansion of the phase term in []'s in m about $m = \nu$, and keeping only the first two terms. The resulting expression for $\langle \dot{w}_1 \rangle$ is

$$\langle \dot{w}_1 \rangle = 1 - \alpha^2 \frac{\sin\{2[(r^2 - \nu^2)^{1/2} + \nu \sin^{-1}(\nu/r)]\}}{\sin(\pi\nu)} \frac{\nu(r^2 - \nu^2)^{1/2}}{r^4}. \tag{4.4.20}$$

From (4.4.20) we derive the threshold

$$\alpha^2 = -\epsilon \frac{\sin(\pi\nu)}{\sin\{2[(r^2 - \nu^2)^{1/2} + \nu \sin^{-1}(\nu/r)]\}} \frac{r^4}{\nu^2(r^2 - \nu^2)^{1/2}}. \tag{4.4.21}$$

Note that (4.4.18) and (4.4.21) give the same scaling for α on both ν and r.

The last limit to consider is $r \approx \nu$ and $\nu \gg 1$. For this we need the intermediate argument expansions of the Bessel function and its derivative (eqs. 9.3.23 and 9.3.27, Abramowitz and Stegun, 1964). The magnitude of $J_n'(r)$ has a maximum of $1.1/\nu^{2/3}$ at $r \approx n + 1.8\, n^{1/3}$. Substituting this into (4.4.5) we obtain

$$\alpha = \left| \frac{\nu^{2/3}}{1.1} \delta \right|. \tag{4.4.22}$$

Since J_n' has its maximum amplitude (as a function of r) at this point, (4.4.22) gives the minimum threshold for first order islands at a given ν. For higher order islands we again compute, for $m \approx \nu$

$$\tfrac{1}{4}\partial^2 J_m{}^2[(2\tilde{I}_1)^{1/2}]/\partial\tilde{I}_1{}^2 \approx -2^{1/3} m^{-10/3}[R\,\mathrm{Ai}^2(-R) - \mathrm{Ai}'^2(-R)], \tag{4.4.23}$$

where $R = (r - m)(2/m)^{1/3}$ and we have used the differential equation governing the Airy function (eq. 10.4.1, Abramowitz and Stegun, 1964). We do not attempt to carry out the sum in this case, wishing only to find how the threshold scales with ν in this limit. So we assume that $\nu \approx n$ so that only the $m = n$ contributes in (4.4.23). Taking $r \approx n + 1.8\, n^{1/3}$, where the combination of Airy function in []'s in (4.4.23) has a maximum, we obtain a threshold of

$$\alpha = \frac{\nu^{2/3}}{0.8} \sqrt{\epsilon\delta}. \tag{4.4.24}$$

Again note that (4.4.24) has the same scaling as (4.4.22). In fact, we obtain nearly the correct threshold for first order islands by setting $\epsilon = \delta \ll 1$ in any of (4.4.17), (4.4.21) or (4.4.24). The resulting expressions for α overestimate the thresholds given by the correct expression for the first order islands, (4.4.14), (4.4.18) and (4.4.22) by a factor of $\sqrt{2}$.

To illustrate these results more graphically we plot in Fig. 4.4.1 $\langle \dot{w}_1 \rangle$ as given by (4.4.4) and (4.4.20) for the parameters in Fig. 3.2.4 (at these parameters the motion has just become stochastic). As α increases the curve of $\nu/\langle \dot{w}_1 \rangle$ grows away from the line $\langle \dot{w}_1 \rangle = 1$. This causes new islands to appear, and crowds up the existing islands. At the stochasticity threshold this causes the islands to overlap, leading to their breakup, with its attendent stochasticity.

Figure 4.4.2 shows the dependence of the island thresholds on ν. We have plotted (4.4.18) and (4.4.21) (with the sin term equal to unity) against ν for $29\frac{1}{2} < \nu < 30\frac{1}{2}$, for various s/p and for $r \approx 47.5$ (the middle of the r scale in the plots of Sec. 3.2). We also show some numerically observed island thresholds. Note that the analytic thresholds are in good agreement with the numerical ones. Note that for α large many islands are predicted for all ν, not very close to n (= 30). In this figure we have also given the numerically observed stochasticity thresholds. Note that this field is insensitive to δ varying by about 20% for δ between $-\frac{1}{2}$ and $\frac{1}{2}$. Now the island thresholds (4.4.5) and (4.4.11) consist of a slowly varying factor which depends on r and ν multiplying a function of δ and ϵ. The stochasticity threshold will likewise consist of the same factor of r and ν multiplying some function of δ [ϵ is only defined in reference to a particular chain of islands (4.4.12)]. The evidence of Fig. 4.4.2 is that this function of δ is essentially a constant. Thus to obtain an analytic expression for the stochasticity threshold we just take the either (4.4.18) or (4.4.21) and replace δ and ϵ by appropriate constants. (It won't matter which equation we do this to, since they both have the same scaling with r and ν.) For instance we can substitute $\delta = \frac{1}{4}$ into (4.4.18) observing that for this δ the stochasticity theshold coincides with the threshold for first order islands. We can further generalize this result for arbitrary r by sustituting $\delta = \frac{1}{4}$ into the more general equation, (4.4.5), to give

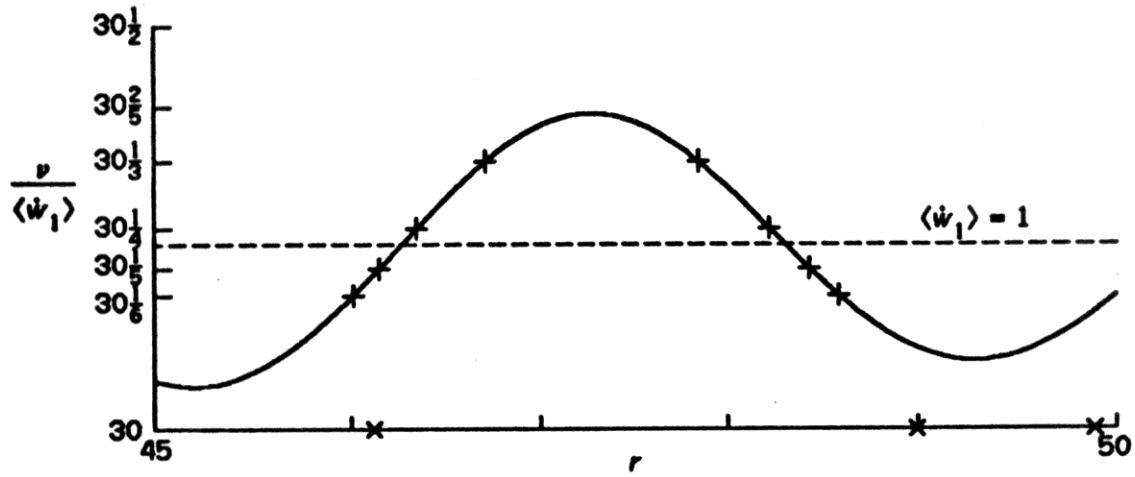

Figure 4.4.1. Plot of $\nu/\langle \dot{w}_1 \rangle$ for higher order islands as given by (4.4.20) for $\nu = 30.23$ and $\alpha = 4$ (cf. Fig. 3.2.4). The plusses (+) indicate the values of r for which $\langle \dot{w}_1 \rangle$ is a simple rational multiple of ν, and where higher order islands form. The crosses (x) show the positions for first order islands as given by (4.4.5).

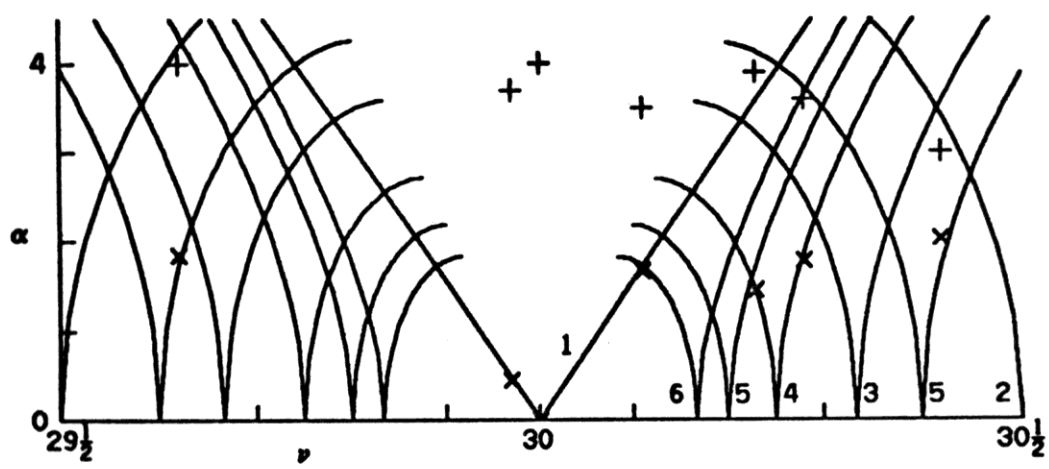

Figure 4.4.2. The threshold α for the formation of islands of various orders (the numbers by the curves) for $r \approx 47.5$ as a function of ν. The lines give the analytically predicted values, (4.4.18) and (4.4.21), and the crosses (x) the numerically observed values. The plusses (+) give the numerically observed stochasticity thresholds.

$$\alpha > \left|\frac{r}{4\nu J_\nu'(r)}\right|. \tag{4.4.25}$$

Again it doesn't matter whether we chose (4.4.5) or (4.4.11) since we have seen that they scale the same way in all limits of interest. We have substituted ν for n here to emphasise that this result is not restricted to values of ν close to an integer. Since the stochasticity threshold is defined in terms of a substantial region of velocity space, the value of J_ν' with the oscillatory part factored out should be used. As with the island thresholds the various limits of (4.4.25) can be found. For $r \gg \nu$ we see that (4.4.25) is the same as the loop overlap condition for the iterated equations, (2.4.16), except that $Q(\delta)$ (Fig. 2.4.5) is replaced by $\frac{1}{4}$. In the limit $r \gg \nu$, (4.4.25) is nearly the same as the result of Fukuyama *et al.* (1977) [see (B.31) and (B.32) in Appendix B]. Their result is only valid in this limit and has factor of 0.15 in the place of the $\frac{1}{4}$ in (4.4.25). As we explained in Sec. 4.3 their results are obtained by finding the overlap of the sub-islands within the large first order islands, so their results are valid only close to a cyclotron harmonic; specifically they require $\delta \ll 0.15$. Of particular interest is the minimum threshold for a given ν. We obtain this by substituting $r \approx \nu$ into (4.4.25) to give

$$\alpha = \nu^{2/3}/4, \tag{4.4.26}$$

or in unnormalized terms,

$$\frac{E_0}{B_0} = \frac{1}{4}\left(\frac{\Omega}{\omega}\right)^{1/3}\frac{\omega}{k}. \tag{4.4.27}$$

Equation (4.4.25) can also be used to determine the region of velocity space that is stochastic. For instance the upper limit can be found expanding (4.4.25) in the limit $r \gg \nu$ and solving for r, giving

$$r = (4\alpha\nu)^{2/3}(2/\pi)^{1/3}. \tag{4.4.28}$$

Since the Bessel function cuts off extremely rapidly for $r < \nu$ the lower limit of the stochastic

region is approximately given by $r = \nu$. However the more strongly nonlinear effect of trapping (Sec. 3.1) is operative here. This allows particles within $\sqrt{\alpha}$ of ν to be accelerated into the stochastic region $r > \nu$. This lowers the lower limit of the stochastic region to

$$r = \nu - \sqrt{\alpha}. \tag{4.4.29}$$

In Fig. 4.4.3 we plot the limits of the stochastic region of velocity space as a function of α as given by (4.4.25) and (4.4.29) for a fixed ν.

As we have seen trapping occurs near $r = \nu$. Also this is the region of velocity space that becomes stochastic first, at a field given by (4.4.26). This suggests that we should be able to derive (4.4.26) from trapping considerations. Indeed this is so, and the scaling of (4.4.26) may be derived if we state that the motion becomes stochastic when trapping is "effective." We define "effective" here to mean that the particle spends at least a trapping bounce time in the trapping region. The trapping region is given by $\dot{y} > \nu - \sqrt{\alpha}$ (see Fig. 4.4.4). The time a particle travelling at ν spends in this region is given by

$$2(2\nu\sqrt{\alpha})^{1/2}, \tag{4.4.30}$$

assuming $\sqrt{\alpha} \ll \nu$, which we can check *a posteriori*. The bounce time (inverse bounce frequency) is

$$1/\sqrt{\alpha}. \tag{4.4.31}$$

Equating (4.4.30) and (4.4.31) gives (4.4.26), as required.

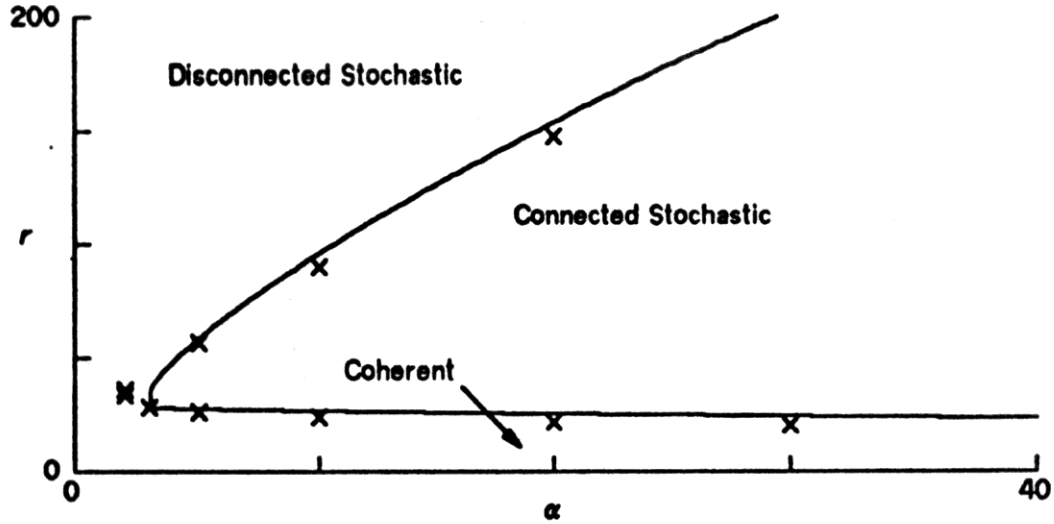

Figure 4.4.3. The limits of the stochastic region of velocity space as given by (4.4.25) and (4.4.29) for $\nu = 30.23$. The crosses (x) give the numerically observed values. The terms "Diconnected Stochastic" and "Connected Stochastic" are used to distinguish motion of the type shown in Figs. 3.2.3 and 3.2.4 respectively.

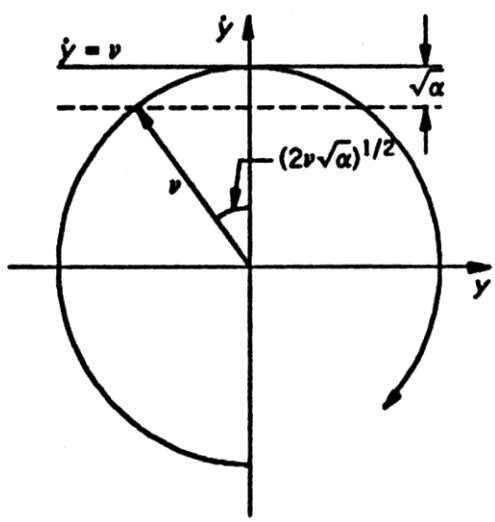

Figure 4.4.4. Derivation of stochasticity threshold in terms of trapping.

Section 4.5. Inclusion of Small Parallel Propagation.

The discussion up till now has been on the interaction of an ion with an electrostatic wave propagating exactly perpendicular to the magnetic field. This makes the analytic and numerical work considerably easier, since we can completely ignore the parallel motion. However lower hybrid waves used for RF heating always have a slight parallel component to their electric field (if they did not they would not penetrate the plasma). Thus if we are to determine the interaction of a particle with a lower hybrid wave, we must include the effect of parallel propagation.

First we must generalize our notation somewhat. We will normalize lengths to $|\mathbf{k}|^{-1}$; thus in normalized terms

$$\mathbf{k} = [0, \sin\theta, \cos\theta] = [0, \xi, \zeta], \tag{4.5.1}$$

where θ is the angle $\mathbf{k}$ makes with the magnetic field $B_0\hat{\mathbf{z}}$, and its direction cosines are ξ and ζ. The normalized electric field is given by $\alpha = qkE_0/(m\Omega^2)$. As a vector $\bar{\alpha}$ is given by

$$\bar{\alpha} = [0, \xi, \zeta]. \tag{4.5.2}$$

The equation of motion is then

$$\frac{d\mathbf{v}}{dt} = \bar{\alpha}\cos(\mathbf{k}\cdot\mathbf{r} - \nu t - \phi) + \mathbf{v}\times\hat{\mathbf{z}}. \tag{4.5.3}$$

As in Sec 2.1 the x component of (4.5.3) may be integrated to give $\dot{x} = y$, giving for the other components

$$\ddot{y} + y = \xi\alpha\cos(\xi y + \zeta z - \nu t - \phi), \tag{4.5.4}$$

$$\ddot{z} = \zeta\alpha\cos(\xi y + \zeta z - \nu t - \phi). \tag{4.5.5}$$

Now for ζ sufficiently small (in a sense we will make precise in a moment) we can replace (4.5.5)

by $\ddot{z} = 0$. Then the solution for z is

$$z = z_0 = v_{\parallel} t + \text{const}, \tag{4.5.6}$$

where $v_{\parallel}$ is a constant. Now if (4.5.6) is substituted into (4.5.4), it is clear that the constant may be absorbed into the ϕ. The resulting equation reads

$$\ddot{y} + y = \xi\alpha\cos[\xi y - (\nu - \zeta v_{\parallel})t - \phi], \tag{4.5.7}$$

or multiplying by ξ

$$\xi\ddot{y} + \xi y = \xi^2\alpha\cos[\xi y - (\nu - \zeta v_{\parallel})t - \phi]. \tag{4.5.8}$$

If we compare (4.5.8) with the orbit equation (2.1.10) we see that (4.5.8) is identical if we make the following replacements in (2.1.10):

$$y \to \xi y, \;\; \alpha \to \xi^2\alpha, \;\; \nu \to \mu \equiv \nu - \zeta v_{\parallel}. \tag{4.5.9}$$

Thus the solution to (4.5.8) is the same as (2.1.10). Making the above replacements in (4.4.25) we know that motion becomes stochastic above the stochasticity threshold

$$\alpha > \left|\frac{r\xi^{-1}}{4\mu J_{\mu}'(\xi r)}\right|. \tag{4.5.10}$$

Remember that (4.5.10) was derived assuming that $\ddot{z} = 0$. We must now go back and check for what parameters this is valid. To do this we solve for z by integrating (4.5.5) along unperturbed orbits ($y_0 = r\sin t$, $z_0 = v_{\parallel}t$), i.e. we solve

$$\begin{aligned}\ddot{z}_1 &= \zeta\alpha\cos(\xi r\sin t - \mu t - \phi)\\ &= \zeta\alpha\,\Sigma_m\, J_m(\xi r)\cos[(m - \mu)t - \phi],\end{aligned} \tag{4.5.11}$$

where $z = z_0 + z_1$, $z_1(t = 0) = 0$. As we know from Sec. 2.2 the solution to (4.5.11) is secular if $\mu = \ell$, an integer. We consider only this case as it leads to the largest values of z_1, and hence gives the tightest restriction on the validity of (4.5.10). Including only the $m = \ell$ term in (4.5.11) and taking the cosine term to be unity, we obtain

$$z_1 = \tfrac{1}{2}\zeta\alpha J_\ell(\xi r)t^2. \tag{4.5.12}$$

Now we argue that the stochastic nature of the motion for fields satisfying (4.5.10) is something that is established on the time scale of a cyclotron period. Thus as long as the phase factor ζz_1 appearing in the perpendicular equation of motion is small at $t = 1$ then the presence of this phase factor at later times won't alter the fact that the motion is stochastic. Expressing this condition as a condition on α we find that

$$\alpha \ll \left|\frac{2\zeta^{-2}}{J_\ell(\xi r)}\right|, \tag{4.5.13}$$

for (4.5.10) to be valid. The results of Smith and Kaufman (1975) are that the motion is stochastic if

$$\alpha > \left|\frac{\zeta^{-2}}{16J_\ell(\xi r)}\right|. \tag{4.5.14}$$

Thus we see that if (4.5.13) is not obeyed, so that the stochasticity condition (4.5.10) cannot be applied, the motion is still stochastic, since (4.5.14) is then satisfied. We may combine (4.5.10) and (4.5.14) to give the general stochasticity condition

$$\alpha > \mathrm{Min}\left[\left|\frac{\zeta^{-2}}{16J_\mu(\xi r)}\right|, \left|\frac{r\xi^{-1}}{4\mu J_\mu{}'(\xi r)}\right|\right]. \tag{4.5.15}$$

(For uniformity we have replaced ℓ by μ; this incurs negligible error.)

If Fig. 4.5.1 we plot what region of velocity space becomes stochastic as a function of α and at a constant θ, close to 90°. Since both of the terms in (4.5.15) rapidly become large for $\xi r < \mu$,

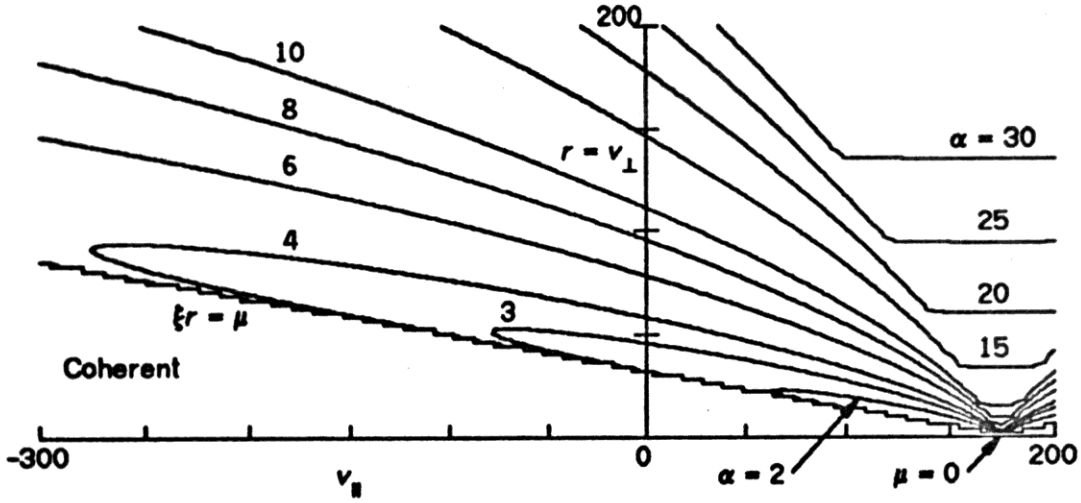

Figure 4.5.1. The stochastic regions of velocity space, as given by (4.5.15), for various α (marked by the curves), and for $\nu = 30.23$, $\theta = 80^\circ$. (The jaggedness is an artifact of the plotting routine.)

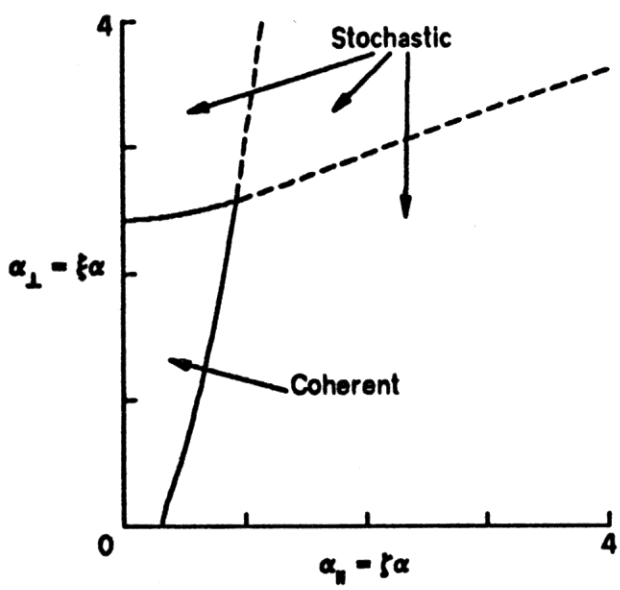

Figure 4.5.2. Variation of the stochasticity threshold with θ, as given by (4.5.16), for the region of velocity space $r \approx \nu/\xi$, $v_\parallel \approx 0$.

the motion is "never" stochastic in this region (although as we discussed in Sec 4.4, trapping does cause the edge of this region to become stochastic). At a particular α the stochastic region of velocity space is closed and has the line $\xi r = \mu$ as one of its boundaries. The region is symmetric about $v_{\parallel} = \nu\zeta^{-1}$ (i.e. $\mu = 0$). The boundaries that are nearly parallel to the $v_{\parallel}$ axis are due to the expression of Smith and Kaufman (1975), the first term in (4.5.15). The other boundaries are due to our result, the second term in (4.5.15).

To show the dependence of (4.5.15) angle we pick the region of velocity space $r \approx \nu/\xi$, $v_{\parallel} \approx 0$, i.e. just inside the $\xi r > \mu$ region. For ν large we use the appropriate limits of the Bessel functions (eqs. 9.3.23 and 9.3.27, Abramowitz and Stegun, 1964) (4.5.15) becomes

$$\alpha = \mathrm{Min}\left[\frac{\nu^{1/3}}{10\zeta^2}, \frac{\nu^{2/3}}{4\xi^2}\right] \tag{4.5.16}$$

(see Fig. 4.5.2). The second term is the smaller in (4.5.16) for $\zeta < 0.6\,\nu^{-1/6}$, approximately, or

$$\theta > \tfrac{1}{2}\pi - 0.6\,\nu^{-1/6}. \tag{4.5.17}$$

For lower hybrid waves ν is typically between 20 and 40, while ζ is around $\sqrt{m_e/m_i}$ ($\approx 1/40$ for hydrogen plasmas). Thus the second term is applicable in this case. Since ζ is small, $\xi \approx 1$ and (4.5.16) reduces to the original stochasticity threshold, (4.4.26).

Section 4.6. Inclusion of Weak Magnetic Field Inhomogeneity.

The other important effect omitted from our analysis thus far is magnetic field inhomogeneity. In tokamaks this inhomogeneity is primarily due to the $1/R$ drop-off of the toroidal magnetic field. However because of the complicated way the lower hybrid ray spirals around the tokamak (Kulp *et al.*, 1976), the inhomogeneity in general appears in all three of the coordinates our cartesian coordinate system (with $\hat{\mathbf{z}}$ along the magnetic field and $\mathbf{k}$ parallel to $\hat{\mathbf{y}}$). We would be surprised if weak inhomogeneity effected our results significantly for two reasons: the stochasticity condition (4.4.25) is not dependent on cyclotron harmonic resonances; and stochasticity is known to occur in many systems with inhomogeneous magnetic field (Dunnett *et al.*, 1968; Jaeger *et al.*, 1972; Lieberman and Lichtenberg, 1973). For these reasons we have not made an exhaustive study of the problem. We will consider here two special cases

(Case I)
$$\mathbf{B} = B_0(1 + \beta k y)\hat{\mathbf{z}}, \tag{4.6.1}$$

and

(Case II)
$$\mathbf{B} = B_0(1 + \beta k x)\hat{\mathbf{z}}. \tag{4.6.2}$$

where β is a measure of the change of $\mathbf{B}$ in a wavelength.

Considering first Case I where $\mathbf{B}$ is given by (4.6.1), we see that, as with the homogeneous magnetic field case (Sec. 2.1), the x component of the Lorentz force law is again trivially integrated to give

$$\dot{x} = y + \tfrac{1}{2}\beta y^2, \tag{4.6.3}$$

where as before we have set the integration constant to zero by choice of the y origin. The reason we able to do this is that the ∇B and $\mathbf{E}\times\mathbf{B}$ drifts are parallel to one another. Thus one component (y) of the guiding center position remains fixed. Substituting this into the y component

of the equation gives

$$\ddot{y} + y = \alpha\cos(y - \nu t - \phi) - \tfrac{3}{2}\beta y^2 - \tfrac{1}{2}\beta^2 y^3. \tag{4.6.4}$$

Since (4.6.4) is identical to (2.1.10), except that the force term has some additional terms. Therefore only a slight modification of the numerical routines used to integrate (2.1.10) is needed to integrate (4.6.4). In Figs. 4.6.1 and 4.6.2 we show the surface of section plots for $\beta = 10^{-3}$. We see in these plots the same behaviour as for $\beta = 0$. At intermediate fields there are chains of islands and part of phase space is stochastic. At higher fields the islands have overlapped, leading to widespread stochasticity.

In order to understand this behaviour in more detail we look at the Hamiltonian for the system. It is then readily ascertained that the Hamiltonian,

$$H = I_1 - \alpha\sin(\sqrt{2I_1}\sin w_1 - w_2) + \tfrac{1}{2}\beta(2I_1)^{3/2}\sin^3 w_1 + \tfrac{1}{8}\beta^2(2I_1)^2\sin^4 w_1, \tag{4.6.5}$$

where $y = \sqrt{2I_1}\sin w_1$, describes this system. We follow the same prescription given by Walker and Ford (1969) as we followed in Sec. 4.4. This enables us to put the angle dependent terms depending on β into some angle independent terms, and angle dependent terms which are $O(\beta^2)$. The transformed Hamiltonian becomes

$$H = I_1 - \tfrac{3}{4}\beta^2 I_1{}^2 + \nu I_2 - \alpha\sin(\sqrt{2I_1}\sin w_1 - w_2) + \beta^2 \text{ x (angle dependent terms)}. \tag{4.6.6}$$

Since β is small, the presence of the angle independent β^2 term does not effect the analysis presented in Sec. 4.4 deriving the first and higher order islands thresholds. Thus the effect of finite β is just to cause an additional shift in $\langle\dot{w}_1\rangle$ that get added into both (4.4.4) and (4.4.8). This additional shift is just

$$\Delta\langle\dot{w}_1\rangle = (\partial/\partial I_1)(-\tfrac{3}{4}\beta^2 I_1{}^2) = -\tfrac{3}{4}\beta^2 r^2. \tag{4.6.7}$$

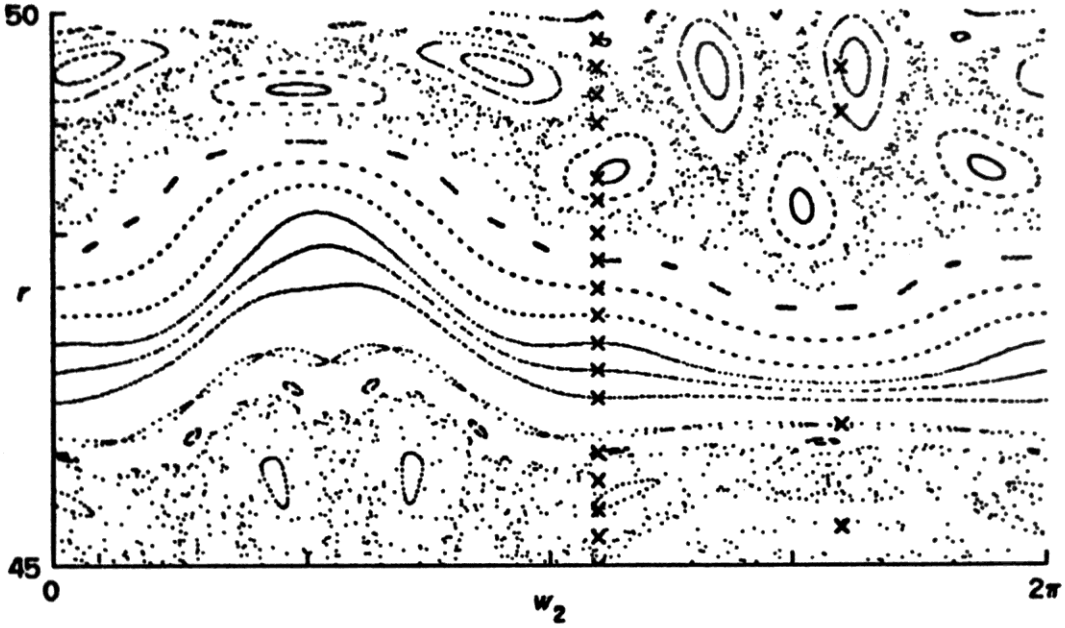

Figure 4.6.1. The surface of section, Σ, for $\nu = 30.23$, $\alpha = 2.4$, and magnetic field given by (4.6.1) with $\beta = 10^{-3}$. Crosses (x) denote the initial positions of the particles and dots (·) subsequent crossings. The particles are followed for 300 crossings of the $w_1 = \pi$ plane.

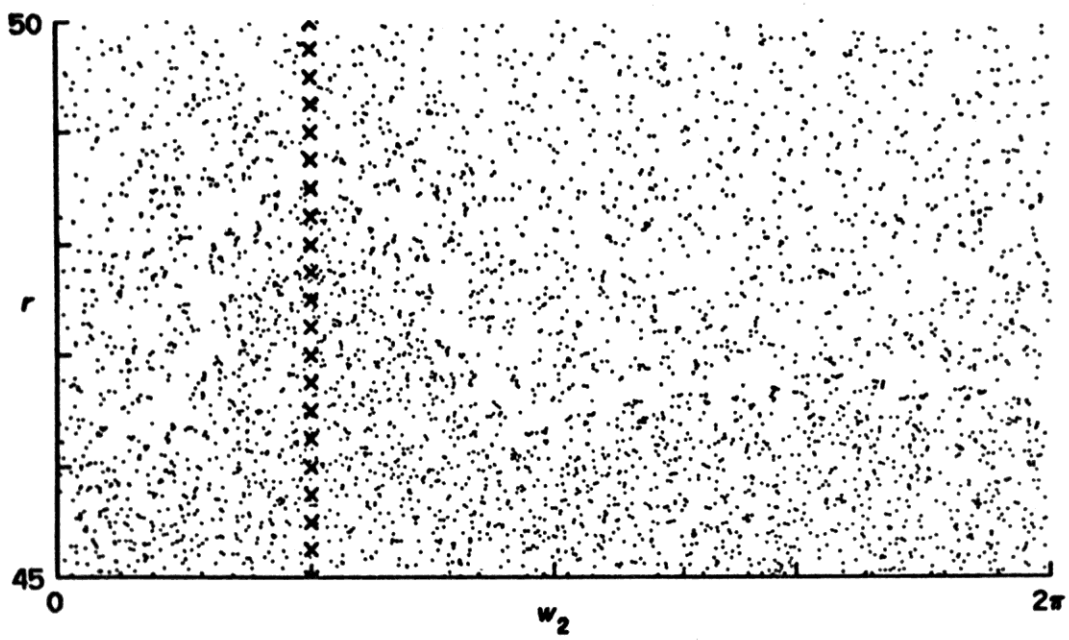

Figure 4.6.2. Same as Fig. 4.6.1, but $\alpha = 4$.

The shift in $\langle \dot{w}_1 \rangle$ is second order in β because the y coordinate of the guiding center is constant, and so to first order it samples a constant magnetic field. The corresponding change in $\nu/\langle \dot{w}_1 \rangle$ (see Fig. 4.4.1) is $\frac{3}{4}\beta^2 \nu r^2$. For the parameters of Figs. 4.6.1 and 4.6.2 this shift varies from 0.046 at $r = 45$ to 0.057 at $r = 50$. Since this shift does not vary much for the range of r plotted, we are effectively seeing in Fig. 4.6.1 the island structure characteristic of $\beta = 0$, $\alpha = 2.4$, and $\nu = 30.23 + 0.05 = 30.28$. In confirmation, we note that the two chains of fourth order islands visible in Fig. 4.6.1 are centered at around $r = 49$, where the sine factor in the denominator of (4.4.21) is positive, indicating that $\epsilon < 0$, and that the effective ν is greater that $30\frac{1}{4}$. Since the stochasticity condition is independent of δ, small changes in the effective wave frequency do not change the field at which the motion becomes stochastic.

The island structure is determined by $\nu/\langle \dot{w}_1 \rangle$; thus we may argue that the stochasticity thresholds (4.4.25) and (4.4.26) may be applied when $\beta \neq 0$ as long as the change in $\nu/\langle \dot{w}_1 \rangle$ due to β meets two conditions. Firstly the fractional change must be small compared to unity. Secondly the change in $\nu/\langle \dot{w}_1 \rangle$ when r changes by unity must be small. This latter condition is requirement that the islands cannot "feel" the effect of β over the scale length of the island structure (~ 1). Stated more concisely these conditions read

$$\beta \ll r^{-1} \text{ and } \beta \ll (\nu r)^{-1/2}. \tag{4.6.8}$$

For $r > \nu$ the first of these conditions is the more stringent. We may state it as follows: The fractional change of B over a Larmor radius must be small; a condition that is well satisfied in Tokamaks.

We turn now to Case II where the magnetic field is given by (4.6.2). In this case we cannot simply integrate either component of the Lorentz force equation, since the $\mathbf{E} \times \mathbf{B}$ motion due to the wave is perpendicular to the ∇B drift, so that neither component of the guiding center position is conserved. To derive the Hamiltonian we begin by writing down 4.1.1 with

$$\mathbf{A} = -B_0 y(1 + \beta k x)\hat{\mathbf{x}}. \tag{4.6.9}$$

We normalize the Hamiltonian as in Sec. 4.1, and transform it using the generating function

$$F_2 = (P_x - \nu t - \phi)(x + \tfrac{1}{2}\beta x^2) + P_y(y - \nu t - \phi + P_x) \tag{4.6.10}$$

[cf. (4.1.5)], and then using the generating function (4.1.8) to obtain

$$H = I_1 + \nu I_2 - \alpha \sin(\sqrt{2I_1}\sin w_1 - w_2) - \beta(I_2 + \sqrt{2I_1}\cos w_1)2I_1 \sin^2 w_1, \tag{4.6.11}$$

where

$$y = \sqrt{2I_1}\sin w_1 - w_2 + \nu t + \phi, \quad x + \tfrac{1}{2}\beta x^2 = -I_2 - \sqrt{2I_1}\cos w_1. \tag{4.6.12}$$

Note that $\dot{w}_2$ is no longer a constant. We again perform a transformation converting the β dependent terms in (4.6.11) into angle independent terms plus terms proportional to β^2. The resulting Hamiltonian reads

$$H = I_1 + \nu I_2 - \beta(I_2 + \tfrac{1}{2}\beta I_2{}^2)I_1 - \tfrac{3}{4}\beta^2 I_1{}^2 - \alpha \sin(\sqrt{2I_1}\sin w_1 - w_2)$$

$$+ \beta^2 \times \text{(angle dependent terms)}. \tag{4.6.13}$$

Evaluating $\langle \dot{w}_1 \rangle$ and $\langle \dot{w}_2 \rangle$ we find that

$$\langle \dot{w}_1 \rangle = 1 - \beta(I_2 + \tfrac{1}{2}\beta I_2{}^2) - \tfrac{3}{2}\beta^2 I_1 + (\alpha \text{ dependent terms}), \tag{4.6.14}$$

$$\langle \dot{w}_2 \rangle = \nu - \beta I_1(1 + \beta I_2). \tag{4.6.15}$$

There are new terms appearing in both expressions. The terms in ()'s in (4.6.14) arise because the $\mathbf{E}\times\mathbf{B}$ motion of the ion is parallel to the magnetic field gradient, and thus can move the particle's guiding center into regions of different magnetic field; note that from (4.6.12), the

negative of I_2 is a measure of the x coordinate of the guiding center. The additional terms appearing in $\langle \dot{w}_1 \rangle$ are due to the fact that the ∇B drift of the ion is parallel to the wavevector of the wave, causing a Doppler shift in the wave frequency as seen by the ion. We now ask under what circumstances the stochasticity thresholds, (4.4.25) and (4.4.26), can be applied. Since the $\frac{3}{2}\beta^2 I_1$ term that appears in (4.6.6) also appears in (4.6.14), the conditions (4.6.7) must still be satisfied. For the other terms we use the same reasoning as in Case I but this time to $\langle \dot{w}_2 \rangle / \langle \dot{w}_1 \rangle$. The requirement that the fractional change in $\langle \dot{w}_2 \rangle / \langle \dot{w}_1 \rangle$ be small means that $\beta I_1 \ll \nu$ in (4.6.15) (note that we can choose the x origin so that I_2 is small, so there are no additional constraints due to the I_2 dependent terms). Since H is a constant of the motion a change in r of unity (i.e. a change in I_1 of r) leads to a change in I_2 of r/ν. Thus we require that the change in $\langle \dot{w}_2 \rangle / \langle \dot{w}_1 \rangle$ when either I_1 changes by r or I_2 changes by r/ν, be small; that is $\beta \ll r^{-1}$, which is already specified. The former condition is slightly more stringent than (4.6.7) giving

$$\beta \ll \nu r^{-2}, \tag{4.6.16}$$

although (4.6.16) and (4.6.7) are the same in the limit $r \approx \nu$. Also it should be noted that all the conditions given on the applicability of the stochasticity thresholds have been *sufficient* conditions. Equations (4.4.25) and (4.4.26), or slight modifications of them, may be correct when these conditions fail. However the conditions we have given do enable us to directly apply the results of Sec. 4.4 to tokamak-type plasmas.

Chapter 5. APPLICATION TO RF HEATING.

Section 5.1. Simulated Heating Experiment.

One problem with the approach of the last chapter is that it takes a static view of the ion motion. The results of that chapter tell us that above a certain field the ions will get heated, but they don't tell us how fast they get heated. The results of Sec. 3.1 are helpful in this regard: there, we computed the average energy gain per cyclotron period as a function of the initial velocity of the particle. In this section we wish to extend those results to longer times.

We start by asking the question: What happens to a distribution function of ions when a uniform wave is turned on at $t = 0$? For realistic parameters the perpendicular phase velocity of lower hybrid wave is at least a few times the ion thermal speed, $v_{Ti} = \sqrt{T_i/m_i}$. Thus the bulk of the ion distribution function satisfies $r < \nu - \sqrt{\alpha}$, placing those ions in the coherent region of velocity space. These ions will not exchange energy (on the average) with the wave, but are responsible for supporting the wave; that is they provide the real part of the ion susceptibility. Only a very few particles in the tail of the ion distribution function which satisify $r > \nu - \sqrt{\alpha}$ will exchange any time-averaged energy with the wave. Thus we were justified in not treating the interaction between the wave and the ions self-consistently, neglecting the action of the ions on the wave. If the distribution function is a Maxwellian then we incur negligible error by assuming that all the particles in the stochastic region have a perpendicular speed corresponding to the minimum energy side of the stochasic region, i.e. $r > \nu - \sqrt{\alpha}$. Thus an adequate model of the distribution function of the interacting particle at $t = 0$ is a delta function just inside the stochastic region.

Figures 5.1.1 and 5.1.2 show the results of integrating the orbits of 50 particles with the same initial speeds, but with evenly distributed phases with respect to the wave. The other parameters are: $\nu = 30.23$, $\alpha = 20$. The horizontal axis is the number of cyclotron orbits, which is

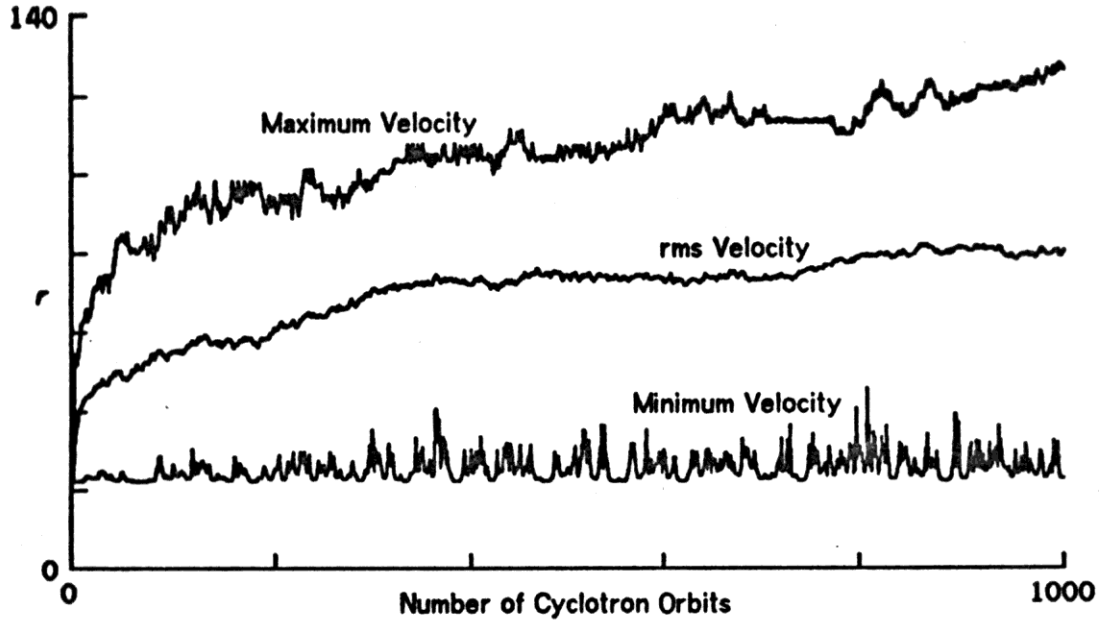

Figure 5.1.1. Heating of a group of 50 particles with $\alpha = 20$, $\nu = 30.23$, initial velocity $r = 23$, and evenly distributed phase.

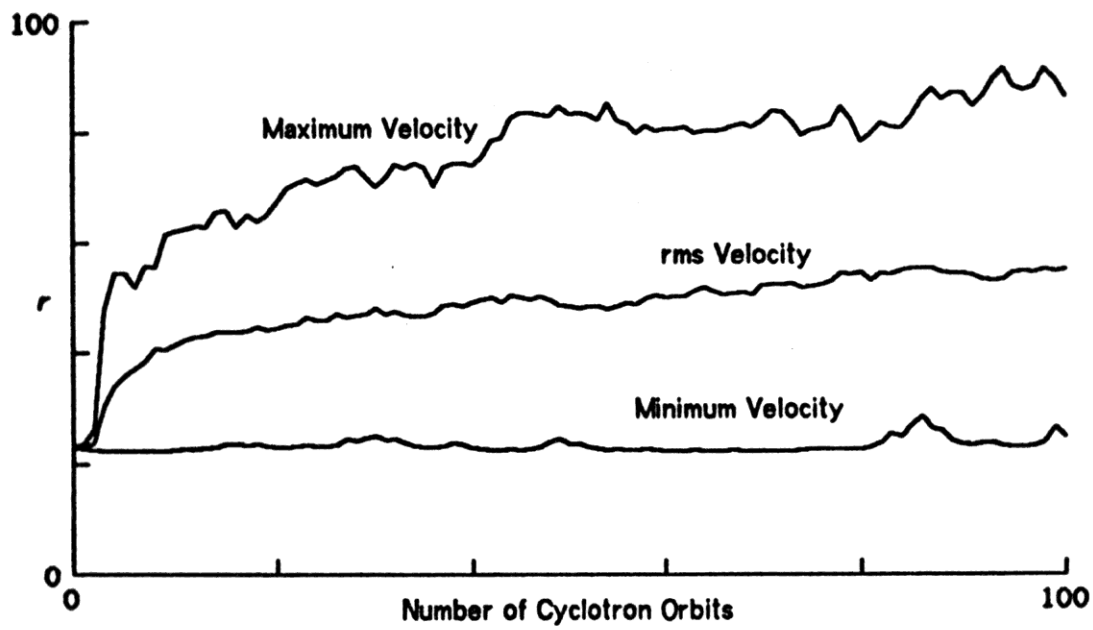

Figure 5.1.2. Same as Fig. 5.1.1 but on a larger scale.

nearly proportional to time. Initially there is a rapid increase in the rms velocity of the particles. This is followed at about the 10th cylotron orbit by a slower heating of the particles. This heating continues for longer than 1000 cyclotron orbits. From Fig. 4.4.3, we see that the stochastic region of velocity space extends up to $r = 150$ for the parameters of Figs. 5.1.1 and 5.1.2. Thus by the 1000th cyclotron orbit the particles are occupying a substantial fraction of the stochastic region of velocity space.

In Fig. 5.1.3 we plot the distribution function, f, of the particles at late times. This was obtained by averaging over the cyclotron orbits 800 - 1000. We have defined f such that

$$\int 2\pi r f\, dr = 1. \tag{5.1.1}$$

Thus f represents the distribution function in two dimensional perpendicular velocity space, before the cyclotron angle has been integrated out. Note that, except at high velocities, f is quite flat; the distribution function is plateaued in two dimensional velocity space.

Discussion of the final state of the particles is rather academic, since lower hybrid waves excited from a waveguide array are not uniform. We model this by saying that a particle spends only a finite time, $W/v_{\parallel}$, in the region where the waves are (W is the total width of the waveguide array). Taking $v_{\parallel} \sim v_{Ti}$ implies, as we will see, a time on the order of 10 - 20 cyclotron periods. On this time scale the most important effect is the initial rapid energy gain by the ions. Since this energy gain is experienced by particles just inside the trapping region, it is related to the trapping velocity. In fact the rms velocity after a few cyclotron orbits is around $\nu + \sqrt{\alpha}$, so the energy gain per particle on a single pass through the lower hybrid ray is given by the expressions for $\langle \Delta \mathcal{E} \rangle_{max}$, (3.1.5) and (3.1.6). The flux of ions entering the ray is $n_0 v_{Ti}$ (particles per second per unit area in the perpendicular plane), where we use v_{Ti} as a representative parallel velocity for the ions. Assuming that the ion distribution function is Maxwellian, then only a fraction,

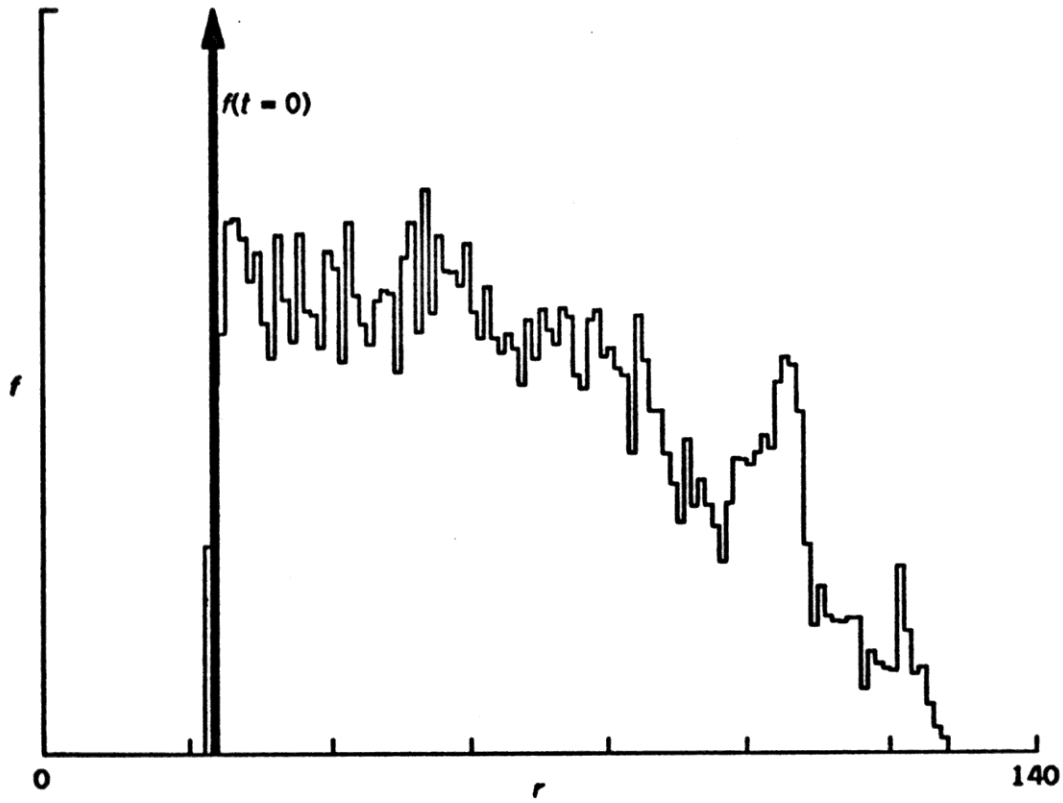

Figure 5.1.3. Perpendicular velocity distribution function for the particles in Fig. 5.1.1 averaged over orbits 800 - 1100. (This is the two dimensional distribution function before the Larmor angle has been integrated out.) Normalization is such that $\int 2\pi r f \, dr = 1$.

$$\exp[-\tfrac{1}{2}(\omega/k - v_{tr})^2/v_{Ti}^2], \tag{5.1.2}$$

of the particles are in the stochastic region of perpendicular velocity space, and most of these particles will be travelling at $\omega/k - v_{tr}$. Thus we can estimate the energy gain of the ions to be,

$$2m_i(\omega/k)v_{tr}\, n_0 v_{Ti} \exp[-\tfrac{1}{2}(\omega/k - v_{tr})^2/v_{Ti}^2]. \tag{5.1.3}$$

The dimension of this quantity is energy per second per unit area of the ray in the perpendicular plane.

Section 5.2. Role of Collisions.

In deriving (5.1.3) we modeled the spatially inhomogeneous field as a field that is turned on at $t = 0$ and off again at W/v_{Ti}. In practice an ion has many encounters with the lower hybrid ray. Assuming the lower hybrid ray subtends a poloidal angle $\Delta\theta$ then the mean time between encounters with the field is

$$t_0 = (2\pi R/v_{Ti})(2\pi/\Delta\theta). \tag{5.2.1}$$

Thus a more realistic model for the field would be to have switched on for a time W/v_{Ti} with a duty cycle of t_0. The most uncertain aspect of extending (5.1.3) to this case is the assumption that the distribution function of ions entering the lower hybrid ray is Maxwellian. Such an assumption will give the right answer for the number of particles in the stochastic region, but the distribution function of particles within the stochastic region will not in general be part of a Maxwellian, because these ions will have been affected by previous transits through the field. If there were no collisions then the effect of subsequent passes through the ray would be just to continue on the curves in Fig. 5.1.1, which results in much slower heating. The effect of collisions, if they are sufficiently frequent, is to reinstitute a Maxwellian tail while the ion is streaming

outside the ray, so that (5.1.3) remains valid. In this section we will determine how collisional the ions must be for this to be so.

The effect of one transit through the ray on the distribution function is to create a plateau in perpendicular velocity space at ω/k with a size of about v_{tr}. This is usefully regarded as the sum of a Maxwellian and a perturbation, $f_p(\mathbf{v})$. The perturbation is centered at $v_\perp = \omega/k$, has an extent of about v_{tr}, and has velocity space integral of zero. If the perturbation is small (true when $\omega/k > v_{Ti}$) then the equation for the relaxation of the perturbation to zero may be written as (Trubnikov, 1965)

$$\left.\frac{\partial f_p}{\partial t}\right|_{coll} = -\sum_\beta \nabla_{\mathbf{v}} \cdot \mathbf{J}^{p/\beta}, \tag{5.2.2}$$

where

$$\mathbf{J}^{\alpha/\beta} = \mathbf{F}^{\alpha/\beta} f_\alpha/m_\alpha - \mathbf{D}^{\alpha/\beta} \cdot \nabla_{\mathbf{v}} f_\alpha, \tag{5.2.3}$$

$$\mathbf{D}^{\alpha/\beta} = -L^{\alpha/\beta}\, \nabla_{\mathbf{v}}\nabla_{\mathbf{v}}\psi_\beta, \tag{5.2.4}$$

$$\mathbf{F}^{\alpha/\beta} = -L^{\alpha/\beta}\, \nabla_{\mathbf{v}}\varphi_\beta\, m_\alpha^2/m_\beta, \tag{5.2.5}$$

$$L^{\alpha/\beta} = \lambda\left[\frac{q_\alpha q_\beta}{\epsilon_0 m_\alpha}\right]^2, \tag{5.2.6}$$

$$f_\beta = \nabla_{\mathbf{v}}^2\varphi, \quad \varphi_\beta = \nabla_{\mathbf{v}}^2\psi_\beta, \tag{5.2.7}$$

and λ is the Coulomb logarithm $\ln(r_{max}/r_{min})$, which is typically about 16 to 20. If the field particle distribution functions, f_β, are Maxwellian then $\mathbf{J}$ becomes

$$\mathbf{J}^{\alpha/\beta} = -m_\alpha/(m_\alpha + m_\beta)\nu_s^{\alpha/\beta}\mathbf{v} f_\alpha - \tfrac{1}{4}\nu_\perp^{\alpha/\beta} v^2 \nabla_{\mathbf{v}} f_\alpha + \tfrac{1}{2}(\tfrac{1}{2}\nu_\perp^{\alpha/\beta} - \nu_\parallel^{\alpha/\beta})\mathbf{v}\mathbf{v} \cdot \nabla_{\mathbf{v}} f_\alpha, \tag{5.2.8}$$

where ν_s, $\nu_\parallel$, and $\nu_\perp$ are the slowing down, parallel diffusion, and perpendicular diffusion frequencies ("parallel" and "perpendicular" here refer to the direction of the test particle velocity,

not the direction of the magnetic field). [Expressions for these frequencies may be found in the NRL Plasma Formulary (1976); note, however, that (5.2.8) differs in several respects from the formula given there.]

To understand the evolution of the perturbation, f_p, we look at a simple case for f_α, namely

$$f_\alpha = \delta(v_\perp - v_{\perp\alpha})\,\delta(v_\parallel - v_{\parallel\alpha})/(2\pi v_{\perp\alpha}). \tag{5.2.9}$$

This is a ring distribution function in velocity space. We are interested in finding how f_α diffuses in perpendicular velocity space. From (5.2.8) we compute

$$\frac{d}{dt}\langle(v_\perp - \langle v_\perp\rangle)^2\rangle = \nu_\parallel^{\alpha/\beta} v_{\perp\alpha}^{\;2} + \tfrac{1}{2}\nu_\perp^{\alpha/\beta} v_{\parallel\alpha}^{\;2}. \tag{5.2.10}$$

Now we are intested in an f_p for which $v_{\perp p} = \omega/k$ and $v_{\parallel p} \approx v_{Ti}$, so that $v_{\perp p} > v_{\parallel p}$. Also f_p disappears once it has spread a distance v_{tr} in perpendicular velocity space, for then the positive and negative parts of it would cancel out. Thus the time it takes for collisions to destroy the plateau is given by

$$\tau = \nu_\parallel^{-1} v_{tr}^{\;2}/(\omega/k)^2, \tag{5.2.11}$$

where for $\nu_\parallel$ we use the sum of $\nu_\parallel^{i/e}$ and $\nu_\parallel^{i/i}$. In the usual case we have $v_{Te} > \omega/k > v_{Ti}$, in which case, assuming $T_e \approx T_i$ and the plasma is hydrogen, $\nu_\parallel^{i/e} < \nu_\parallel^{i/i}$ holds for $\omega/k < 5v_{Ti}$. However we will require that this latter condition be satisfied so that there be an appreciable number of particles in the stochastic region. Thus in cases of interest we may use $\nu_\parallel = \nu_\parallel^{i/i}$ in (5.2.11), where from the NRL Plasma Formulary (1976)

$$\nu_\parallel^{i/i} = 5.1\times10^{-13}\lambda_{ii} n_0 T_i^{-3/2}[\omega/(kv_{Ti})]^{-5}\ \mathrm{s}^{-1}, \tag{5.2.12}$$

where n_0 is in m^{-3} and T_i is in eV. In this case the smoothing out of the plateau results in bulk heating of the ions. If t_0, the time between encounters with the field, is greater than τ then

(5.1.3) may be used for each transit through the ray. If $t_0 < \tau$ then (5.1.3) can only be applied approximately every τ/t_0 encounters with the field.

Section 5.3. Design of Experiment.

Let us summarize the results so far: The motion becomes stochastic above the threshold field

$$\frac{E_0}{B_0} > \frac{1}{4}\left(\frac{\Omega}{\omega}\right)^{1/3}\frac{\omega}{k}. \tag{4.4.27}$$

The stochastic region of velocity space is close to $v_\perp = \omega/k$, extending approximately $v_{tr} = \sqrt{qE_0/mk}$ below ω/k. These results were derived for a wave propagating perpendicular to the homogeneous magnetic field, but we may apply them in cases where θ, the angle of $\mathbf{k}$ to the magnetic field, differs from $\frac{1}{2}\pi$ by no more than $0.6(\Omega/\omega)^{1/6}$ [see (4.5.17)], and if there is negligible change in the magnetic field over a Larmor orbit of a particle with $v_\perp = \omega/k$. Since the scale length of magnetic field variation is R, the major radius, this latter condition is automatically satisfied if the ions are confined. We have modeled the effect of a spatially finite ray by saying that a particle spends only W/v_{Ti} in the ray. Assuming that this is several cyclotron periods and that the distribution function of ions entering the ray is Maxwellian, the rms velocity gained by the particle on travelling through the ray is $2v_{tr}$. The condition under which we may assume that the entering distribution function is Maxwellian is that τ be shorter than the mean time between encounters with the field, t_0, where

$$t_0 = (2\pi R/v_{Ti})(2\pi/\Delta\theta), \tag{5.2.1}$$

$$\tau = \nu_{\parallel}^{-1} v_{tr}^2/(\omega/k)^2. \tag{5.2.11}$$

and $\nu_{\parallel}$ is given by (5.2.12). If this is the case, then energy gain by the ions per second per unit

area of the ray in the perpendicular plane is

$$2m_i(\omega/k)v_{tr}\, n_0 v_{Ti} \exp[-\tfrac{1}{2}(\omega/k - v_{tr})^2/v_{Ti}^2]. \tag{5.1.3}$$

We will now see whether stochastic heating can be used to heat a realistic tokamak plasma. Our purpose is to uncover the issues involved in designing an experiment. In order to focus the discussion we will pick two sets of plasma parameters, as follows:

	Case I	Case II
Plasma	H	H
n_0	3×10^{19} m^{-3} (3×10^{13} cm^{-3})	10^{21} m^{-3} (10^{15} cm^{-3})
B_0	2 T (20 kG)	10 T (100 kG)
T_e	800 eV	2 keV
T_i	400 eV	2 keV
ω_{LH}	5.4×10^{9} s^{-1} (860 MHz)	2.9×10^{10} s^{-1} (4.7 GHz)
ω_{LH}/Ω_i	28	31
R	1 m	1 m
a	0.2 m (20 cm)	0.2 m (20 cm)
I	100 kA	1 MA

These values are those of the central plasma. For simplicity we will assume that n_0, T_e, and T_i scale proportionally to one another as a function of minor radius. In practice the electron temperature profile is more peaked than the density and ion temperature profiles. The goal is to design a waveguide array such that the lower hybrid waves that it excites can appreciably heat the plasma. If we look at (5.1.3) we immediately recognise that the exponential is the dominant factor; if the power dissipated is not to be negligible then the exponent in (5.1.3) must not be too negative. As we will see later, we are generally interested in fields such that $v_{tr} \ll \omega/k$, in which case we demand that $\omega/(k_\perp v_{Ti})$ must not be large, or typically

$$\omega/(k_\perp v_{Ti}) < 4. \tag{5.3.1}$$

The first task is to see if lower hybrid waves satisfying (5.3.1) can be excited in a plasma. We assume for the time being that the stochasticity threshold, (4.4.27), can be satisfied (we will check this later). There are a number of constraints we must satisfy. The first is that the parallel wavenumber must satisfy the accessibility condition (Golant, 1971; Troyon and Perkins, 1974; Theilhaber, 1976). Using the results of Theilhaber (1976) we find that $n_\parallel = k_\parallel c/\omega$ must satisfy

$$n_\parallel^2 > [1 - \omega^2/(\Omega_e\Omega_i)]^{-1}, \tag{5.3.2}$$

if $\omega^2 < \Omega_e\Omega_i$ and $\omega_{pi}^2/\omega^2 > \omega^2/(\Omega_e\Omega_i - \omega^2)$, and

$$n_\parallel^2 > 1 + 2\frac{\omega_{pe}^2}{\Omega_e^2} - \frac{\omega_{pi}^2}{\omega_2^2} + 2\frac{\omega_{pe}}{\Omega_e}\left[1 + \frac{\omega_{pe}^2}{\Omega_e^2} - \frac{\omega_{pi}^2}{\omega_2^2}\right]^{1/2}, \tag{5.3.3}$$

otherwise. Here the plasma frequencies are evaluated at the center of the plasma. In practice we will find that the accessibility condition becomes approximately $n_\parallel > 2$. Except for parallel wavenumbers close to this accessibility condition and in the very low density region the waves propagate according to the electrostatic dispersion relation,

$$K_\perp(x)\, k_\perp^2 + K_\parallel(x)\, k_\parallel^2 - a(x)k_\perp^4 - b(x)k_\perp^2 k_\parallel^2 - c(x)k_\parallel^4, \tag{5.3.4}$$

where

$$K_\perp = 1 + \frac{\omega_{pe}^2}{\Omega_e^2} - \frac{\omega_{pi}^2}{\omega^2},\ K_\parallel = -\frac{\omega_{pe}^2}{\omega^2}, \tag{5.3.5}$$

$$a = \frac{3}{4}\frac{\omega_{pe}^2}{\Omega_e^2}\frac{v_{Te}^2}{\Omega_e^2} + 3\frac{\omega_{pi}^2}{\omega^2}\frac{v_{Ti}^2}{\omega^2},\ b = -\frac{\omega_{pe}^2}{\omega^2}\frac{v_{Te}^2}{\Omega_e^2} + 6\frac{\omega_{pi}^2}{\omega^2}\frac{v_{Ti}^2}{\omega^2},$$

$$c = 3\frac{\omega_{pe}^2}{\omega^2}\frac{v_{Te}^2}{\omega^2} + 3\frac{\omega_{pi}^2}{\omega^2}\frac{v_{Ti}^2}{\omega^2}. \tag{5.3.6}$$

We have defined v_{Ts} as $\sqrt{T_s/m_s}$, and have assumed that $\Omega_i \ll \omega \ll \Omega_e$. The coefficients describing the finite temperature effects are found by expanding the Harris dispersion relation (Harris, 1961)

for small k. In writing (5.3.4) we have assumed a slab geometry, where the density and temperature are functions only of x, the distance from the wall of the tokamak. In Fig. 5.3.1 we have plotted the solution of (5.3.4) against $n_0(x)$, for Case II and with $n_\parallel = 4$, $\omega = 1.3\ \omega_{LH,\,max}$. For simplicity we have assumed that the temperatures are proportional to the density, and that the magnetic field is constant. The curve of $n_\perp$ stays quite close to the cold plasma solution, the dashed line in Fig. 5.3.1, until ω is close to the local lower hybrid frequency, where $n_\perp$ starts to increase rapidly leading eventually to wave conversion to a ion thermal wave.

As the wave penetrates two direct heating mecahnisms may become operative: electron Landau damping (Bers *et al.*, 1976a) and the stochastic ion heating we have been discussing. [There are also a number of other processes which can effect to penetration of the ray or can lead to heating, e.g. parametric decay (Porkolab, 1974) and filamentation (Morales and Lee, 1975). Also nonlinear effects may modify the process of electron Landau damping (Bers *et al.*, 1976a).] The effectiveness of both heating mechanisms increases exponentially as a certain factor decreases. This factor is $\omega/(k_\perp v_{Ti})$ for the stochastic heating and $\omega/(k_\parallel v_{Te})$ for Landau damping, and both factors decrease as the wave penetrates into the plasma. The decrease is due to the increase of the temperature and also, in the case of the stochastic heating, to the increase of $k_\perp$ with increasing density (see Fig. 5.3.1). We will begin by assuming that the wave is very heavily damped once either of these factors drops below 4. At the outside of the plasma where $k_\perp \sim k_\parallel$, we have $\omega/(k_\perp v_{Ti}) > \omega/(k_\parallel v_{Te})$. However due to the increase in $k_\perp$ both due to cold and warm plasma effects this situation can reverse at some point as the wave penetrates. The wave will have damped on the electrons if this crossover point occurs for $\omega/(k_\parallel v_{Te}) < 4$; however if this is not the case and if $k_\perp$ becomes sufficiently large then the wave may damp on the ions. Thus the increase of $k_\perp$ close to wave conversion is very important, since it leads to a slowing down of the wave and makes (5.3.1) easier to satisfy. From (5.3.4) we can find the value of $k_\perp$ at wave conversion

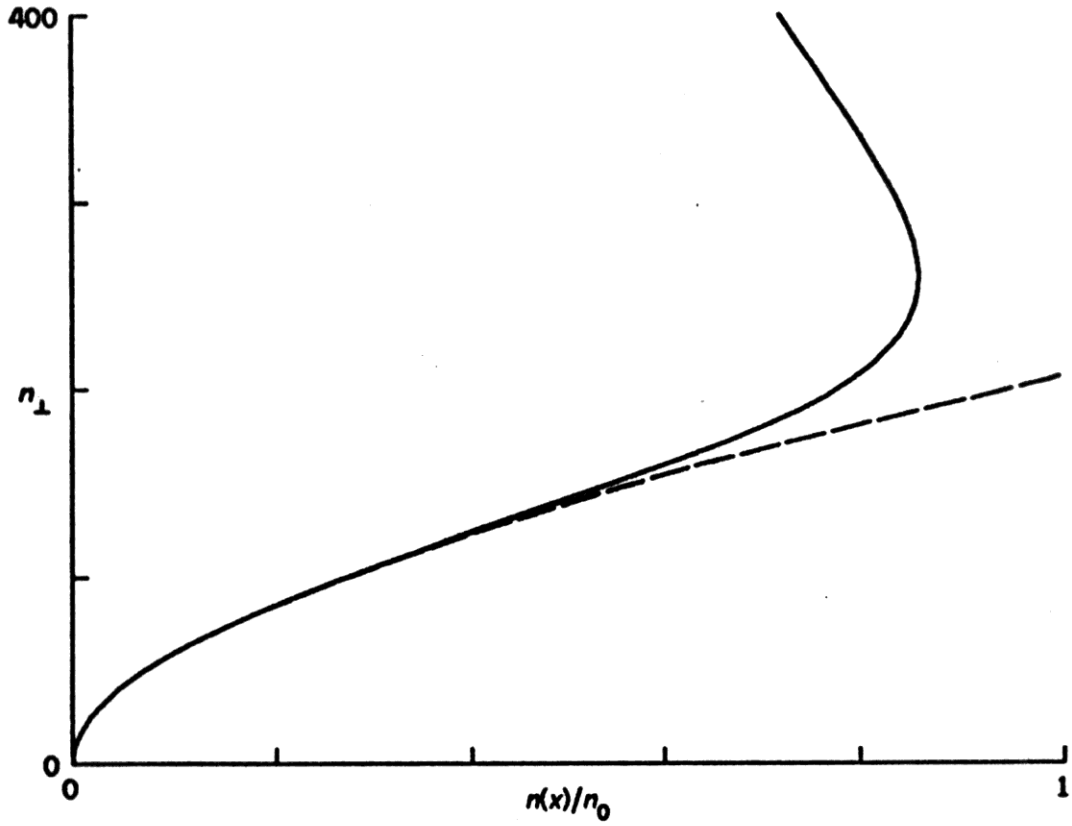

Figure 5.3.1. Plot of $n_\perp$ against density, $n(x)$, for the parameters of Case II, and $\omega = 1.3\ \omega_{LH,\ max}$, $n_\parallel = 4$. The solid line in the electrostatic dispersion relation given by (5.3.4), and the dashed line is the cold electrostatic dispersion relation, (5.3.4) with $a(x)$, $b(x)$, and $c(x) = 0$.

$$k_\perp^4 = (|K_\parallel| k_\parallel^2 + c k_\parallel^4)/a. \tag{5.3.7}$$

In order for the wave to reach this wave conversion point electron Landau damping must be small. In that case we can drop the second term in the numerator in (5.3.7) (we may check this afterwards). In addition for Cases I and II, the ion term in the expression for a, (5.3.6), dominates over the electron term at wave conversion. Then (5.3.7) becomes

$$\frac{\omega}{k_\perp v_{Ti}} = \left[\sqrt{3}\,\frac{\omega}{k_\parallel v_{Te}}\left(\frac{T_e}{T_i}\right)^{1/2}\right]^{1/2}. \tag{5.3.8}$$

At wave conversion the wave frequency is related to the local lower hybrid frequency by

$$\frac{\omega}{\omega_{LH}} = \left[1 + 2\sqrt{3}\,\frac{k_\parallel v_{Te}}{\omega}\left(\frac{T_i}{T_e}\right)^{1/2}\right]^{1/2}. \tag{5.3.9}$$

This equation shows us that if the wave is to reach wave conversion before being Landau damped then ω must be quite close to ω_{LH}, although it is still possible that the wave will damp by stochastic ion heating before reaching the wave conversion point.

In Figs. 5.3.2 and 5.3.3 we show plots of both $\omega/(k_\perp v_{Ti})$ and $\omega/(k v_\parallel v_{Te})$ as a function of density (again assuming that the temperatures are proportional to density). In these plots ω is fixed and is close to the central value of ω_{LH} and curves for various $n_\parallel$'s are shown. Note that the low $n_\parallel$'s propagate to the maximum density without getting damped on either the ions or the electrons; for intermediate values of $n_\parallel$ the wave is damped on the ions close to the center of the plasma; and for the highest values they are damped on the electrons closer to the outside of the plasma. Of interest then is the values of $n_\parallel$ at these transitions and the position in the plasma where the heating changes from electron Landau damping to stochastic ion heating. Figures 5.3.4 and 5.3.5 show the transistion values of $n_\parallel$ as a function of ω/ω_{LH} for our two cases. Note that if the frequency is too high the curves cross, indicating that there is no range of $n_\parallel$ which will heat the ions. Also shown in these figures are curves showing the accessibility condition, (5.3.2) and (5.3.3). Figures 5.3.6 and 5.3.7 show the curves of the density at which the wave changes from

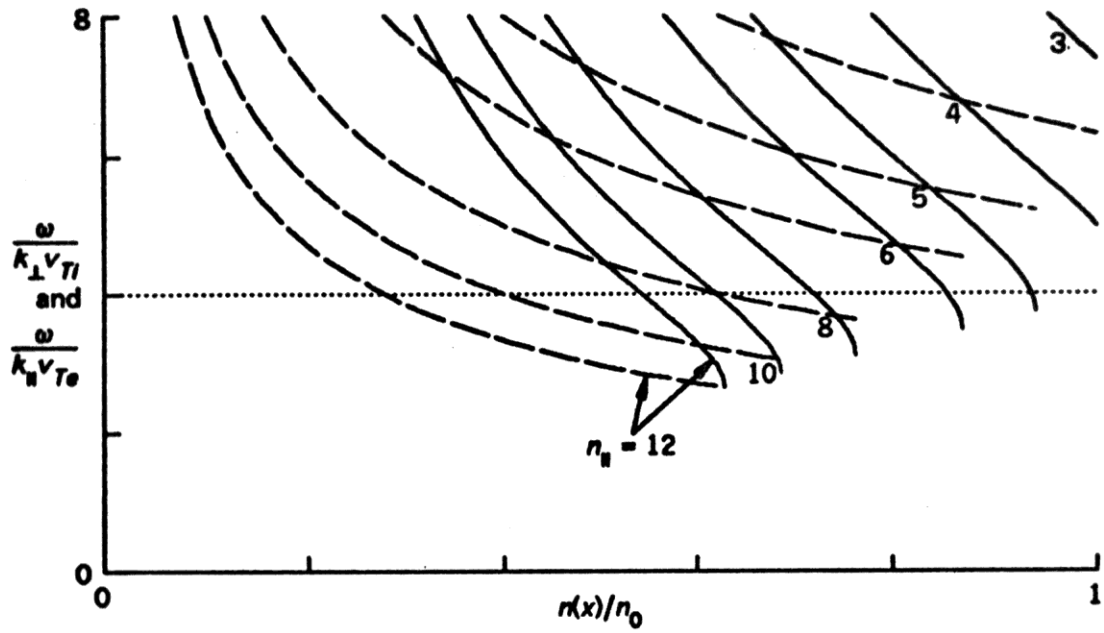

Figure 5.3.2. Plots of $\omega/k_\perp v_{Ti}$ (the solid lines) and $\omega/k_\parallel v_{Te}$ (the dashed lines) against $n(x)$ for Case I, $\omega/\omega_{LH,\,max} = 1.2$, and various $n_\parallel$'s (shown by numbers on the figure). The wave is assumed to be heavily damped if either $\omega/k_\perp v_{Ti}$ or $\omega/k_\parallel v_{Te}$ drops below to dotted line.

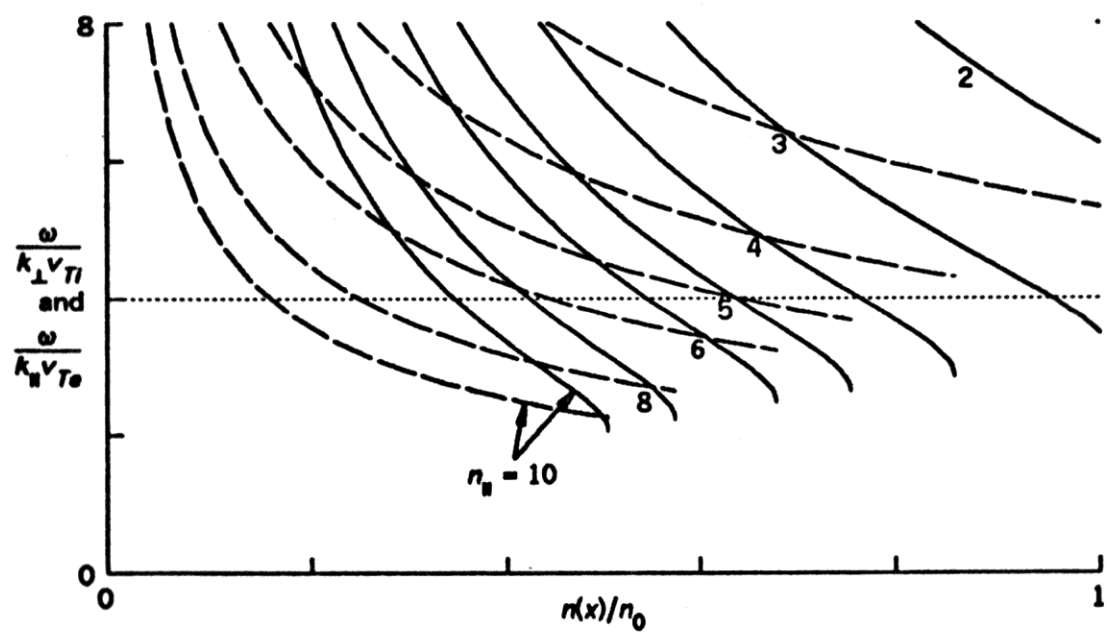

Figure 5.3.3. Same as Fig. 5.3.2 except for Case II and $\omega/\omega_{LH,\,max} = 1.3$.

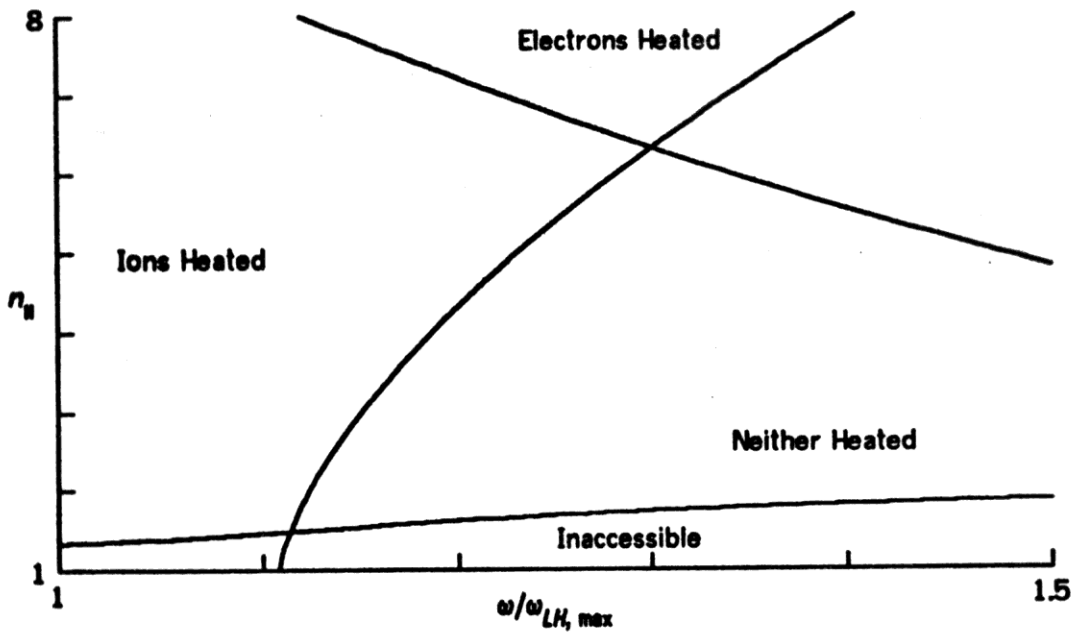

Figure 5.3.4. Graph showing what species the various Fourier components heat, as a function of ω, for Case I. The lowest curve gives the accessibility condition, (5.3.2) and (5.3.3).

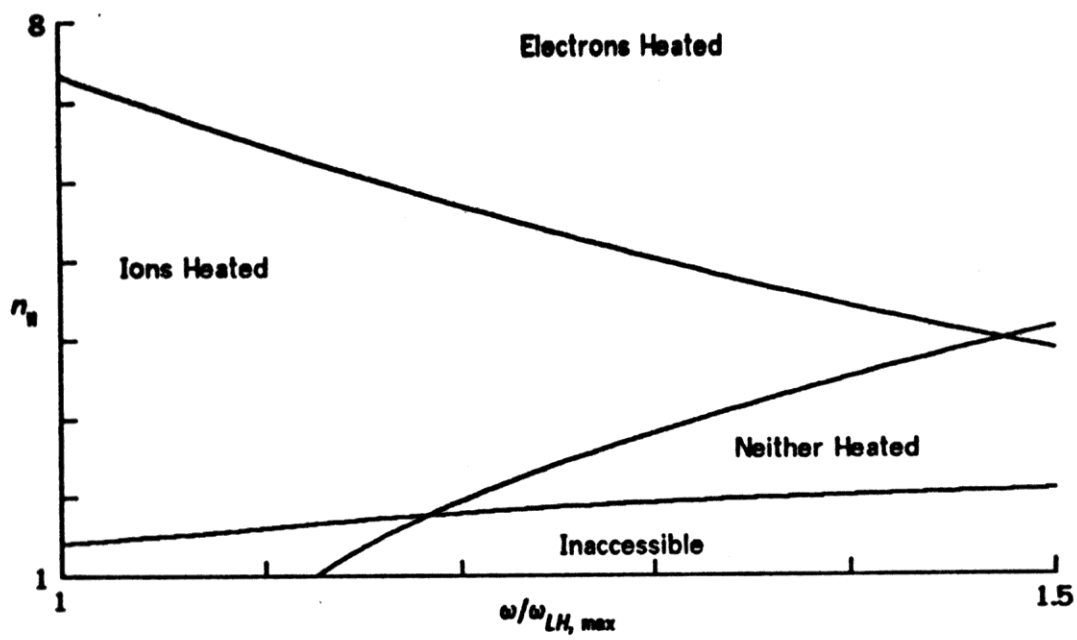

Figure 5.3.5. Same as Fig. 5.3.4 except for Case II.

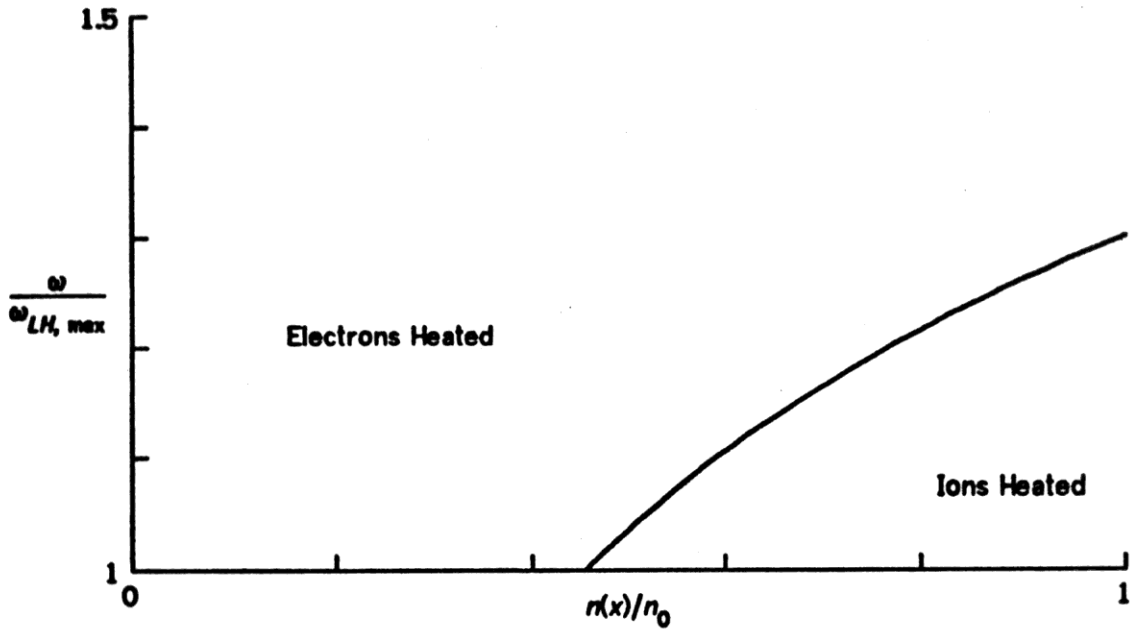

Figure 5.3.6. The density at which the wave changes from heating the electrons to heating the ions for Case I.

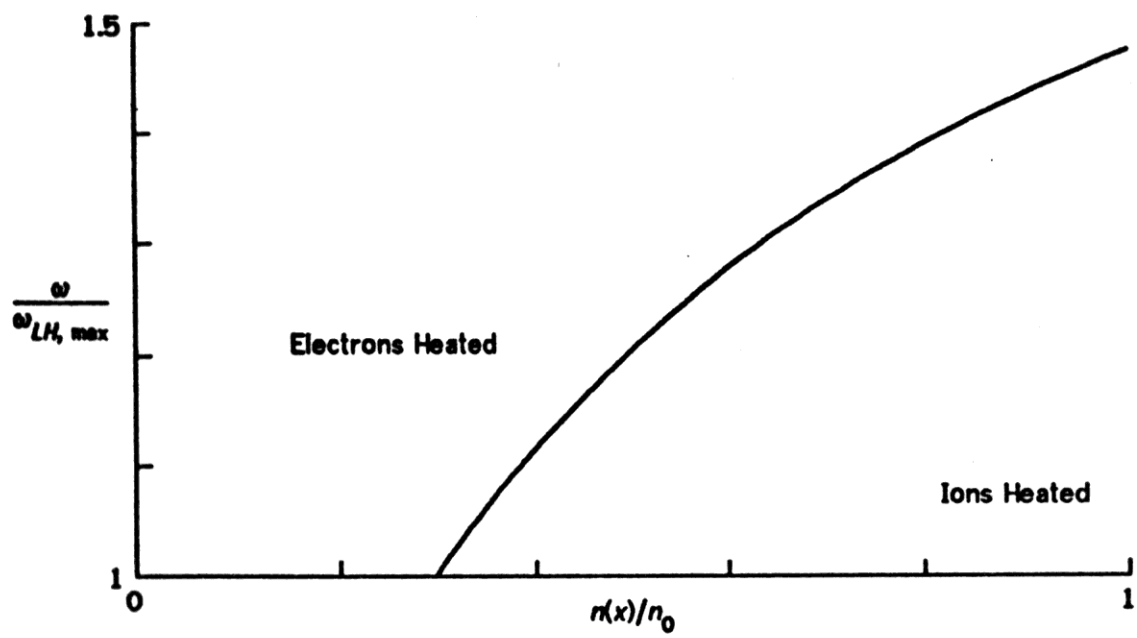

Figure 5.3.7. The same as Fig. 5.3.6 except for Case II.

heating the electrons to heating the ions. These plots confirm the simple picture we gave by looking just at the wave conversion point. They indicate that only quite close to the lower hybrid frequency can stochastic ion heating be realized. The maximum frequency that can be used may be found by substituting $\omega/(k_\perp v_{Ti}) = \omega/(k_\parallel v_{Te}) = 4$ in (5.3.4) and assuming that the ion term of a is the only thermal term to come into play. The resulting expression for the maximum frequency is

$$\left(\frac{\omega}{\omega_{LH}}\right)^2 = 1\tfrac{3}{16} + \frac{T_i}{T_e}. \tag{5.3.10}$$

This gives values 1.3 and 1.5 for ω/ω_{LH} for Cases I and II, close to the more exact values given in Figs. 5.3.4 and 5.3.5. We will pick the following parameters to describe the wave:

	Case I	Case II
ω	$6.5\times10^9\ s^{-1}$ (1 GHz)	$3.8\times10^{10}\ s^{-1}$ (6 GHz)
ω/ω_{LH}	1.2	1.3
$n_{\parallel,\,min}$	4.3	2.8
$n_{\parallel,\,max}$	7.2	5
$n_{min}(x)/n_0$	0.77	0.64

The value of $n_{min}(x)$ is the minimum density which can be heated by these waves. For these frequencies the lower hybrid wave propagates close to perpendicular to the magnetic field so that (4.4.27) is the correct stochasticity condition. Designing an array so that the bulk of the field lies in the bounds on $n_\parallel$ given above appears to pose no particular problem; see, for instance, Bers and Karney (1974).

We now must check that the field amplitude is sufficient for the stochasticity condition (4.4.27) to be met. Substituting (5.3.2) into (4.4.27) we obtain

$$\frac{E_0/B_0}{v_{Ti}} > \left(\frac{\Omega}{\omega}\right)^{1/3}. \tag{5.3.11}$$

The right hand side of (5.3.11) shows only a weak dependence on ω and is equal to about $\frac{1}{3}$ for both Cases I and II. The magnitude of E_0 in the center of the plasma must be at least 120 kV/m (1.2 kV/cm) in Case I and 1.3 MV/m (13 kV/cm) in Case II. If the widths of the waveguide arrays are 0.1 m (10 cm) and 50 mm (5 cm) in the two cases, then it take a thermal particle 16 and 17 cyclotron periods to go through the lower hybrid cone. Thus the power gain formula, (5.1.3), that we derived for short times in valid. We may compute v_{tr} for these fields, and we find that in both cases $v_{tr}/(\omega/k)$ is about 5%. The time it takes for the plateau to disappear, τ, is 70 and 19 μs; these times are less than the times between encounters with the field, t_0, in our two cases, which are 130 and 60 μs, respectively (we have assumed that $\Delta\theta = \frac{1}{2}\pi$). Thus collisions are effective in channelling the energy gain by the tail particles to the bulk ions.

The fields we have quoted are the values of the electric field where the stochastic heating is taking place. We would like to express this as a field amplitude and power density at the edge of the plasma. To do this we use the WKB enhancement factor derived by Briggs and Parker (1972). As long as the wave obeys the cold plasma electrostatic dispersion relation then the amplitude of $\mathbf{E}_0$ is proportional to

$$\frac{|k_\perp|/k_\parallel}{(K_\perp|K_\parallel|)^{1/4}}. \tag{5.3.12}$$

Close to the slow wave cutoff, $\omega \approx \omega_{pe}$, and so $K_\perp \approx -K_\parallel \approx 1$ and $k_\perp \approx -k_\parallel$ thus (5.3.12) gives the WKB enhancement of the electric field compared with the field just inside the cutoff. Evaluating (5.3.12) at the maximum density using the cold plasma dispersion relation gives amplification factors of 10.9 in Case I and 7.9 in Case II. Thus the fields near cutoff in the two cases are 11 kV/m (110 V/cm) and 160 kV/m (1.6 kV/cm) respectively. The power flow in the lower hybrid waves is given by the electrostatic power flow formula (Bers, 1975):

$$\mathbf{S} = -\tfrac{1}{4}\epsilon_0|\mathbf{E}|^2\omega\left[\frac{(\mathbf{K}+\mathbf{K}_\dagger)\cdot\mathbf{k}}{k^2} + \frac{k_\dagger k_\dagger}{k^2}\frac{\partial K_{\dagger\dagger}}{\partial \mathbf{k}}\right], \tag{5.3.13}$$

where **K** is the dielectric tensor, and $\mathbf{K}_t$ its tranpose. Close to cutoff the waves are not influenced by finite temperature effects so **K** is independent of **k** and the second term in []'s is zero. Computing the power flow perpendicular to the wall then gives

$$S_{\perp} = \frac{1}{2}\frac{\omega}{k_{\parallel}}\epsilon_0 E_{\parallel}^{2}, \tag{5.3.14}$$

where again the evaluation is just beyond the slow cutoff at a point where $K_{\parallel} \approx -1$. Using central values of $n_{\parallel}$ $[(n_{\parallel,\,max} + n_{\parallel,\,min})/2]$ and the minimum values of the fields we derived above then the power flow is 28 kW/m^2 and 9 MW/m^2 in the two cases.

In order to have a measurable effect on the ion temperature, we demand that the RF power equal the ohmic heating power. Assuming that the energy confinement time is not a strong function of temperature this would enable us to roughly double the ion temperature. If we take the loop voltage in our examples to be 3 V, them the ohmic power input is (VI) 300 kW in Case I and 3 MW in Case II. With Case I it is obvious that if we used the minimum power of 28 kW/m^2, we would have to use too large an area of waveguides. However the field strength in this case could be increased several-fold. Unfortunately increasing the field results in an increase in the time it takes for collisions to smooth out the plateau caused by the field; thus the wave would have to penetrate somewhat further into the plasma where $\omega/(kv_{Ti})$ is smaller. In Case II, the area of waveguides required is $\frac{1}{3}$ m^2. Again this is larger than we would like. In this case the field near the plasma wall is quite high (1.6 kV/cm), and, due to the lack of experimental data, it is not clear how much this can be increased. If the field cannot be increased signifiicantly, it would suggest that a feasible solution might be to bring the RF power to the wall of the tokamak with only a few waveguides, and to couple to the plasma with a "leaky" waveguide; this would allow the power to be spread over a large area of the tokamak, with a minimum of external waveguides.

Section 5.4. Conclusion.

We have shown that a lower hybrid wave can cause stochastic ion motion. The conditons for this are summaraized in the beginning of Sec. 5.3. It should be emphasized that this is a *nonlinear* process, and so it does not utilize linear damping at cyclotron harmonics. One of the important results of this work is that there is no cyclotron harmonic "structure" left above the stochasticity threshold; thus the results apply equally well to cases where the magnetic field is non-uniform. In Sec. 5.3 we showed how this phenomenon can provide a direct method of heating the ions using a lower hybrid wave in a present-day tokamak. However such heating will only take place if the wave frequency is just above the central lower hybrid frequency, and thus in an experimental situation it would be important to have good control of the density.

Scaling our results up to reactor-sized tokamaks presents some problems that still need to be resolved. Since the ion temperature is high in a reactor, the collisions will be less effective in channelling the energy of the heated tail particles into the bulk. Since the distribution function is less readily Maxwellianized, it may be necessary to account for the slower stochastic heating that takes place after the rapid initial heating.

Parametric instabilties have been observed in a number of lower hybrid heating experiments (e.g. Porkolab *et al.*, 1977), and are expected to take place in lower hybrid heating in a reactor. The decay products of the injected lower hybrid wave always are at a lower frequency than the injected wave and they often have a larger k ($k\lambda_{De} \sim \frac{1}{4}$). Thus the phase velocity of the decay products may be considerably lower than that of the injected wave, and, if the stochasticity condition is met, ions closer to the bulk ion distribution can be heated. The work of Reiman (1977) will enable us to make an estimate of the amplitude of the decay products, and so check whether the stochasticity threshold will be met.

The hot ion tails that have been observed in recent experiments are probably due to

trapping and stochastic heating either by the injected wave or its decay products. Similarly the energy gained by the neutral beam diagnostic in the ATC experiment (Bernabei *et al.*, 1976) is probably due to these processes.

Lastly our results may be important in the problem of ion cyclotron resonance heating. Our analysis has been carried out assuming that the wave frequency is much above the cyclotron frequency. However numerical solutions, similar to those shown in Sec. 3.2, indicate that if the wave is of sufficient amplitude, then the motion becomes stochastic even at low harmonics.

Appendices.

Appendix A. Numerical Integration Scheme for Orbit Equations.

We give here the method for numerically solving the equations of motion (2.1.9) and (2.1.10). The Adams predictor-corrector method is used (eqs. 25.5.3-4, Abramowitz and Stegun, 1964). The integration is started by a Runge-Kutta method (eq. 25.5.10, Abramowitz and Stegun, 1964). Both methods are accurate to order Δt^5. The coordinate, x, is also computed [from (2.1.9)] to provide a check on the computation. The differential equation is written as

$$\ddot{y} = f(t, y),$$

where

$$f(t, y) = \alpha \cos(y - \nu t - \phi) - y.$$

In the following $t_n = t_0 + n\Delta t$, $y_n = y(t_n)$ etc.

The Runge-Kutta Method.

Given: $t_n, x_n, y_n, \dot{y}_n$.

returns: $x_{n+1}, y_{n+1}, \dot{y}_{n+1}$.

$$a_1 \leftarrow \Delta t\, y_n, \qquad b_1 \leftarrow \Delta t\, \dot{y}_n, \qquad c_1 \leftarrow \Delta t\, f(t_n, y_n),$$

$$a_2 \leftarrow \Delta t(y_n + \tfrac{1}{2}b_1), \qquad b_2 \leftarrow \Delta t(\dot{y}_n + \tfrac{1}{2}c_1), \qquad c_2 \leftarrow \Delta t\, f(t_n + \tfrac{1}{2}\Delta t, y_n + \tfrac{1}{2}b_1),$$

$$a_3 \leftarrow \Delta t(y_n + \tfrac{1}{2}b_2), \qquad b_3 \leftarrow \Delta t(\dot{y}_n + \tfrac{1}{2}c_2), \qquad c_3 \leftarrow \Delta t\, f(t_n + \tfrac{1}{2}\Delta t, y_n + \tfrac{1}{2}b_2),$$

$$a_4 \leftarrow \Delta t(y_n + b_3), \qquad b_4 \leftarrow \Delta t(\dot{y}_n + c_3), \qquad c_4 \leftarrow \Delta t\, f(t_n + \Delta t, y_n + b_3),$$

$$x_{n+1} \leftarrow x_n + \tfrac{1}{6}(a_1 + 2a_2 + 2a_3 + a_4),$$

$$y_{n+1} \leftarrow y_n + \tfrac{1}{6}(b_1 + 2b_2 + 2b_3 + b_4),$$

$$\dot{y}_{n+1} \leftarrow \dot{y}_n + \tfrac{1}{6}(c_1 + 2c_2 + 2c_3 + c_4).$$

The Adams predictor-corrector Method.

Given: $t_n, x_{n-3}, x_{n-2}, x_{n-1}, x_n, y_{n-3}, y_{n-2}, y_{n-1}, y_n, \dot{y}_{n-3}, \dot{y}_{n-2}, \dot{y}_{n-1}, \dot{y}_n, \ddot{y}_{n-3}, \ddot{y}_{n-2}, \ddot{y}_{n-1}, \ddot{y}_n$.

returns: $x_{n+1}, y_{n+1}, \dot{y}_{n+1}, \ddot{y}_{n+1}$.

$$\dot{y}_{n+1,p} \leftarrow \dot{y}_n + \tfrac{1}{24}\Delta t(55\ddot{y}_n - 59\ddot{y}_{n-1} + 37\ddot{y}_{n-2} - 9\ddot{y}_{n-3}),$$

$$y_{n+1,p} \leftarrow y_n + \tfrac{1}{24}\Delta t(9\dot{y}_{n+1,p} + 19\dot{y}_n - 5\dot{y}_{n-1} + \dot{y}_{n-2}),$$

$$\ddot{y}_{n+1,p} \leftarrow f(t_{n+1}, y_{n+1,p}),$$

$$\dot{y}_{n+1} \leftarrow \dot{y}_n + \tfrac{1}{24}\Delta t(9\ddot{y}_{n+1,p} + 19\ddot{y}_n - 5\ddot{y}_{n-1} + \ddot{y}_{n-2}),$$

$$y_{n+1} \leftarrow y_n + \tfrac{1}{24}\Delta t(9\dot{y}_{n+1} + 19\dot{y}_n - 5\dot{y}_{n-1} + \dot{y}_{n-2}),$$

$$x_{n+1} \leftarrow x_n + \tfrac{1}{24}\Delta t(9y_{n+1} + 19y_n - 5y_{n-1} + y_{n-2}),$$

$$\ddot{y}_{n+1} \leftarrow f(t_{n+1}, y_{n+1}).$$

A check on the accuracy of the integration was given by computing the energy $\mathcal{E}$ (2.1.14). The integration of the equations proceeded as follows:

(1) Specify x_0, y_0, $\dot{y}_0$ and t_0.

(2) Use the Runge-Kutta method to compute x_i, y_i, and $\dot{y}_i$

at $i = 1$ ($n \leftarrow 0$, $\Delta t \leftarrow \Delta t$),

$i = -1$ ($n \leftarrow 0$, $\Delta t \leftarrow -\Delta t$),

$i = -2$ ($n \leftarrow -1$, $\Delta t \leftarrow -\Delta t$).

(3) Use for i in [-2, -1, 0, 1] set $\ddot{y}_i \leftarrow f(t_i, y_i)$.

(4) Use the Adams predictor-corrector method to integrate the equations for subsequent times (n in [1, 2, . . .]).

(5a) For the plots of single cyclotron orbits store the values of x_i, y_i *and* $\dot{y}_i$ for selected i and terminate step (4) at a specified time, t_N.

(5b) For the plots of the crossings of the $w_1 = \pi$ plane, exit step (4) after the first crossing of the $w_1 = \pi$ plane. Determine $r = -y$ and $w_2 = (\nu t + \phi)_{\text{mod } 2\pi}$ at $w_1 = \pi$ by linear interpolation. Set $t \leftarrow 0$ and $\phi \leftarrow w_2$ (this ensures that t does not become so large as to impair the accuracy of the trigonometric routines). Return to step (4) until the desired number of crossing has been made.

The computations were carried out in MACSYMA on the Macsyma Consortium DEC KL-10 at the Laboratory for Computer Science at M.I.T. The integration routines given above were written in LISP using single precision arithmetic (8 bits for exponent, 27 bits for fraction, and 1 bit for the sign). The routines that called the integration routines and stored and plotted the results were written in MACSYMA.

The surface of section plots were all computed using a step size, Δt of 10^{-3}. The running time with this step size was about 2 s of CPU time per cyclotron orbit. Of this about 6 ms was needed for LISP storage management activities ("garbage collection"). As a check on the accuracy of the surface of section plots we have repeated the calculation of Fig. 3.2.3 using step sizes of 10^{-2} (Fig. A.1) and 10^{-4} (Fig. A.2). We see that there is excellent agreement between the plots for all three step sizes. If we check the value of $\mathcal{E}$, we see that it is accurately conserved. For instance, consider the particle whose initial position is $r = 47.25$ and $w_2 = \frac{1}{2}\pi$ in Fig. 3.2.4 ($\nu = 30.23$, $\alpha = 4$, $\Delta t = 10^{-3}$). (The motion of this particle is stochastic.) Initially $\mathcal{E}$ is 1577.208; after 300 cyclotron orbits it is 1577.232, a change of only 1.5×10^{-3}%. The simulation experiment (Figs. 5.1.1-3) was run with $\Delta t = 3\times10^{-3}$.

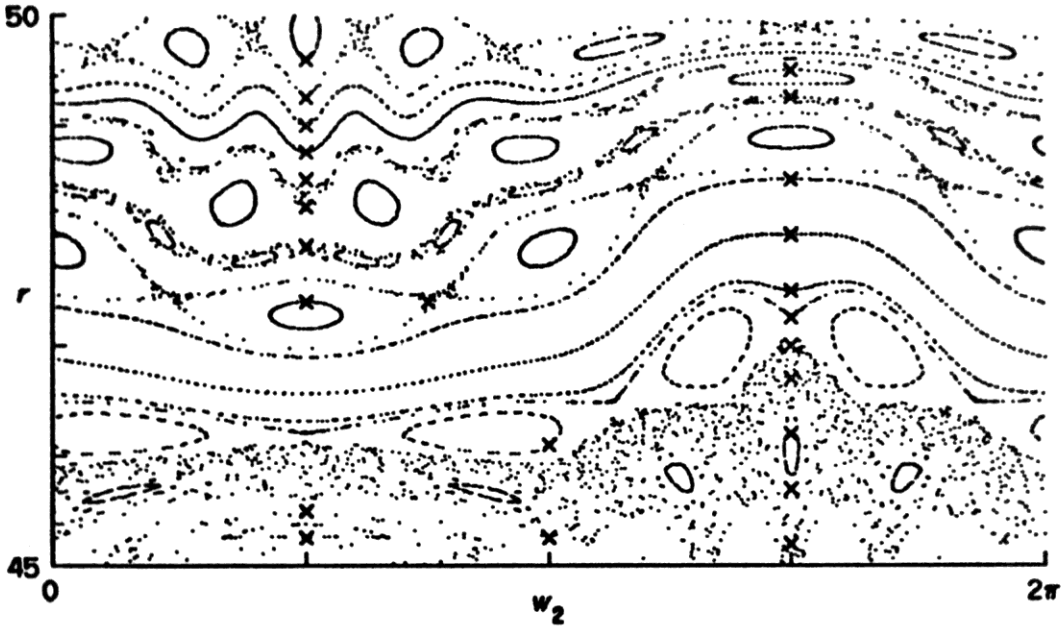

Figure A.1. The surface of section, Σ, the same parameters as Fig. 3.2.3, and computed using a step size, $\Delta t = 10^{-2}$.

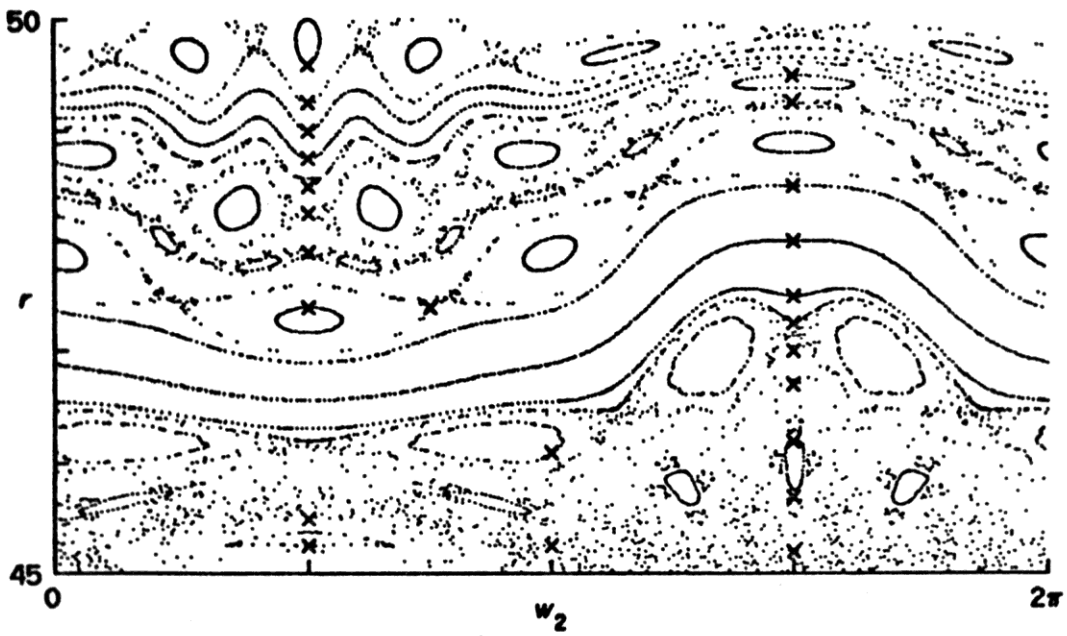

Figure A.2. Same as Fig. A.1, except that $\Delta t = 10^{-4}$.

Appendix B. Calculation of Overlap Condition near a Harmonic.

We present in this appendix the derivation of the overlap condition for islands for the case where ω is close to a cyclotron harmonic ($\nu \approx n$). This calculation was first done by Fukuyama *et al.* (1977). This analysis begins with the Hamiltonian expressed in the rotating frame that was derived in Sec. 4.2:

$$\hat{H} = (n - \nu)\hat{I}_1 + \nu\hat{I}_2 - \alpha\, \Sigma_m\, J_m[(2n\hat{I}_1)^{1/2}]\sin[m\hat{w}_1/n - (1 - m/n)\hat{w}_2]. \tag{4.2.12}$$

Because $\hat{w}_1$ is slowly varying, the dominant contribution to the motion is given by the $m = n$ term in the sum. This is the term that gives the large first order islands seen in Figs. 3.2.7 and 4.2.1. The motion around such islands is that of a nonlinear oscillator. To derive the overlap condition we will transform to the action-angle variables of this nonlinear oscillator. The next most slowly varying terms in the sum ($m = n \pm 1$) are then added as a perturbation. Since the oscillator is nonlinear its frequency can resonate with the Fourier components of the perturbation leading to the formation of sub-islands. The overlap condition is then given by comparing the size of the sub-islands with their separation.

Including only the terms $m - n = 0, \pm 1$ in (4.2.12) we obtain in the limit $\nu \gg 1$

$$\hat{H} = (n - \nu)\hat{I}_1 + \nu\hat{I}_2 - \alpha\, J_n[(2n\hat{I}_1)^{1/2}]\sin\hat{w}_1 - \alpha\, \Sigma_{m=n\pm1}\, J_m[(2n\hat{I}_1)^{1/2}]\sin(\hat{w}_1 \mp \hat{w}_2/n). \tag{B.1}$$

For simplicity we expand the Bessel functions in the limit $r \gg \nu$ (eq. 9.2.1, Abramowitz and Stegun, 1964). Since in this limit the amplitude of the Bessel function is slowly varying compared with the oscillatory part, we will regard the amplitude as a constant. In the same spirit we may replace the argument of the Bessel functions by its Taylor series expansion about some point, so that

$$(2n\hat{I}_1)^{1/2} \approx (2n\hat{I}_{10})^{1/2} + n(\hat{I}_1 - \hat{I}_{10})/(2n\hat{I}_{10})^{1/2} = r + n\Delta\hat{I}_1/r, \tag{B.2}$$

where $r = (2n\hat{I}_{10})^{1/2}$ is the position of a maximum of J_n. Then (B.1) may be written as

$$\hat{H} = \delta\Delta\hat{I}_1 + \nu\hat{I}_2 - \alpha\sqrt{2/\pi r}\cos(n\Delta\hat{I}_1/r)\sin\hat{w}_1 + 2\alpha\sqrt{2/\pi r}\sin(n\Delta\hat{I}_1/r)\cos\hat{w}_1\sin(\hat{w}_2/n) \tag{B.3}$$

($\delta = \nu - n$). We transform (B.3) to a new set of conjugate variables using

$$M = n\hat{H}/r,\ v = n\Delta\hat{I}_1/r,\ u = \hat{w}_1 - \tfrac{1}{2}\pi,\ J_2 = n^2\hat{I}_2/r,\ \theta_2 = \hat{w}_2/n \tag{B.4}$$

(note that v and u are shifted and scaled versions of I_1 and w_1). The Hamiltonian, M, is than

$$M = -\delta v + J_2 - \Gamma\cos u\cos v - 2\Gamma\sin u\sin v\sin\theta_2. \tag{B.5}$$

The quantitly Γ is defined by

$$\Gamma = \alpha\sqrt{2/\pi}\,nr^{-3/2}, \tag{B.6}$$

and it gives the frequency of oscillation around the first order islands; note that it is proportional to α. Now if we are very close to a cyclotron harmonic, or, more specifically, if $\delta \ll \Gamma$ then the first term in (B.5) may be neglected. The lowest order motion is then determined by

$$M_0 = J_2 - \Gamma\cos u\cos v. \tag{B.7}$$

This gives oscillations about points for which u and v are multiples of π. The trajectories are similar to those shown in Fig. 4.2.1. For simplicity we will concentrate on the motion centered at $u = v = 0$. The Hamiltonian equations given by (B.7) are straightforwardly integrated to give

$$\sin v = q\,\mathrm{sn}[\Gamma(t - t_0)|q^2],\ \sin v = q\,\mathrm{cd}[\Gamma(t - t_0)|q^2], \tag{B.8}$$

where sn and cd are Jacobian elliptic functions (Chapter 16, Abramowitz and Stegun, 1964) and

$$q^2 = 1 - M_0^2/\Gamma^2. \tag{B.9}$$

The period of the elliptic functions is $4K(q^2)$ [K is the complete elliptic integral of the first kind (Sec. 17.3, Abramowitz and Stegun, 1964)]. Thus the frequency of oscillation is

$$\Gamma\Omega = \frac{\Gamma\pi}{2K(q^2)}. \tag{B.10}$$

This varies from Γ at the center of the first order islands ($M_0 = -\Gamma$, $q = 0$) to 0 at the separatrix between islands ($M_0 = 0$, $q = 1$). We may write M_0 in the action-angle variables, J_1 and θ_1, as

$$M_0 = M_0(J_1) + J_2, \tag{B.11}$$

where J_1 is given in terms of M_0 by

$$J_1 = \frac{1}{2\pi}\oint v\,du = \frac{2}{\pi}\int_0^q \frac{q}{(1-q^2)^{1/2}} K(q^2)\,dq. \tag{B.12}$$

A plot of M_0 as a function of J_1 is given in Fig. B.1. The frequency, $\Gamma\Omega$, (B.10), may also be computed from $\partial M_0/\partial J_1$; in Fig. B.2, $\Gamma\Omega$ is plotted against J_1. The variables u and v are given in terms of J_1 and θ_1 as

$$\sin u = q(J_1)\,\mathrm{sn}(\theta_1/\Omega|q^2), \quad \sin v = q(J_1)\,\mathrm{cd}(\theta_1/\Omega|q^2), \tag{B.13}$$

where $q(J_1)$ is defined by (B.9).

We now add in the perturbation, the last term of (B.5). Substituting (B.13) we obtain

$$M = M_0(J_1) + J_2 - 2\Gamma q^2(J_1)\,\mathrm{sn}(\theta_1/\Omega|q^2)\,\mathrm{cd}(\theta_1/\Omega|q^2)\sin\theta_2, \tag{B.14}$$

In order to determine the effect of the perturbation we take its Fourier transform. The product of a sn and cd function is expressible as a single sn function using eqs. 16.14.1 and 16.14.2 of Abramowitz and Stegun (1964). This sn function may be Fourier transformed using eq. 16.23.1 of Abramowitz and Stegun (1964) to give

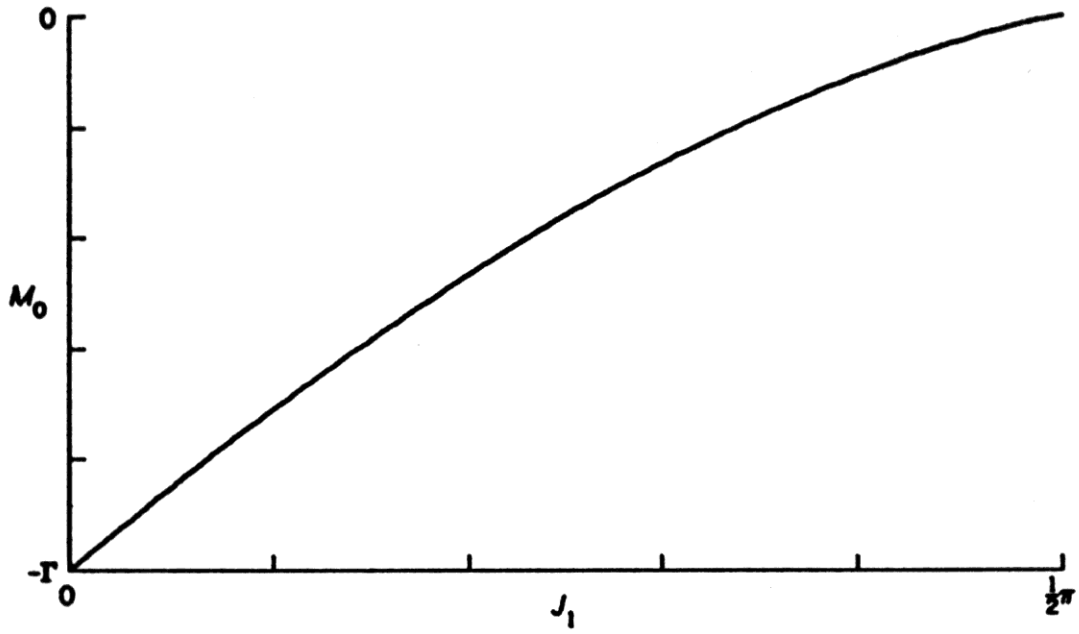

Figure B.1. Plot of the Hamiltonian, $M_0(J_1)$, as a function of action, J_1. See (B.12).

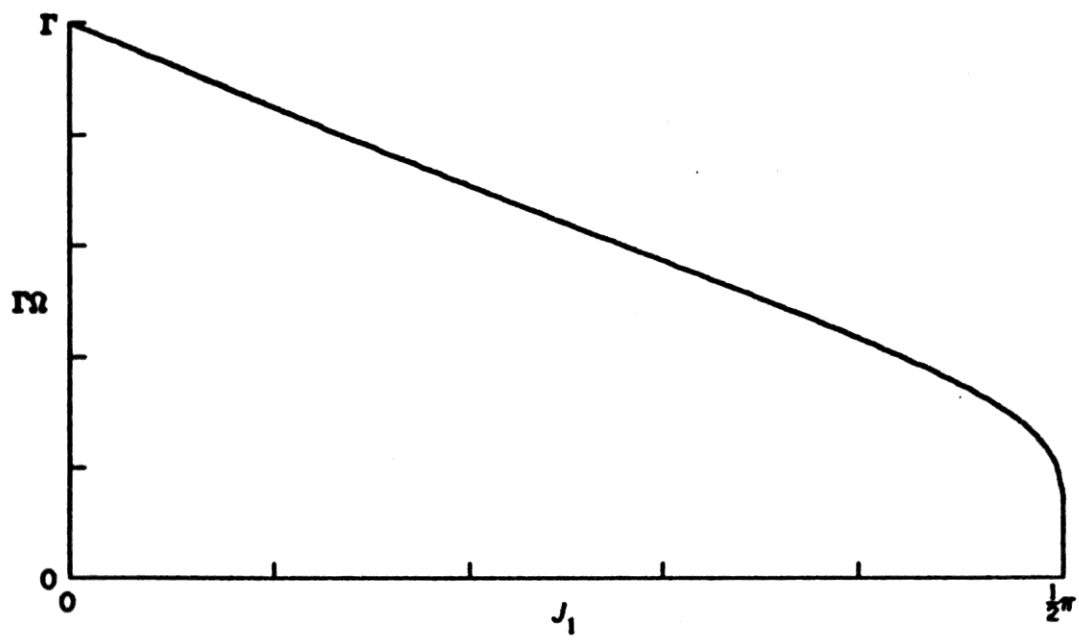

Figure B.2. Plot of the frequency, $\Gamma\Omega(J_1)$, against action. See (B.10).

$$\mathrm{sn}(\theta_1/\Omega|q^2)\,\mathrm{cd}(\theta_1/\Omega|q^2) = \mathrm{sn}(2K\theta_1/\pi|q^2)\,\mathrm{cd}(2K\theta_1/\pi|q^2) = \sum_{m=0}^{\infty} A_m \sin[2(2m+1)\theta_1], \tag{B.15}$$

where

$$A_m = \frac{2\pi}{K(q^2)q^2}\,\mathrm{cosech}\left[\frac{(2m+1)\pi K(1-q^2)}{K(q^2)}\right]. \tag{B.16}$$

(B.13) then becomes

$$M = M_0(J_1) + J_2 - \Gamma q^2(J_1) \sum_{m=-\infty}^{\infty} A_m \cos[2(2m+1)\theta_1 - \theta_2]. \tag{B.17}$$

The motion descibed by (B.17) is that of two oscillators, a nonlinear one, $M_0(J_1)$, and a linear one, J_2. The last term in (B.17) couples these two oscillators. Normally the coupling is weak; however if the frequency of θ_2 (as given by J_2) is $2(2s+1)$ times the frequency of θ_1 (as given by $M_0(J_1)$) then there is a resonance. The $m = s$ term in the sum in (B.17) will then be slowly varying, and can perturb the motion significantly.

The value of J_1 at which this resonance occurs is given by

$$\Gamma\Omega(J_{1,s}) = \left.\frac{\partial M_0(J_1)}{\partial J_1}\right|_{J_1 = J_{1,s}} = \frac{1}{2(2s+1)}. \tag{B.18}$$

We may determine how the motion become perturbed in this case by ignoring all but the $m = s$ term in the sum. Since the motion of given by $M_0(J_1)$ is nonlinear, this term will only be important for J_1 close to $J_{1,s}$; thus we may Taylor expand $M_0(J_1)$ about $J_1 = J_{1,s}$ giving

$$M_0(J_1) \approx M_0(J_{1,s}) + \Delta J_1/[2(2s+1)] + \tfrac{1}{2}\Gamma(\partial\Omega/\partial J_1)|_{J_{1,s}}\,\Delta J_1^{\,2}, \tag{B.19}$$

where $\Delta J_1 = J_1 - J_{1,s}$. The Hamiltonian then becomes

$$\Delta M = \frac{\Delta J_1}{2(2s+1)} + \tfrac{1}{2}\Gamma\frac{\partial\Omega}{\partial J_{1,s}}\Delta J_1^{\,2} + J_2 - \Gamma q^2(J_{1,s})A_m\cos[2(2s+1)\theta_1 - \theta_2]. \tag{B.20}$$

We now transform into a rotating frame using a similar generating function to (4.2.10). The

relation between the variables is

$$\Delta J_1 = 2(2s+1)\hat{J}_1, \quad J_2 = \hat{J}_2 - \hat{J}_1, \quad \hat{\theta}_1 = 2(2s+1)\theta_1 - \theta_2, \quad \hat{\theta}_2 = \theta_2, \tag{B.21}$$

and the transformed Hamiltonian is

$$\hat{M} = \tfrac{1}{2}\Gamma(\partial\Omega/\partial J_{1,s})4(2s+1)^2\hat{J}_1^{\,2} + \hat{J}_2 - \Gamma q^2(J_{1,s})A_s\cos\hat{\theta}_1 . \tag{B.22}$$

The motion given by $\hat{J}_1$ and $\hat{\theta}_1$ is identical to the motion of a particle in an electrostatic wave. The trapped orbit give the sub-islands; their overall width is

$$\frac{2}{2s+1}\left|\frac{q^2(J_{1,s})A_s}{\partial\Omega/\partial J_{1,s}}\right|^{1/2} .$$

This may be expressed as a width in J_1 as

$$\Delta J_{1,s} = 4\left|\frac{q^2(J_{1,s})A_s}{\partial\Omega/\partial J_{1,s}}\right|^{1/2} . \tag{B.23}$$

Now the separation between the $m = s$ and $m = s+1$ resonances is $J_{1,s+1} - J_{1,s}$. This may be simply estimated by Taylor expanding $\Omega(J_1)$ about $J_{1,s}$ and assuming s is large. Then

$$J_{1,s+1} - J_{1,s} \equiv \delta J_{1,s} \approx \frac{4\Gamma\Omega^2}{|\partial\Omega/\partial J_{1,s}|} . \tag{B.24}$$

See Fig. B.3 for the relation of $\Delta J_{1,s}$ to $\delta J_{1,s}$. Neighbouring islands overlap when their width exceeds their separation,

$$\Delta J_{1,s} > \delta J_{1,s}, \tag{B.25}$$

or

$$S \equiv \left(\frac{\Delta J_1}{\delta J_1}\right) = \frac{q^2 A_s}{\Gamma^2\Omega^4}\left|\frac{\partial\Omega}{\partial J_1}\right| > 1 . \tag{B.26}$$

(Although our analysis breaks down here since we should not neglect neighbouring resonances).

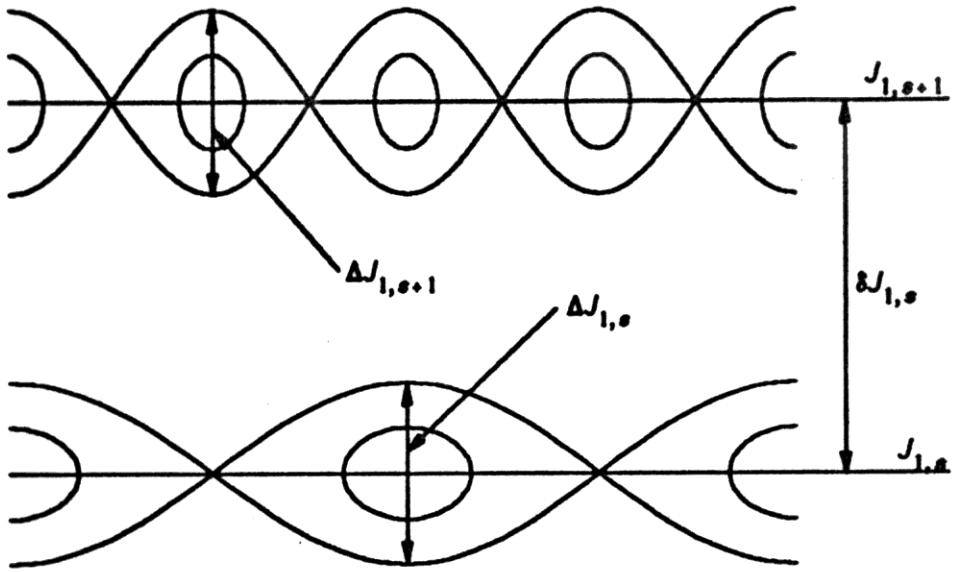

Figure B.3. Schematic picture showing the relation between the sub-island width, $\Delta J_{1,s}$, and the separation between the sub-islands, $\delta J_{1,s}$.

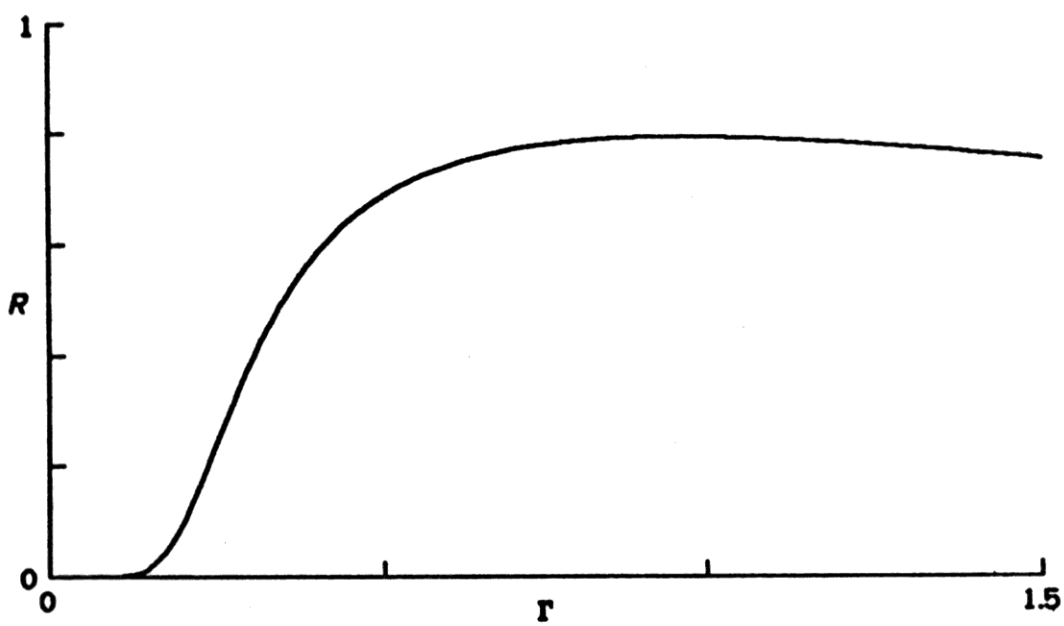

Figure B.4. The fraction, R, of phase space that is stochastic as a function of the field, Γ. See (B.29).

Eliminating Ω, s, and A_s using (B.10), (B.18), and (B.16) and using

$$\frac{dK(q^2)}{dq} = \frac{E(q^2) - (1 - q^2)K(q^2)}{(1 - q^2)q} \tag{B.27}$$

(E is the elliptic integral of the second kind) when evaluating $\partial\Omega/\partial J_1$, (B.26) becomes

$$S = \frac{8}{\Gamma^2\pi}\,\mathrm{cosech}\left[\frac{K(1 - q^2)}{\Gamma}\right]\frac{E(q^2) - (1 - q^2)K(q^2)}{(1 - q^2)^{1/2}q^2} > 1. \tag{B.28}$$

Equation (B.28) gives the stochasticity threshold as defined by Zaslavskii and Chirikov (1972). The last factor in (B.28) becomes $\frac{1}{4}\pi$ as $q \to 0$ and it diverges as $(1 - q^2)^{-1/2}$ as $q \to 1$. As $q \to 0$ the cosech term goes to zero as $2(q/4)^{1/\Gamma}$, and as $q \to 1$ it goes to a constant, $\mathrm{cosech}(\frac{1}{2}\pi/\Gamma)$. Thus near the separatrix, $q \approx 1$, S diverges (for nonzero Γ) while it is zero at the center of the first order islands. This means that there is always a strip of stochasticity close to the separatrix. We can estimate the area of the surface of section (or the volume of phase space) that is stochastic, by finding the value of J_1 at which $S = 1$. Since J_1 is proportional to the area of a first order island in the plots of Σ in Figs. 3.2.7-9, see (B.12), the fraction of phase space that is stochastic is given by

$$R = 1 - J_1[q(S = 1)]/J_1(q = 1). \tag{B.29}$$

In Fig. B.4, R is plotted as a function of Γ. R is extremely small for Γ small; in fact for $\Gamma \to 0$

$$R \to \frac{32}{\pi^2\Gamma^3}\exp\left(-\frac{\pi}{2\Gamma}\right). \tag{B.30}$$

Now (B.30) is a non-analytic function of Γ, having an essential singularity at $\Gamma = 0$, and the formal expansion of R for $\Gamma > 0$ is zero to all orders in Γ. This is of interest because it shows how the theorem of Kruskal (1962), that the perturbed action is conserved to all orders in the perturbation parameter (Γ), is not inconsistent with the fact that the motion is stochastic for finite Γ. The curve rises quite steeply for $\Gamma > 0.15$. Thus the stochasticity threshold, the field at which particles can move freely past the first order islands, is given by

$$\Gamma > 0.15, \tag{B.31}$$

or

$$\alpha > 0.15\ \sqrt{\pi/2}\, r^{3/2}/n. \tag{B.32}$$

This result should be compared with (4.4.25) in the limit $r \gg \nu$. The assumption that $\delta \ll \Gamma$ that we made above now becomes $\delta \ll 0.15$.

References.

R. E. Aamodt, *Particle Motion in the Presence of Three-Dimensional Finite Amplitude Harmonic Cyclotron Waves*, Phys. Fluids *13*, 2341 (1970).

M. Abramowitz and I. A. Stegun (eds.), *Handbook of Mathematical Functions*, (National Bureau of Standards, 1964).

V. I. Arnold and A. Avez, *Ergodic Problems of Classical Mechanics*, (W. A. Benjamin, Inc., New York, 1968).

L. A. Artsimovitch, *Tokamak Devices*, Nucl. Fusion *12*, 215 (1972).

S. Bernabei, C. Daughney, W. M. Hooke, R. W. Motley, M. Porkolab, T. Nagashima, and S. Suckewer, *Lower Hybrid Heating Experiments on the ATC Tokamak*, Symposium on Plasma Heating on Toroidal Devices, Varenna (1976).

A. Bers, *Linear Waves and Instabilities*, in *Plasma Physics* (*Les Houches 1972*), (Gordon and Breach, New York, 1975).

A. Bers, C. F. F. Karney, and D. C. Watson, *Ion Heating in Tokamaks by Externally Applied RF Power*, Proc. Seventh European Conference on Controlled Fusion and Plasma Physics, Lausanne, Switzerland, p. 193 (1975).

A. Bers, F. W. Chambers, and N. J. Fisch, *RF Heating by Electron Landau Damping of Lower Hybrid Waves*, PRR 76/23, Research Laboratory of Electronics, Massachusetts Institute of Technology (July 1976a).

A. Bers, F. Y. F. Chu, G. L. Johnston, and C. F. F. Karney, *Nonlinear Propagation of Lower Hybrid Cones from a Plane Boundary*, Paper 8C-1, Bull. Am. Phys. Soc. *21*, 1156 (1976b).

P. Blanc, W. Hess, G. Ichtchenko, P. Javel, P. Lallia, C. Mahn, T. K. Nguyen, W. Ohlendorf, G. W. Pacher, H. D. Pacher, S. Takamura, G. Tonon, and J. G. Wegrowe, *Experiments at the Lower Hybrid Frequency in the WEGA Tokamak*, Proc. Int. Conf. on Plasma Physics and Controlled Thermonuclear Fusion Research, Berchtesgaden, (1976).

N. N. Bogoliubov and Y. A. Mitropolsky, *Asymptotic Methods in the Theory of Nonlinear Oscillations*, (Hindustan Publishing Corp., Delhi, 1961).

M. Brambilla, *Slow-Wave Launching at the Lower Hybrid Frequency using a Phased Waveguide Array*, Nucl. Fusion *16*, 47 (1976).

R. J. Briggs and R. R. Parker, *Transport of RF Energy to the Lower Hybrid Resonance in an Inhomogeneous Plasma*, Phys. Rev. Lett. *29*, 852 (1972).

L. Chen and R. L. Berger, *Anomalous Spatial Depletion of the Lower Hybrid Cone Through Parametric Decay*, PPPL-1306, Plasma Physics Laboratory, Princeton University (1976).

C. T. Dum and T. H. Dupree, *Nonlinear Stabilization of High-Frequency Instabilities in a Magnetic Field*, Phys. Fluids *13*, 2064 (1970).

D. A. Dunnett, E. W. Laing, and J. B. Taylor, *Invariants in the Motion of a Charged Particle in a Spatially Modulated Magnetic Field*, J. Math. Phys. *9*, 1819 (1968).

O. C. Eldridge, A. H. Kritz, and A. C. England, *Ion Cyclotron Heating Near the Lower Hybrid Resonance*, Paper 6A4, Bull. Am. Phys. Soc. *20*, 1313 (1975).

J. Ford, *The Statistical Mechanics of Classical Analytic Dynamics*, in *Fundamental Problems in Statistical Mechanics, Vol. 3*, pp. 215-255, Editor E. D. G. Cohen (North-Holland Publishing Co., Amsterdam, Neth. 1975).

A. Fukuyama, H. Momota, R. Itatani, and T. Takizuka, *Stochastic Acceleration by an Electrostatic Wave near Ion Cyclotron Harmonics*, Phys. Rev. Lett. *38*, 701 (1977).

V. M. Glagolev, *Propagation and Absorption of Ion Hybrid Waves in a Weakly Inhomogeneous plasma - I* and *II*, Plasma Phys. *14*, 301 and 315 (1972).

V. E. Golant, *Plasma Penetration near the Lower Hybrid Frequency*, Zh. Tekh. Fiz. *41*, 2492 (1971) [Sov. Phys. Tech. Phys. *16*, 1980 (1972)].

H. Goldstein, *Classical Mechanics* (Addison-Wesley Press, Inc., Cambridge, Mass., 1951).

E. G. Harris, *Plasma Instabilities Associated with Anisotropic Velocity Distributions*, J. Nucl. Energy *C2*, 138 (1961).

W. Hess, P. Blanc, G. Ichtchenko, P. Javel, P. Lallia, C. Mahn, T. K. Nguyen, W. Ohlendorf, G. W. Pacher, H. D. Pacher, S. Takamura, G. Tonon, and J. G. Wegrowe, *Experiments in the WEGA Tokamak at the Lower Hybrid Frequency*, Paper 5D-3, Bull. Am. Phys. Soc. *21*, 1107 (1976).

W. M. Hooke and S. Bernabei, *Observation of a Parametric Instability near the Lower Hybrid-Resonance Frequency*, Phys. Rev. Lett. *29*, 1218 (1972).

W. M. Hooke, *Lower Hybrid Frequency Plasma Heating in the ATC Tokamak*, Paper 6A6, 7, 8, Bull. Am. Phys. Soc. *20*, 1313 (1975).

E. F. Jaeger and A. J. Lichtenberg, *Resonant Modification and Destruction of Adiabatic Invariants*, Ann. Phys. *71*, 319 (1972).

F. Jaeger, A. J. Lichtenberg, and M. A. Lieberman, *Theory of Electron Cyclotron Resonance Heating, I. Short Time and Adiabatic Effects*, Plasma Phys. *14*, 1073 (1972).

C. F. F. Karney and A. Bers, *Nonlinear Orbit Perturbation and Ion Heating*, PRR 76/7, Research Laboratory of Electronics, Massachusetts Institute of Technology (January 1976a).

C. F. F. Karney and A. Bers, *Stochastic Ion Heating by a Perpendicularly Propagating Electrostatic Wave*, PRR 76/24, Research Laboratory of Electronics, Massachusetts Institute of Technology (July 1976b).

C. F. F. Karney and A. Bers, *Direct Heating of the Ion Tail by RF Power near the Lower Hybrid Frequency*, Paper 8C-3, Bull. Am. Phys. Soc. *21*, 1157 (1976c).

C. F. F. Karney and A. Bers, *Stochastic Ion Heating by a Perpendicularly Propagating Electrostatic Wave*, PRR 76/35-2, Research Laboratory of Electronics, Massachusetts Institute of Technology (March 1977a).

C. F. F. Karney and A. Bers, *Stochastic Ion Heating by Lower Hybrid Waves*, Paper D9, Proc. Annual Controlled Fusion Theory Conference, San Diego (May 1977b).

C. F. F. Karney, A. Bers, and D. C. Watson, *Linear and Nonlinear Absorption of RF Power near the Lower Hybrid Frequency*, Paper 6A3, Bull. Am. Phys. Soc. *20*, 1313 (1975).

J. M. Kindel, M. Okuda, and J. M. Dawson, *Parametric Instabilites and Anomalous Heating of Plasmas near the Lower Hybrid Frequency*, Phys. Rev. Lett. *29*, 995 (1972).

M. Kruskal, *Asymptotic Theory of Hamiltonian and other Systems with all Solutions Nearly Periodic*, J. Math. Phys. *3*, 806 (1962).

J. L. Kulp, G. L. Johnston, and A. Bers, *Lower Hybrid Wave Group Velocity Trajectories in Toroidal Geometry*, PRR 76/9, Research Laboratory of Electronics, Massachusetts Institute of Technology (January 1976).

P. P. Lallia, G. W. Pacher, and H. D. Pacher, *Ion Measurements during Lower Hybrid Experiments in WEGA*, Symposium on Plasma Heating on Toroidal Devices, Varenna (1976).

M. A. Lieberman and A. J. Lichtenberg, *Theory of Electron Cyclotron Resonance Heating, II. Long Time and Stochastic Effects*, Plasma Phys. *15*, 125 (1973).

G. J. Morales and Y. C. Lee, *The Nonlinear Filamentation of Lower-Hybrid Cones*, Phys. Rev. Lett. *35*, 930 (1975).

T. M. O'Neil, *Collisionless Damping of Nonlinear Plasma Oscillations*, Phys. Fluids *8*, 2255 (1965).

NRL Plasma Formulary, Naval Research Laboratory (Last revisions dated November 1, 1976).

E. Ott, *Decay Instability of Lower Hybrid Waves*, Phys. Fluids *18*, 566 (1975).

M. Porkolab, *Theory of Parametric Instability near the Lower Hybrid Frequency*, Phys. Fluids *17*, 1432 (1974).

M. Porkolab, S. Bernabei, W. M. Hooke, R. W. Motley, and T. Nagashima, *Observation of Parametric Instabilities in Lower-Hybrid Radio-Frequency Heating of Tokamaks*, Phys. Rev. Lett. *38*, 230 (1977).

A. B. Rechester and T. H. Stix, *Magnetic Braiding due to Weak Asymmetry*, Phys. Rev. Lett. *36*, 587 (1976).

A. H. Reiman, *Space-Time Evolution of the Nonlinear Three-Wave Interaction in an Inhomogeneous Medium*, Ph.D. Thesis, Physics Dept., Princeton University (to be submitted 1977)

B. Richards and R. R. Parker, *Ion Heating in Alcator near the Lower Hybrid Resonance*, Paper 6A5 Bull. Am. Phys. Soc. *20*, 1313 (1975).

J. P. M. Schmitt, *Nonlinear Theory of RF Heating at Cyclotron Harmonics*, Phys. Fluids *19*, 245 (1976).

A. Sen, C. F. F. Karney, and A. Bers, *Two Dimensional Depletion of Lower Hybrid Pump by Quasi-Mode Excitations*, Paper D16, Proc. Annual Controlled Fusion Theory Conference, San Diego (May 1977).

D. J. Sigmar and J. D. Callen, *Wave-Particle Transfer and Wave-Amplitude Limiting Effects for a Flutelike High-Frequency Mode*, Phys. Fluids *14*, 1423 (1971).

M. D. Simonutti, *Propagation and Collisionless Absorption of Linearly Converted Lower Hybrid Plasma Waves*, Phys. Fluids, *18*, 1524 (1975).

G. R. Smith and A. N. Kaufman, *Stochastic Acceleration by a Single Wave in a Magnetic Field*, Phys. Rev. Lett. *34*, 1613 (1975).

T. H. Stix, *Radiation and Absorption via Mode Conversion in an Inhomogeneous Collision-Free Plasma*, Phys. Rev. Lett. *15*, 878 (1965).

R. Sugihara and Y. Midzuno *Trapping and Detrapping in a Single Wave and Particle Acceleration in a Magnetoplasma*, IPPJ-263, Institute of Plasma Physics, Nagoya Universtiy (October 1976).

K. S. Theilhaber, *Micorwave Heating of a Plasma by Whistler Waves*, S.M. Thesis, Dept. of Electrical Engineering and Computer Science, M.I.T. (1976).

A. V. Timofeev, *Confinement of Charged Particles in Adiabatic Traps in the Presence of Monochromatic Cyclotron Oscillations*, Nucl. Fusion *14*, 165 (1974).

F. Troyon and F. W. Perkins, *Lower-Hybrid Heating in Large Tokamak*, Proc. Second Topical Conf. on RF Plasma Heating, Lubbock, Texas (1974).

B. A. Trubnikov, *Particles Interaction in a Fully Ionized Plasma*, in *Reviews of Plasma Physics, Vol. 1*, pp. 105-204, Editor M. A. Leontovich (Consultants Bureau, New York, 1965).

G. H. Walker and J. Ford, *Amplitude Instability and Ergodic Behavior for Conservative Nonlinear Oscillator Systems*, Phys. Rev. *188*, 416 (1969).

G. M. Zaslavskii and B. V. Chirikov, *Stochastic Instability of Non-Linear Oscillations*, Usp. Fiz. Nauk *105*, 3 (1971) [Sov. Phys. Usp. *14*, 549 (1972)].

G. M. Zaslavskii and N. N. Filonenko, *Stochastic Instability of Trapped Particles and Conditions of Applicability of the Quasi-Linear Approximation*, Zh. Eksp. Teor. Fiz. *54*, 1590 (1968) [Sov. Phys. JETP 25, 851 (1968)].

Biographical Note.

Charles Fielding Finch Karney was born in England in 1951. He obtained a Bachelor of Arts degree from Cambridge University in 1972 and a Master of Science degree from Massachusetts Institute of Technology in 1974. He will go to Princeton Plasma Physics Laboratory in September 1977.

Errata

p. 2, line 5: "Philosphy" → "Philosophy".
p. 3, line 1: "Acknowledgements" → "Acknowledgments".
p. 3, line 5: "proof-read" → "proofread".
p. 4, line 3: "Acknowlegements" → "Acknowledgments".
p. 8, para. 2: omit sentence "Antonsen and Ott (1976) ... exactly."
p. 18, eq. (2.2.16): "y_o" → "y_0".
p. 25, eq. (2.3.9), first line: integral should include dt'.
p. 26, eq. (2.3.16): "]" → "$\Big]$".
p. 32, eq. (2.4.10): "$\sqrt{2/\pi}$" → "$-\sqrt{2/\pi}$".
p. 34, eq. (2.4.14): "$2\pi\delta - 2\pi A(r,\nu)\ldots$" → "$2\pi\delta + 2\pi A(r,\nu)\ldots$".
p. 38, fig. 3.1.1, line 2: "*and*" → "and".
p. 52, eq. (4.1.1): "." → ",".
p. 53, eq. (4.1.5): "." → ",".
p. 55, line 1: "(4.1.13)" → "(4.1.12)".
p. 55, eq. (4.1.18): "." → ",".
p. 65, line following eq. (4.3.2): "w_2" → "w_1".
p. 70, last line: "computing" → "compute".
p. 73, line before eq. (4.4.11): "susbtitute" → "substitute".
p. 79, line 10: "has factor" → "has a factor".
p. 80, eq. (4.4.30): "$(2\nu\sqrt{\alpha})$" → "$(2\nu^{-1}\sqrt{\alpha})$".
p. 81, fig. 4.4.4: "$(2\nu\sqrt{\alpha})$" → "$(2\nu^{-1}\sqrt{\alpha})$".
p. 83, eq. (4.5.10): ">" → "=".
p. 85, caption for fig. 4.5.2: append "and for $\nu = 30.23$".
p. 86, line 7: "dependence of (4.5.15) angle" → "dependence of (4.5.15) on angle".
p. 86, eq. (4.5.16): "$\nu^{1/3}/(10\zeta^2)$" → "$\nu^{1/3}/(16\zeta^2)$".
p. 86, eq. (4.5.17) and line preceding: "0.6" → "$\frac{1}{2}$".
p. 88, eq. (4.6.5): "$H = I_1 - \ldots$" → "$H = I_1 + \nu I_2 - \ldots$".
p. 88, 2 lines before eq. (4.6.7): "get" → "gets".
p. 93, 6 lines before end: "stochasic" → "stochastic".
p. 94, caption to fig. 5.1.1: "phase" → "phases".
p. 95, line before eq. (5.1.1): "1000" → "1100".
p. 98, eq. (5.2.7): "$\nabla^2_{\mathbf{v}}\phi$" → "$\nabla^2_{\mathbf{v}}\phi_\beta$".
p. 116, line 8: "$r = -y$" → "$r = -\dot{y}$".
p. 118, eq. (B.1): "$\sin(\hat{w}_1 \mp \hat{w}_2/n)$" → "$\sin(\hat{w}_1 \pm \hat{w}_2/n)$".
p. 119, eq. (B.3): "$\delta\,\Delta\hat{I}_1$" → "$-\delta\,\Delta\hat{I}_1$". "$\ldots + 2\alpha$" → "$\ldots - 2\alpha$".
p. 119, eq. (B.8): first "$\sin y$" → "$\sin u$".
p. 127, ref. Bernabei *et al.* (1976): "M. Porkolab, T. Nagashima" → "T. Nagashima, M. Porkolab". "on Toroidal Devices" → "in Toroidal Devices".
p. 130, ref. Theilhaber (1976): "Micorwave" → "Microwave".
p. 131, ref. Zaslavskii and Filonenko (1968): "Sov. Phys. JETP **25**" → "Sov. Phys. JETP **27**".